Numerical simulation of coastal flood hazard in the Acadian Peninsula region of New Brunswick

Ferguson, Sean; Provan, Mitchel; Murphy, Enda; Kim, Joseph

Technical Report (National Research Council of Canada. Ocean, Coastal and River Engineering Research Centre); no. NRC-OCRE-2021-TR-060, 2022-03-01

NRC·CNRC

Numerical Simulation of Coastal Flood Hazard in the Acadian Peninsula Region of New Brunswick

Report No.: NRC-OCRE-2021-TR-060

Prepared for:
Defence Research and Development Canada's
Canadian Safety and Security Program

Prepared by:
Ocean, Coastal and River Engineering Research Centre
National Research Council Canada
Ottawa, ON

Authors: Sean Ferguson, Mitchel Provan,
Enda Murphy, Joseph Kim

Date: March 2022

National Research Council Canada | Conseil national de recherches Canada

Canada

Revision History

Document Version	Name	Affiliation	Date of Changes	Comments
0.1	SF	NRC-OCRE	31-03-2022	Final Report

Executive Summary

The work described in this report was completed as part of the Coastal Flood Mitigation Canada project, which aims to: bring together researchers, practitioners, and communities to share knowledge and expertise in support of disaster risk reduction strategies for coastal storm surge and tsunami risks; develop and promote an evidence based approach for coastal storm and tsunami disaster risk reduction decisions; and demonstrate best practise approaches. Three case studies are underway, one for each of Canada's Atlantic, Arctic, and Pacific coasts, in which the project team has conducted, or is working to complete, a coastal flood hazard and risk assessment. Knowledge gained from each case study will support the development of guidelines summarizing best practices and methods for coastal flood hazard assessment in support of risk-based analyses.

An assessment of present-day and future storm surge-driven flood hazards on the Acadian Peninsula, New Brunswick, was conducted in support of the Atlantic Coast case study. The study objectives and scope were developed in consultation with project partners, local experts, academia, private/non-profit groups, and government and community representatives. The hazard assessment was based on regional-scale and community-scale numerical hydrodynamic models, developed to simulate storm surges in Canada's Atlantic coastal waters, including detailed simulation of overland flooding in seven Acadian Peninsula coastal communities.

The regional storm surge model covers much of Canada's Atlantic coast and continental shelf and is large enough to capture storm surges generated by synoptic meteorological forcing. Regional model skill was assessed using data available from tide gauge records. The effects of sea-ice on storm surges, and the potential contribution of wave set-up to total water levels on the east coast of the Acadian Peninsula were investigated at the regional scale. The results of the analysis indicated that wave setup caused by sustained, strong winds from the east or north-east has potential to contribute to elevated water levels at the coast. Conversely, the analysis indicated that high concentrations of sea ice can attenuate storm surge. Methods to incorporate impacts of sea-ice into hydrodynamic modelling of storm surge were explored and applied with some success; these results provide a foundation for potential future research focused on the evolution of coastal flood hazard in the Gulf of Saint Lawrence in the context of diminishing sea-ice under future climate change scenarios.

The community-scale model, focused specifically on the Acadian Peninsula, is nested within the regional model and contains high spatial resolution (approximately 10 m) in seven Acadian Peninsula communities including Maisonnette, Caraquet, Bas-Caraquet, Pointe-Brûlée, Shippagan, Le Goulet, and Lamèque. Owing to a scarcity of tide gauge records in the vicinity of the Acadian Peninsula, non-conventional methods were explored to support calibration and validation. The community-scale model was calibrated using surveyed high water-level indicators provided by Government of New Brunswick. Model skill was also assessed based on photographic and video evidence of flooding.

Most extreme storm surge events on the Acadian Peninsula occur during the winter season between October and March, with a large proportion occurring between November and February. Most of the events coincide with storm surges driven by extratropical winter storms. However, a small proportion of the events represent storm surges driven by post-tropical cyclones, which tend to occur in the summer and fall seasons. Adopting a risk-based approach, coastal flood hazard was assessed for a range of likelihoods. To support this analysis, synthetic storm surge events were developed, each with a unique annual exceedance probability (AEP) or likelihood. A number of statistical methods were explored to investigate

the likelihood and magnitude of storm surge hazards in the Acadian Peninsula including univariate extreme value analyses of storm surge and water levels, and multivariate methods that incorporate the joint-probability of tides and storm surge. Six synthetic storm surge hazard events were developed based on data available from the Belledune tide gauge to represent storm surge events with prescribed annual exceedance probabilities under present-day sea level conditions. An additional 18 storm surge hazard events were developed, representing the same storm surge events but under three different relative sea-level rise scenarios.

Each of the 24 storm surge- and sea-level rise-driven flood hazard events were modelled at the regional and community-scales. Maps illustrating peak flood depths, flood extents, and flow-induced hazards during each event within each of the seven Acadian Peninsula communities were generated. Where possible, model results were compared with existing flood maps available from existing literature and developed using alternative techniques. Key findings are summarized below:

- Model results indicate that at least some infrastructure in all of the Acadian Peninsula communities studied in detail, except for Caraquet, is exposed to flood hazards during commonly occurring storm surge events (e.g. AEPs of 50% or 20%) under present-day sea level conditions; in Caraquet, infrastructure remains unexposed to hazard for storm surge events with AEPs of 10% or higher.
- Under present-day sea level conditions, flow-induced hazards exceeding criteria for pedestrian safety and structural damage are uncommon within the communities of interest; flow-induced hazards exceeding criteria for pedestrian safety and structural damage are restricted to localized and discrete locations, coinciding with hydraulic constrictions caused by causeway structures.
- Model results indicate that exposure to flood hazard increases with increasing sea-level rise. In all seven Acadian Peninsula communities, storm surge-driven flood hazards for the 10% AEP event under the 0.5m global sea-level rise (GSLR) scenario resembled the 1% AEP event during present-day sea levels. In general (six out of seven communities), flood hazards associated with the 50% AEP storm surge event under the 0.5m GLSR scenario resembled either the 5% AEP or 2% AEP event under present-day sea level conditions.
- In general, flood extents delineated based on hydrodynamic modelling of storm surge hazard events in this study agreed well with bathtub modelling completed in other studies for comparable event likelihoods. Hydrodynamic modelling offered additional information not available from bathtub modelling pertaining to spatial and temporal flood propagation, flow velocities, and flood durations. Some discrepancies were observed between hydrodynamic model results and bathtub model results in the vicinity of fine-resolution features at the coast (e.g. coastal structures). Results suggested that the discrepancy was linked to differences in model resolution. Although bathtub modelling does not provide information on flow dynamics, the modelling approach allows for high resolution of coastal floodplain features and is well-suited to estimate maximum flood extents and flood depths where dynamic interactions with floodplain topography and features are not important.

Results from the hazard assessment will support risk assessments for the seven Acadian Peninsula communities by Natural Resources Canada. The results will be used to identify infrastructure and other assets exposed to, and impacted by, coastal flooding. Future analyses will focus on assessment of damages and community impacts to inform coastal flood hazard mitigation. Regional model results will also be made available to potential users to support future hazard and risk assessment initiatives in the vicinity of the regional model study area.

Table of Contents

List of Figures

List of Tables

Acronyms and Abbreviations

AEP	Annual Exceedance Probability
AR4	Fourth Assessment Report
AR5	Fifth Assessment Report
CD	Chart Datum
CGVD2013	Canadian Geodetic Vertical Datum of 2013
CGVD28	Canadian Geodetic Vertical Datum of 1928
CHS	Canadian Hydrographic Service
CSS	Centre for Security Science
CSSP	Canadian Safety and Security Program
DEM	Digital Elevation Model
DRDC	Defence Research and Development Canada
DRR	Disaster Risk Reduction
GEBCO	General Bathymetric Chart of the Oceans
GPD	Generalized Pareto Distribution
GPS	Global Positioning System
GSLR	Global Sea-Level Rise
HHWLT	Higher High Water Large Tide
HHWMT	Higher High Water Mean Tide
IPCC	Intergovernmental Panel on Climate Change
MSL	Mean Sea Level
MWL	Mean Water Level
NOAA	National Oceanic and Atmospheric Administration
NONNA	Non-Navigational
NRC	National Research Council Canada
NRCan	Natural Resources Canada
OCRE	Ocean, Coastal, and River Engineering Research Centre
POT	Peaks-Over-Threshold
QAA	Qualitative Assessment Area
RCP	Representative Concentration Pathway
RMSE	Root Mean Square Error
UN	United Nations

1 Introduction and Background

1.1 Project Overview

Natural Resources Canada (NRCan) – in partnership with Fisheries and Oceans Canada, National Research Council Canada, Ocean Networks Canada, University of Victoria, Emergency Management British Columbia, and Indigenous Services Canada – is leading the multi-year Coastal Flood Mitigation Canada project, which aims to develop an improved understanding of coastal flood risk to support disaster risk reduction in Canada. The project is funded by Defence Research and Development Canada's Centre for Security Science (DRDC CSS) through the Canadian Safety and Security Program (CSSP). The main objectives of the project are to:

- Bring together researchers, practitioners, and communities to share knowledge and expertise in support of disaster risk reduction strategies for coastal storm surge and tsunami risks;
- Develop and promote data, tools, evidence-based approaches, and guidelines for assessing coastal flood risk; and
- Demonstrate best practice approaches for coastal flood risk assessment and reduction with communities in regions of the Pacific, Arctic, and Atlantic coast.

The project includes three case studies, focused on regions within each of Canada's Atlantic, Arctic, and Pacific coasts, in which the project team has conducted, or is working to complete, a coastal flood hazard and risk assessment. Knowledge gained from each case study will support the development of guidelines summarizing best practices and methods for coastal flood hazard assessment in support of risk-based analyses. These guidelines will help to provide a basis for understanding coastal flood risk in all its dimensions, a priority of the United Nations (UN) Sendai Framework for Disaster Risk Reduction (DRR), which underpins Canada's DRR policy.

This report summarizes work completed by researchers at the Ocean, Coastal, and River Engineering Research Centre (OCRE) of the National Research Council of Canada (NRC) in support of the Atlantic coast case study. NRC-OCRE was tasked with developing regional-scale and community-scale numerical models to assess coastal flood hazard in the Acadian Peninsula region of New Brunswick. The modelling results discussed in this report will be used to support coastal flood risk assessments for communities on the Acadian Peninsula.

1.2 Coastal Flood Hazard and Risk

The Sendai Framework defines hazard as (United Nations, 2004, 2015): "a potentially damaging physical event, phenomenon or human activity that may cause the loss of life or injury, property damage, social and economic disruption or environmental degradation". The flood hazard can be interpreted as the source of danger (e.g. storm surge driven by a large storm event) and the magnitude of the hazard can be described by various parameters including the depth of the flood water and flow velocities.

Flood risk is defined as "the probability of harmful consequences, or expected losses (deaths, injuries, property, livelihoods, economic activity disrupted or environment damaged) resulting from interactions between natural or human-induced hazards and vulnerable conditions" (United Nations, 2004). In the context of coastal flooding, the risk associated with a specific event can be assessed by investigating the probability or likelihood of a coastal flood event (or hazard) occurring and the associated consequences pertaining to human health, the environment, and the economy.

1.3 Scope

This report summarizes the hazard assessment component of the Atlantic Coast case study for the Coastal Flood Mitigation Canada project, and covers:

- Data available to support assessment of storm surge hazards in the Gulf of Saint Lawrence and the Acadian Peninsula
- The development of a regional-scale numerical hydrodynamic model to support simulation and assessment of storm surge in Canada's Atlantic coastal region
- The development of a community-scale numerical hydrodynamic model to support simulation of coastal flooding caused by storm surge in seven Acadian Peninsula communities including Maisonnette, Caraquet, Bas-Caraquet, Pointe-Brûlée, Shippagan, Le Goulet, and Lamèque
- The development of storm surge hazard events, and associated likelihoods, to support risk-based assessment of coastal flooding in the Acadian Peninsula
- Simulations of 24 storm surge events with defined annual exceedance probabilities (50%, 20%, 10%, 5%, 2%, and 1%) under present-day and future sea-level scenarios

2 Establishing Objectives through Community and Partner Engagement

During the week of March 9, 2020, the project team visited the Acadian Peninsula to meet with community representatives and local experts. The objective of the visit was to gain more insight on the interests and concerns of the local communities, learn about coastal flood hazard in the region, gain a better understanding of local contexts and important assets, learn about past and ongoing research, and establish scope and objectives for the forthcoming hazard and risk modelling.

On March 11, 2020, the project team toured some of the Acadian Peninsula communities with representatives and local experts from Government of New Brunswick and Valorēs. On March 12, 2020, a workshop was held at Valorēs' office in Shippagan, New Brunswick with participation from project partners, local experts, academia, private/non-profit groups, and government and community representatives (Figure 1). Valorēs is a not-for-profit applied science research institute, affiliated with the University of Moncton, and is heavily involved in ongoing research in the Acadian Peninsula focused on identification of, and adaptation to, coastal flooding and erosion. The workshop included a brief presentation by the project team summarizing broad objectives and project progress, followed by group discussion to better understand local contexts and community needs pertaining to coastal flooding. A brief summary report was prepared outlining the workshop agenda, key messages and outcomes, and proposed next steps (NRCan, 2020).

Figure 1. Coastal flood workshop hosted by Valorēs in March, 2020 (photograph credit: NRCan)

During the community-tour and workshop activities, it was requested that the project team focus hazard modelling effort on seven communities including Maisonnette, Caraquet, Bas-Caraquet, Pointe-Brûlée, Shippagan, Le Goulet, and Lamèque. Some assessment of coastal flood hazard has already been conducted in many of the communities under the Project Adaptation PA project, coordinated by Valorēs. It was requested that the project team build upon this research by conducting an independent assessment of coastal flood hazard using a numerical hydrodynamic modelling approach to add further insight to current and future coastal flood hazards in the area.

Data sharing opportunities were also identified. Members from Government of New Brunswick and University of Moncton shared data related to topographic elevations, built infrastructure, drainage infrastructure, and high-water level observations that were invaluable for model development and assessment of model skill.

3 Summary of Previous Research

As discussed, Valorēs is heavily involved in past and ongoing research related to coastal flood hazard in the Acadian Peninsula, conducted under the Projet Adaptation Péninsule Acadienne (https://adaptationpa.ca/en/). The project website includes a summary of the research as well as a repository of project reports. Of particular relevance to the work being conducted for the Coastal Flood Mitigation Canada project is the past research (and associated reports) conducted in Le Goulet, Shippagan, Bas-Caraquet, and Maisonnette (Aubé et al., 2016; Robichaud et al., 2011). The reports summarize assessments of coastal flood inundation extents, whereby spatially uniform and static extreme water levels were mapped over high-resolution topography. This modelling approach is commonly referred to as "bathtub modelling" (Anderson et al., 2018). As described by Didier et al. (2019), bathtub modelling is commonly applied to support investigation of flood hazard and development of associated mapping products (e.g. Aucelli et al., 2017; Creach et al., 2016). The inundation maps resulting from the bathtub modelling conducted for the Projet Adaptation Péninsule Acadienne provide an interesting basis for comparison with the coastal flood hazard assessment presented in this report, which were derived from

numerical hydrodynamic modelling. The research conducted through the Project Adaptation PA project also include insight on erosion risks, which are not addressed in this study.

Previous research has also been conducted to estimate current and future extreme storm surge events and water levels along the New Brunswick coast and the Gulf of Saint Lawrence (Bernier, 2005; Daigle, 2017; Environment Canada, 2006). Broadly speaking, these estimates formed the basis for the inundation modelling conducted under the Project Adaptation PA project and provide a basis for comparison with extreme hazard events estimated in this study.

4 Available Data

The following sections describe available data used to support the regional storm surge modelling and local-scale coastal flood hazard assessments.

4.1 Bathymetry

Three sources of bathymetric data were used to support model development including:

- Canadian Hydrographic Service (CHS) best available bathymetric data (Canadian Hydrographic Service, 2020)
- CHS Non-Navigational (NONNA) bathymetric data (Canadian Hydrographic Service, 2019)
- Data from the General Bathymetric Chart of the Oceans (GEBCO) developed by the Seabed 2030 Project (GEBCO Compilation Group, 2019)

Bathymetric data acquired from CHS are referenced to Chart Datum (CD). Bathymetric data from GEBCO (2019) "are generated by assimilation of heterogeneous data types, assuming all of them to be referred to mean sea level" (MSL). In this study, MSL and mean water level (MWL) are considered equivalent. Hydrographic Vertical Separation Surfaces (HyVSEPs) were provided by CHS to support transformation from CD to MWL and/or the Canadian Geodetic Vertical Datum of 2013 (CGVD2013) (Robin et al., 2016). Bathymetric data were transformed to MWL to support regional-scale and community-scale modelling.

4.2 Topography

Several topographic datasets were used to support community-scale model development including:

- A hydro-enforced 1m-resolution digital elevation model (DEM), representative of the year 2018 with coverage in densely-populated areas of the Acadian Peninsula, including all seven communities of interest (provided by Government of New Brunswick)
- A 1m-resolution DEM (not hydro-enforced), representative of the year 2018 with coverage across the entire Acadian Peninsula (Government of New Brunswick, 2019a)
- A 1m-resolution DEM (not hydro-enforced), representative of the year 2009 with coverage in the vicinity of Le Goulet (provided by Government of New Brunswick)
- LiDAR point data, representative of the year 2018 with coverage across the entire Acadian Peninsula (Government of New Brunswick, 2019d)

The 2018 hydro-enforced DEM includes special alteration of elevation data in the vicinity of culverts and drainage features, allowing more-realistic drainage and connectivity between land parcels. In addition to the hydro-enforced DEM, a complementary shapefile indicating culvert locations was provided by the

Government of New Brunswick. The 2018 DEM and LiDAR point data were downloaded from the Government of New Brunswick's online geographic information repository, GeoNB (Government of New Brunswick, 2021).

4.3 Water Levels

Water levels in coastal regions reflect contributions from a variety of distinct components, including mean sea-level (and changing mean sea-level resulting from relative sea-level change), astronomical tides, and meteorological effects. The tidal component of the water level is cyclical and largely predictable, being generated primarily by the gravitational forces associated with the moon and sun; although the water level response at a given location depends on a combination of astronomical forces and shallow water effects. Meteorological phenomena, such as wind and barometric pressure, influence water levels and manifest in the form of wind set-up (or set-down), barometric set-up (or set-down), and wave effects (including wave set-up). The difference between the theoretical (predicted) astronomical tide and the observed water level is referred to as the water level residual (or non-tidal residual). In this study, storm surge was modelled as the combined effects of wind and barometric set-up only.

4.3.1 Tide Gauges and Measured Water Levels

Measured hourly water level data were obtained from tide gauges managed by Fisheries and Oceans Canada (Fisheries and Oceans Canada, 2019a). Two tide gauges with sufficiently long periods of record to support extreme value statistical analyses were identified in the vicinity of the Acadian Peninsula (Figure 2). The Lower Escuminac gauge (Station Number 2000, hereafter referred to as the Escuminac gauge), located approximately 75km south of Shippagan, contains a nearly-continuous record of water level measurements from 1973 to present-day (47 years at the time of analysis). The Belledune gauge (Station Number 2145), located approximately 85km west of Shippagan contains a nearly-continuous record of water level measurements from 1999 to present-day (20 years at the time of analysis). Water levels recorded prior to June 29, 2019 (i.e. the time of analysis) by each gauge are shown in Figure 3.

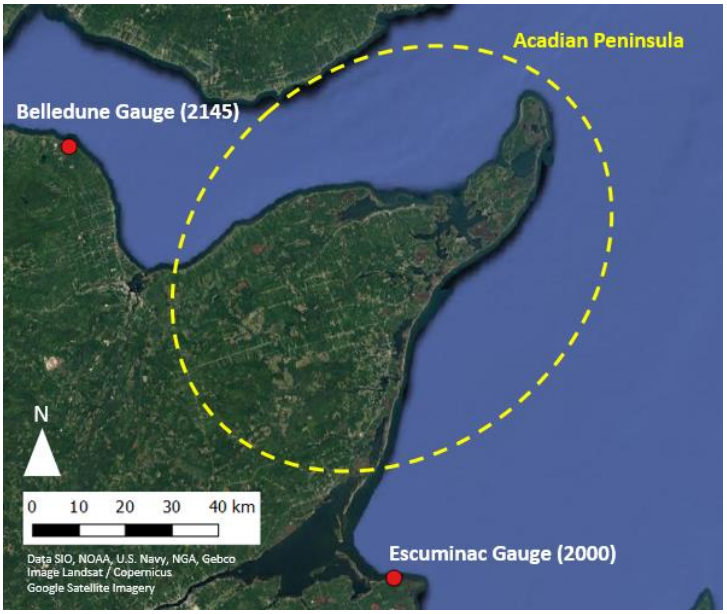

Figure 2. Tide gauges in the vicinity of the Acadian Peninsula

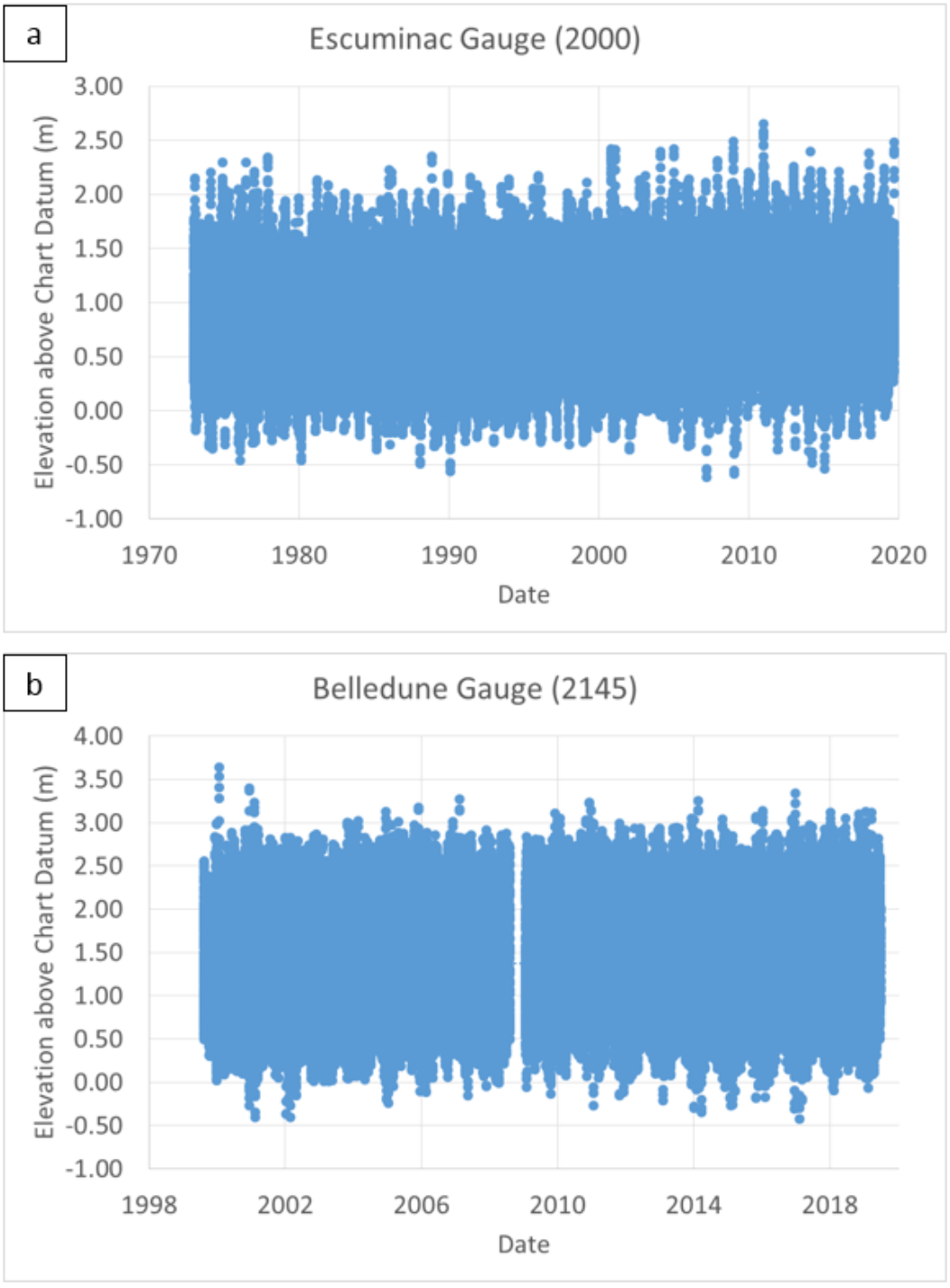

Figure 3. Water level records for the (a) Escuminac gauge and (b) Belledune gauge

4.3.2 Non-Tidal Residuals

Astronomical tide contributions to total water levels were estimated based on tidal constituents for the Escuminac gauge and the Belledune gauge provided by CHS, using the methodology described in Foreman (1977). Residuals were computed as the difference between measured water levels and the theoretical (predicted) astronomical tidal elevation, linearly detrended to remove the effect of relative sea-level rise. This resulted in two sets of residual water levels, one representative of the storm surge observed at the Escuminac gauge, and the other representative of storm surge observed at the Belledune gauge. The 50 largest positive events from the detrended and declustered residuals recorded prior to June 29, 2019[1] are listed in Table 1. It is worth noting that there are some data gaps in the hourly water level records obtained from the tide gauges. Most notably, the Escuminac gauge was not operational during the January 21, 2000 event which is the largest event recorded at the Belledune gauge and is known to be a significant storm surge event in the region (Environment Canada, 2006).

[1] Shortly following the initial assessment of extreme events described in Section 4.3, and the development of the regional model described in Section 6, the post-tropical remnants of Hurricane Dorian passed through the Canadian Atlantic. As described in Section 4.3, the initial water level records used to support analysis truncated at June 28, 2019. To support the hazard event development described in Section 8, the water level records were extended to September 13, 2019 in order to capture the Hurricane Dorian event. For reference, the detrended residual produced by Hurricane Dorian equated to 1.18m and 0.77m at the Escuminac and Belledune tide gauge, respectively. If the Hurricane Dorian event were added to Table 1, it would rank as the 14th and 32nd largest storm surge event on the Escuminac and Belledune gauge, respectively.

Table 1. Largest positive storm surge events observed at proximate tide gauges prior to June 29, 2019

Escuminac Gauge (2000)			Belledune Gauge (2145)		
Event Name	Date	Peak Residual (m)	Event Name	Date	Peak Residual (m)
E1	Dec 22, 2008	1.61	B1	Jan 21, 2000	1.31
E2	Mar 17, 1976	1.58	B2	Jan 5, 2018	1.23
E3	Oct 29, 2000	1.51	B3	Jan 3, 2010	1.17
E4	Jan 3, 2010	1.50	B4	Dec 30, 2016	1.12
E5	Nov 22, 1986	1.49	B5	Feb 14, 2014	1.11
E6	Dec 28, 2010	1.45	B6	Oct 16, 2005	1.05
E7	Jan 4, 1986	1.43	B7	Feb 16, 2015	1.04
E8	Dec 7, 1977	1.31	B8	Nov 14, 2003	0.99
E9	Feb 16, 2015	1.28	B9	Dec 6, 2010	0.96
E10	Dec 4, 2007	1.25	B10	Feb 25, 2012	0.96
E11	Nov 21, 1988	1.21	B11	Oct 29, 2006	0.96
E12	Oct 30, 1998	1.20	B12	Feb 15, 2007	0.95
E13	Feb 18, 2013	1.20	B13	Dec 27, 2010	0.93
E14	Nov 26, 1974	1.17	B14	Feb 18, 2013	0.89
E15	Dec 22, 2010	1.16	B15	Mar 27, 2014	0.88
E16	Dec 27, 2005	1.13	B16	Oct 29, 2000	0.87
E17	Jan 5, 2018	1.09	B17	Jan 10, 2019	0.84
E18	Nov 29, 2018	1.08	B18	Nov 23, 2005	0.84
E19	Jan 14, 2002	1.07	B19	Dec 17, 2007	0.84
E20	Jan 5, 1989	1.06	B20	Jul 5, 2014	0.84
E21	Dec 25, 2017	1.06	B21	Nov 5, 2004	0.83
E22	Mar 17, 1981	1.06	B22	Dec 18, 2003	0.82
E23	Feb 19, 2004	1.05	B23	Mar 9, 2005	0.79
E24	Nov 21, 1974	1.05	B24	Mar 23, 2001	0.79
E25	Oct 5, 2011	1.04	B25	Mar 15, 2017	0.78
E26	Mar 27, 2014	1.03	B26	Jan 11, 2000	0.78
E27	Nov 22, 2008	0.01	B27	Feb 12, 2003	0.78
E28	Feb 14, 2014	1.00	B28	Feb 25, 2019	0.78
E29	Dec 4, 1989	0.99	B29	Feb 12, 2012	0.78
E30	Jan 13, 2016	0.99	B30	Feb 6, 2001	0.78
E31	Sep 12, 2002	0.99	B31	Nov 18, 2002	0.77
E32	Dec 30, 1976	0.98	B32	Jan 13, 2011	0.77
E33	Dec 2, 1995	0.98	B33	Dec 10, 2009	0.77
E34	Jan 12, 1987	0.98	B34	Mar 23, 2019	0.76
E35	Jan 28, 2015	0.98	B35	Dec 2, 2006	0.76
E36	Nov 21, 1989	0.98	B36	Oct 21, 2006	0.75
E37	Mar 7, 1997	0.98	B37	Dec 21, 2010	0.75
E38	Feb 6, 2001	0.97	B38	Feb 20, 2004	0.75
E39	Feb 6, 1974	0.96	B39	Jan 28, 2015	0.75
E40	Nov 3, 2014	0.95	B40	Jan 21, 2019	0.74
E41	Nov 19, 1981	0.95	B41	Mar 10, 2018	0.74
E42	Dec 16, 2016	0.94	B42	Dec 16, 2003	0.74
E43	Nov 12, 1991	0.94	B43	Dec 12, 2000	0.74
E44	Jan 21, 2019	0.94	B44	Feb 2, 2002	0.74
E45	Oct 12, 2004	0.93	B45	Jan 13, 2016	0.74
E46	Jan 13, 2011	0.92	B46	Sep 22, 2010	0.74
E47	Dec 17, 1987	0.92	B47	Feb 13, 2002	0.73
E48	Dec 6, 2010	0.92	B48	Feb 23, 2009	0.71
E49	Feb 9, 2016	0.91	B49	Feb 27, 2011	0.71
E50	Jun 23, 1993	0.90	B50	Dec 27, 2005	0.70

4.3.3 Seasonality of Storm Surge Events

Figure 4 illustrates the seasonality of the 51 largest storm surge events recorded by the Escuminac and Belledune tide gauges (i.e. the events listed in Table 1 plus the Hurricane Dorian event).

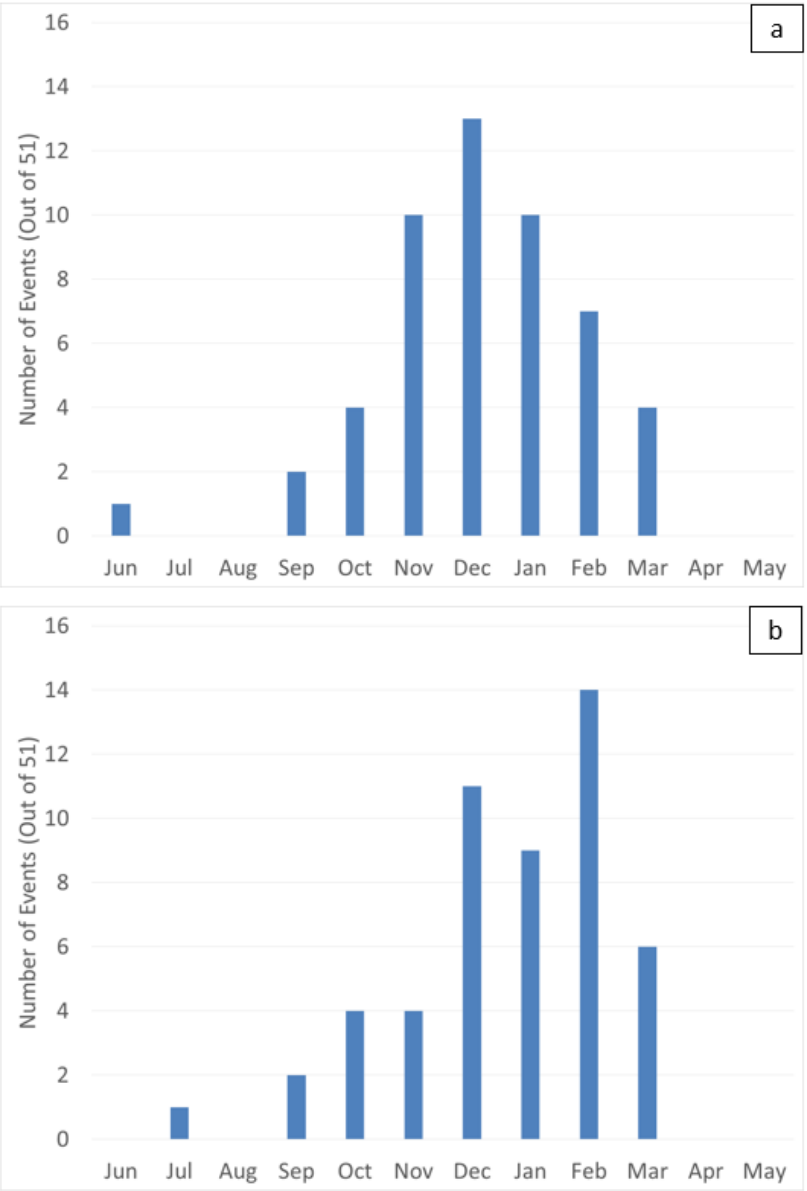

Figure 4. Seasonality of the largest storm surge events recorded by the Escuminac gauge (a) and Belledune gauge (b). Includes the events identified in Table 1 plus the Hurricane Dorian event.

As illustrated, most large storm surge events occurred during the winter season between October and March, with a large proportion occurring between November and February. Most of the events coincided with storm surge driven by extratropical, winter storms. However, a small proportion of the events represent storm surge driven by post-tropical cyclones, which tend to occur in the summer and fall seasons. The National Oceanic and Atmospheric Administration (NOAA) Historical Hurricane Tracks Tool (NOAA, 2021),

was used to determine events that coincide with post-tropical cyclones. Of the 51 largest events recorded by the Escuminac gauge, three events coincided with post-tropical cyclones (two in September and one in October). Of the 51 largest events recorded by the Belledune gauge, four events coincided with post-tropical cyclones (one in July, two in September, and one in October). The findings support Environment Canada's (2006) statement that storm surges in the Gulf of Saint Lawrence are mainly associated with extratropical storm events, but can also be associated with post-tropical cyclones.

4.4 Wind and Atmospheric Pressure

Wind and atmospheric pressure data were used to drive the regional and community-scale storm surge models. The data were obtained from the ERA5 global atmospheric reanalysis dataset (Hersbach et al., 2018). This global data set is produced by the European Centre for Medium-Range Weather Forecasts and contains atmospheric data including atmospheric pressure at mean sea level and wind speeds at an elevation of 10m above the earth surface; the data are provided at a 30km-resolution. At the time of analysis, hourly data were available from 1979 to August 2019.

The ERA5 data was locally validated by comparing the reanalysis to wind and atmospheric pressure measured by two wave buoys (Figure 5); one wave buoy was located in the Gulf of St. Lawrence (wave buoy c44153) and the other was located in the Atlantic Ocean (wave buoy c44139) (Fisheries and Oceans Canada, 2019b). Two metrics were used to assess the quality of the ERA5 data:

- Root mean square error, $RMSE$ – a value that quantifies the differences between the reanalysis and measured data, with smaller values indicating better overall agreement
- Correlation coefficient, *R* – a value between 0 and 1, with higher values indicating a closer correlation between the reanalysis and measured data

The $RMSE$ is calculated by:

$$RMSE = \sqrt{\frac{\sum_i^N (x_{m,i} - x_{o,i})^2}{N}} \quad (1)$$

where $x_{m,i}$ is the reanalysis data, $x_{o,i}$ is the measured data and i = 1 to N are the number of data points being compared.

The correlation coefficient, *R*, is calculated by:

$$R = \frac{\sum_i^N (x_{m,i} - \overline{x_m})(x_{o,i} - \overline{x_o})}{\sqrt{\sum_i^N (x_{m,i} - \overline{x_m})^2 \sum_i^N (x_{o,i} - \overline{x_o})^2}} \quad (2)$$

where $\overline{x_m}$ is the mean of the modelled data, $\overline{x_o}$ is the mean of the measured data, and the remaining variables conform to those shown in equation (1).

Measured data from wave buoy c44139 were compared to data from the ERA5 reanalysis at an approximately collocated grid point for Event E1 (as defined in Table 1). The root mean square error and correlation coefficient were calculated for both atmospheric pressure and wind speeds. The $RMSE$ for the atmospheric pressure was 1.9 kPa with a correlation coefficient of 0.983. The $RMSE$ for the wind speed was 1.31 m/s with a correlation coefficient of 0.953. Based on the calculated statistics, as well as visual comparison of the plotted data (Figure 6), the ERA5 reanalysis data are reasonably consistent with measured storm wind speeds and atmospheric pressure for Event E1 at wave buoy c44139.

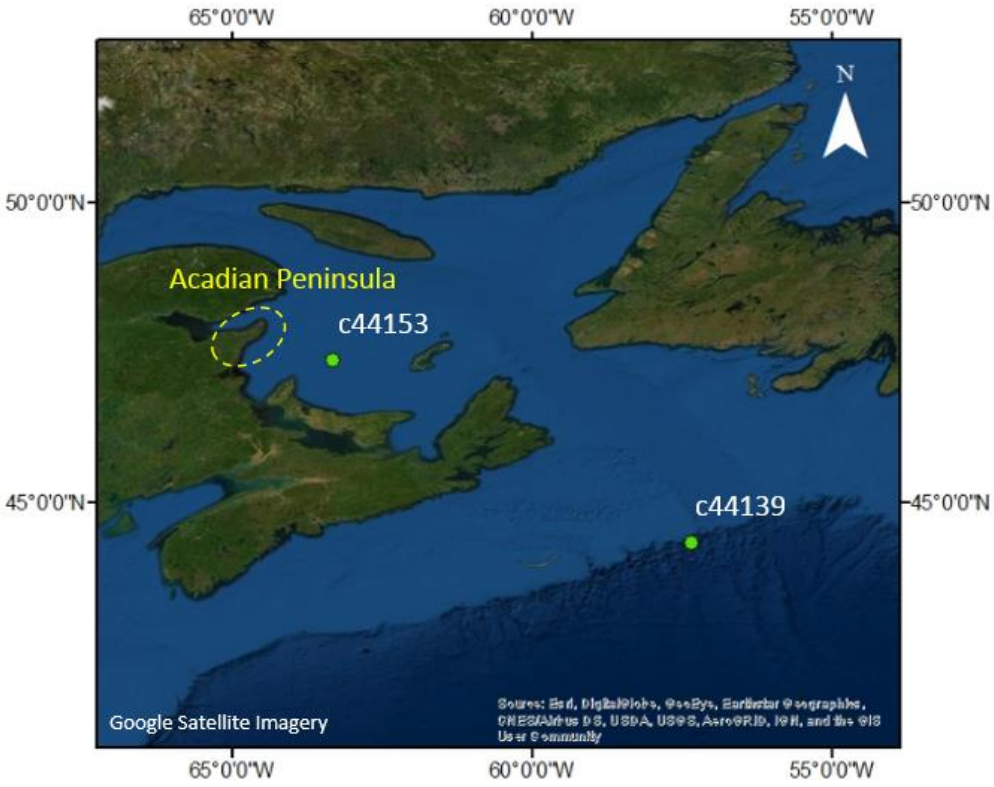

Figure 5. Wave buoy locations.

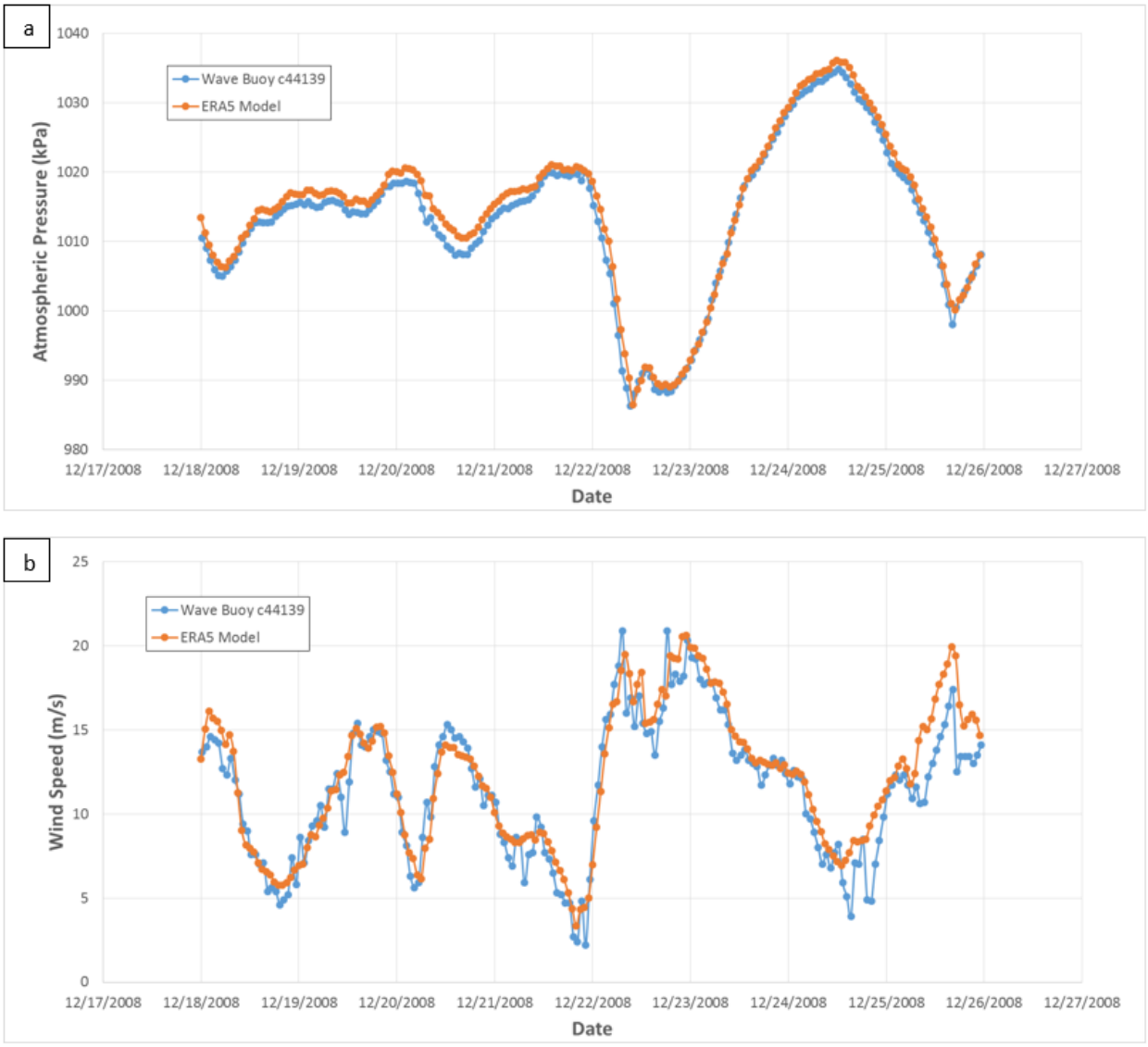

Figure 6. ERA5 model compared against measured atmospheric pressure (a) and wind speed (b) at buoy c44139 (located in the Atlantic Ocean) for Event E1.

Limited measured data were available at wave buoy c44153 (within the Gulf of St. Lawrence). Measured data from the wave buoy were compared to reanalysis data from the ERA5 dataset for Event E33. The $RMSE$ and correlation coefficient were calculated for both the atmospheric pressure and wind speeds for Event E33. The $RMSE$ for the atmospheric pressure was 1.4 kPa with a correlation coefficient of 0.987. The $RMSE$ for the wind speed was 1.03 m/s with a correlation coefficient of 0.969. Based on the calculated statistics, as well as visual comparison of the plotted data (Figure 7), it was concluded that the ERA5 model data are reasonably consistent with measured wind speeds and atmospheric pressure for Event E33 at wave buoy c44153.

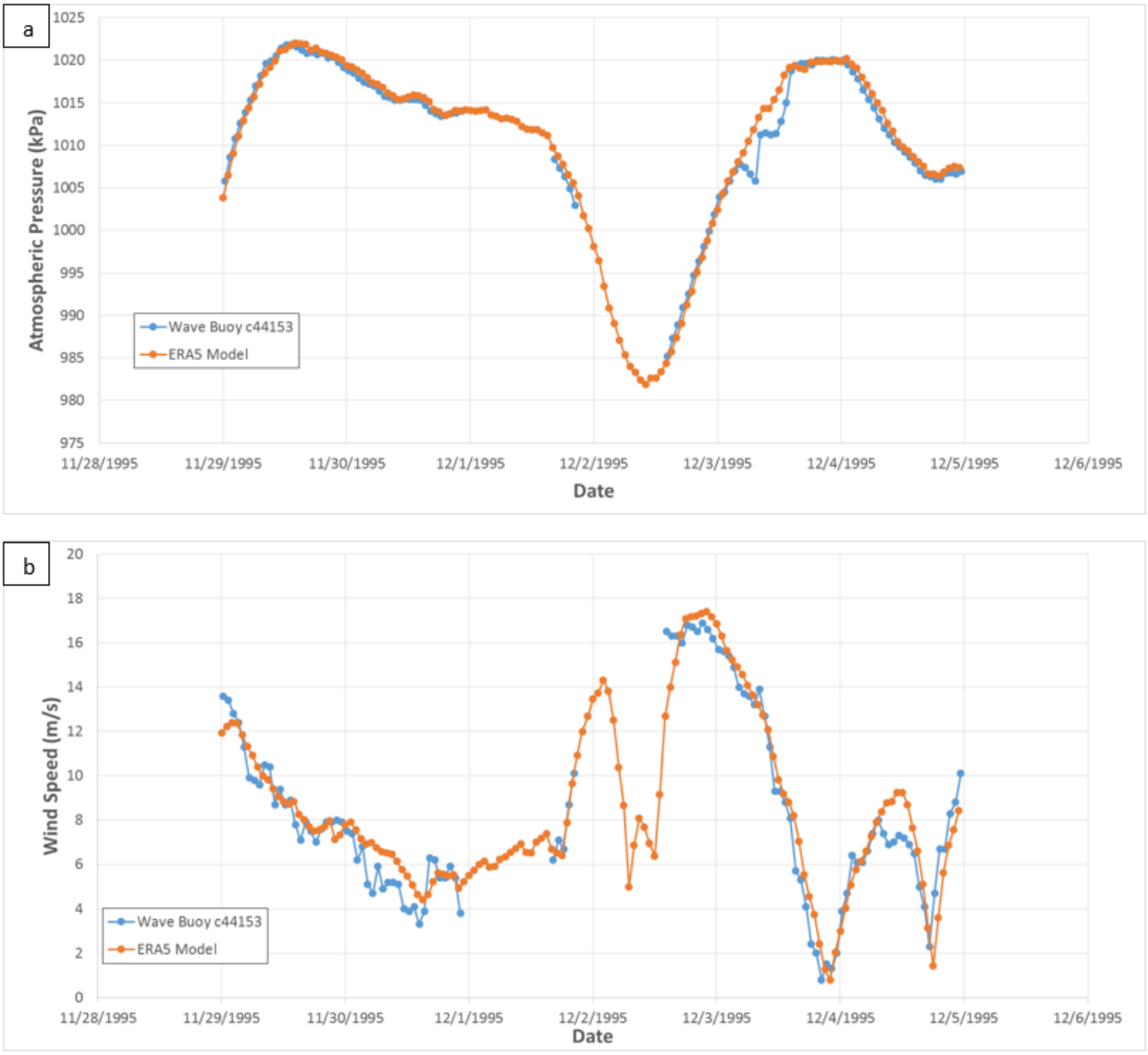

Figure 7. ERA5 renalysis comparison to (a) measured atmospheric pressure and (b) measured wind speed at buoy c44153 (located in the Gulf of St. Lawrence) for Event E33. Note the data gaps in the wave buoy record, indicated by the absence of blue data points.

4.5 Sea Ice Data

Historical weekly ice concentration charts were available online from the Canadian Ice Service Ice Archive (Canadian Ice Service, 2019). Potential impacts of sea ice on storm surge are discussed in Section 6.4.1, where an example of an ice concentration chart coinciding with Event E26 (B15) is shown in Figure 18.

4.6 Land Cover

Land cover data were available from GeoNB. Georeferenced polygons (shapefiles) depicting forested land, non-forested land, and wetlands were downloaded from the online data repository (Government of New Brunswick, 2019e, 2019b, 2019c). The polygon shapefile depicting non-forested land contained attribute data providing further detail regarding the type of non-forested land cover present in specific polygons. Non-forested lands were subcategorized as either: no vegetation; grasses, crops, or other; shrubs; or trees. An example of land cover data near Le Goulet is shown in Figure 8.

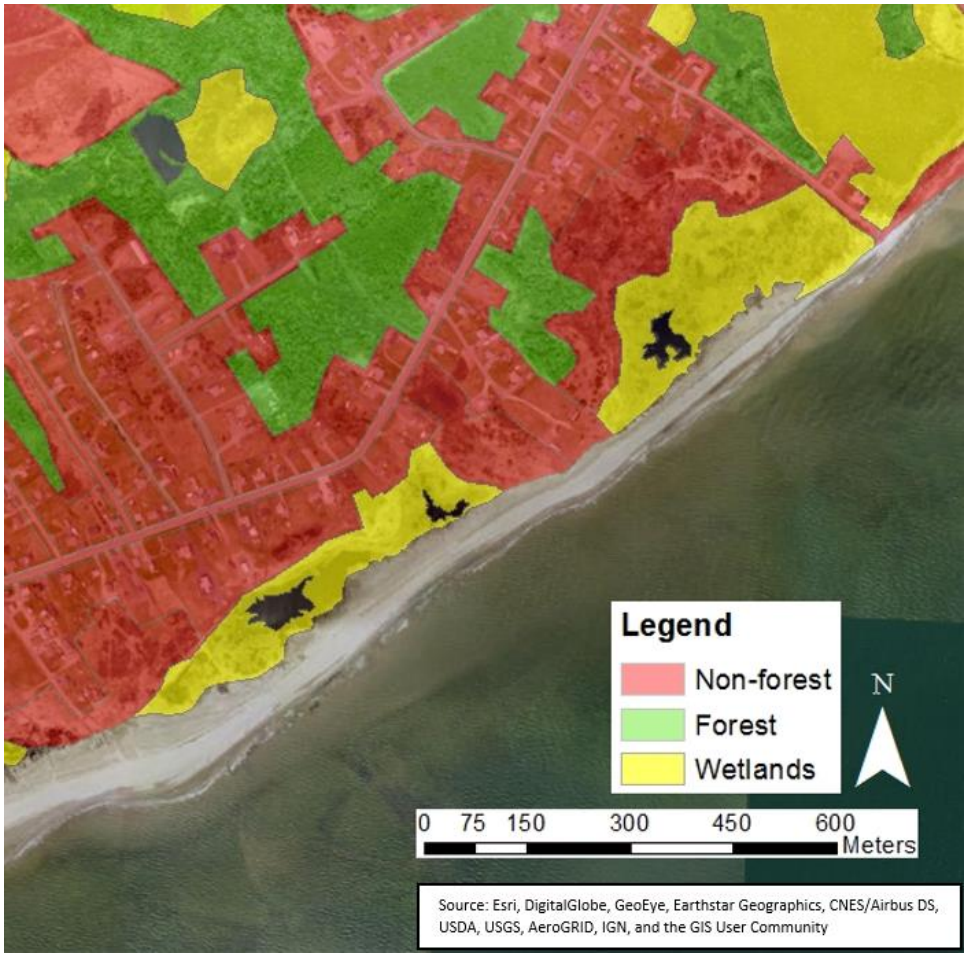

Figure 8. Land cover data near Le Goulet.

4.7 Buildings and Infrastructure

Georeferenced polygons (shapefiles) depicting building and infrastructure footprints were acquired from the Government of New Brunswick. Building and infrastructure footprints were available for all seven communities included in the community-scale modelling. An example of the building and infrastructure footprint data near Maisonnette is shown in Figure 9.

Figure 9. Building and infrastructure footprints near Maisonnette.

4.8 Relative Sea-Level Rise

Georeferenced, gridded surfaces depicting relative sea-level rise projections in the study area were provided by Thomas James of the Geological Survey of Canada. The data reflect projected changes in sea level that occur relative to the solid surface of the Earth, including both changes in sea level as well as land uplift and subsidence (James et al., 2021). The gridded data were provided with a spatial (horizontal) resolution of 0.1°. To support assessment of future storm surge hazards in the Acadian Peninsula, three projections for relative sea-level change were provided corresponding to 0.5m, 1.0m, and 2m of global sea-level rise (GSLR). The three sea-level rise scenarios conform to the following narratives, based on the Fifth Assessment Report (AR5) of the Intergovernmental Panel on Climate Change (IPCC) (Church et al., 2013):

- A global sea-level rise of 0.5m approximately represents a median projection at 2080, assuming the high-emissions scenario Representative Concentration Pathway 8.5 (RCP8.5)
- A global sea-level rise of 1.0m approximately represents the upper 95% percentile projection at 2100, assuming high-emissions scenario RCP8.5
- A global sea-level rise of 2m represents a low probability, high end scenario for the year 2100, or, alternatively, sea-level rise at some time beyond 2100, depending on the climate scenario

The three global sea-level rise scenarios listed above correspond to local sea-level rise values of approximately 0.56m, 1.16m, and 2.37m near the community of Shippagan.

4.9 High Water Level Surveys

High water level indicators that were surveyed following two major storm surge events that occurred on December 6, 2010 and December 21, 2010 (Events E48 (B9) and E15 (B37), respectively). The surveys were conducted by representatives from the Government of New Brunswick, Dominique Bérubé and Marc Desrosiers, using high precision Global Positioning System (GPS) technology (Robichaud et al., 2011). The surveys were conducted on: December 9, 2010 in the vicinity of Le Goulet and Shippagan; June 23, 2011 in the vicinity of Pointe-Brûlée; and June 28, 2011 in the vicinity of Bas-Caraquet. The survey data consist of point measurements indicating horizontal position (X and Y coordinates) and elevation georeferenced to the Canadian Geodetic Vertical Datum of 1928 (CGVD28).

The survey data collected on December 9, 2010 reflect high water levels produced during the December 6, 2010 event. Based on personal communication with Dominique Bérubé, the survey data collected in June 2011 are believed to represent high water levels produced by the December 6, 2010 event, but it is possible that they could actually reflect high water levels associated with the December 21, 2010 event, which produced similar amounts of flooding in the Acadian Peninsula.

Most of the survey data were based on observations of debris (sea-wrack) deposited onshore by the flood water (Figure 10a). The June 28, 2011 survey in Bas-Caraquet reflects observations of gravel deposits forced onshore by the flood water. Some of the December 9, 2010 survey points indicate direct observation of water levels observed during the peak of the flood event, marked with survey flags at the time of observation (Figure 10b). Dominique Bérubé cautioned that, in addition to storm surge and tidal stage, surveyed debris could reflect contributions from wave runup and inundation resulting from wave overtopping or breaching of dunes and barrier islands, which was not accounted for in the modelling described in this report. It is suspected that the contribution of wave runup to total water levels may have been relatively high compared to the tide and storm surge-driven components in Bas-Caraquet, which is exposed to Chaleur Bay, and where observed flood waters did not extend far inland.

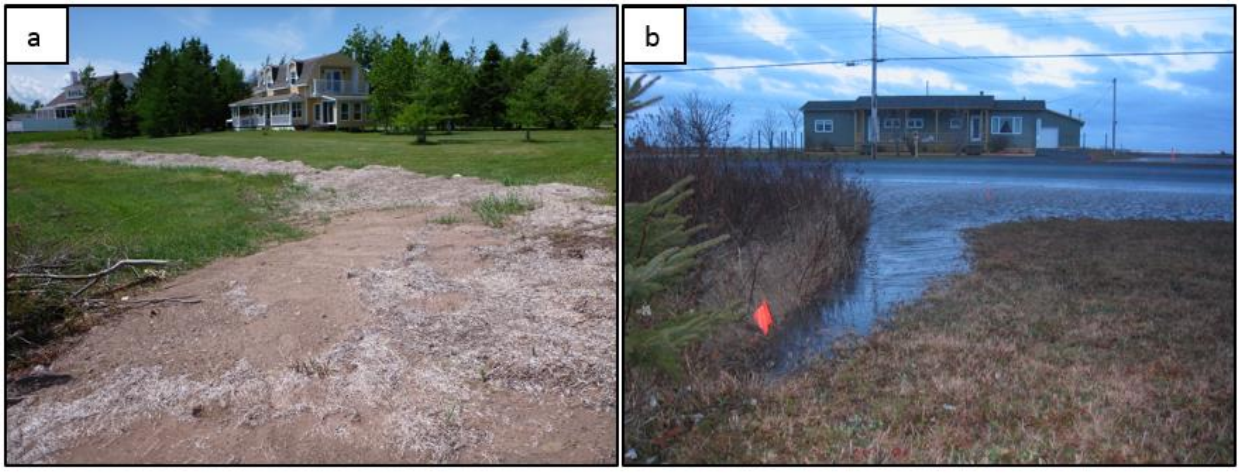

Figure 10. Examples of high water level indicators in (a) Pointe-Brûlée and (b) Le Goulet. Figure (a) shows sea-wrack debris deposited onshore by the flood water, and (b) shows orange flags placed by Dominique Bérubé and Marc Desrosiers, reflecting high water levels observed during the peak of the December 6, 2010 event. Photos provided by Dominique Bérubé and Marc Desrosiers.

4.10 Photographic and Video Evidence of Flooding

Photographic and video evidence of the December 6, 2010 and December 21, 2010 events (i.e. Events E48 (B9) and E15 (B37), respectively) were provided to the research team. Photographic evidence was provided by: Dominique Bérubé (Government of New Brunswick), Marc Desrosiers (Government of New Brunswick), and Dr. André Robichaud (University of Moncton). Video evidence of flooding caused by the December 21, 2010 event was found on YouTube (Doucet, 2010). Dr. André Robichaud provided insight on the locations shown in the YouTube video, and communicated with the owner of the video (Maxime Doucet) to confirm the locations of the footage.

5 Overview of Modelling Approach

Storm surges generated by synoptic-scale meteorological events (such as extratropical storms or post-tropical cyclones) on the Atlantic Canada coast are modified, and in some cases amplified, by interactions with coastal bathymetry and features such as islands, inlets and bays with spatial scales of up to hundreds of kilometres. However, storm surge-driven coastal flood hazards and inundation extents can be influenced by floodplain features (e.g. culverts, road embankments) characterized by spatial scales on the order of metres. Multi-scale (nested) modelling, or dynamical downscaling, approaches are often required to resolve important coastal flood-generating processes at these distinctly different spatial (and temporal) scales (e.g. Barnard et al., 2014) with reasonable computational effort. In this study, modelling was conducted using a multi-scale (or nested-modelling) approach, including development of a regional storm surge model and a community-scale storm surge model.

The regional storm surge model covered much of Canada's Atlantic coast and continental shelf, with a domain large enough to capture storm surges generated by the passage of synoptic-scale meteorological systems. The community-scale flood hazard model, focused specifically on the Acadian Peninsula, was nested (offline, de-coupled) within the regional model and had sufficient spatial resolution and detail to simulate overland propagation of flood water and inundation. The regional model was used to simulate storm surge events in Atlantic Canada coastal regions, and the results from the regional simulation were applied at the offshore boundary of the community-scale model to drive high resolution simulations of storm surge-, tide-, and sea-level rise-driven coastal hazards in the seven Acadian Peninsula communities of interest.

The regional storm surge and community inundation modelling undertaken in this study were both implemented using TELEMAC-2D. TELEMAC-2D solves the two-dimensional (depth-averaged) Saint-Venant equations that describe shallow water hydrodynamics; computations are performed on an unstructured computational mesh using finite-element or finite-volume methods (Ata, 2018). TELEMAC-2D incorporates many of the processes relevant to modelling storm surges in coastal waters including bed friction, Coriolis forces, building drag, turbulence, and forcing by spatially and temporally varying winds and atmospheric pressure.

6 Regional East Coast Storm Surge Model Development

6.1 Model Setup

The computational domain of the regional model, shown in Figure 11, encompasses a large portion of the Canadian Atlantic coast. The model domain covers an area from Portland, Maine at the southern extent to Sandwich Bay, Labrador at the northern extent. The open sea boundary of the model was established offshore of the continental shelf, in water depths exceeding 4000m, to minimize artificial boundary condition influences on simulated storm surges in coastal areas of interest. The model mesh was generated using Blue Kenue software (Barton, 2019; Canadian Hydraulics Centre, 2011). The mesh consists of approximately 476,000 computational nodes with a 200m resolution around the Acadian Peninsula (area of the community-scale model), a ~1700m resolution within the Gulf of St. Lawrence, and a 30km resolution at the offshore boundary. The CHS-NONNA and GEBCO bathymetry data described in Section 4.1 were interpolated to the mesh to create the model bathymetry.

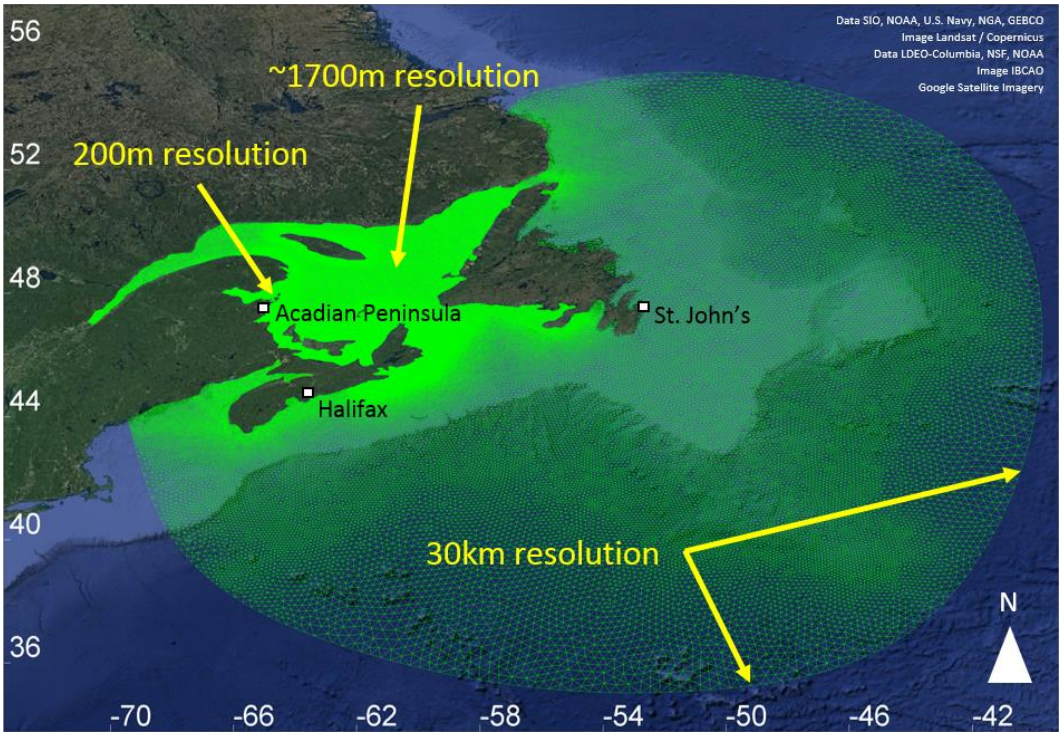

Figure 11. Computational mesh for the regional storm surge model.

6.2 Model Boundary Conditions

The regional storm surge model was forced using the ERA5 wind and atmospheric pressure data described in Section 4.3.3. The wind and atmospheric pressure fields were interpolated to the model mesh nodes for time periods surrounding 44 of the 50 largest positive storm surge events identified from the Escuminac gauge record. Six of the top 50 recorded storm surge events occurred prior to 1979, pre-dating the available ERA5 wind and atmospheric pressure data at the time of analysis, and thus were not simulated. A closed

boundary condition was prescribed at the shoreline and offshore boundaries of the model, meaning that model hydrodynamics were forced only by the wind and atmospheric pressure data (i.e. no depth or flow forcing was applied at the model boundary). This boundary condition design was deemed acceptable for the regional storm surge model as there was sufficient distance between the offshore model boundaries and the key areas of interest (within the Gulf of St. Lawrence) for the storm surge to develop within the model domain. In addition, storm surge is a shallow water phenomenon, so the offshore model boundary was intentionally placed in the deep waters off the continental shelf (water depths >4000m) where minimal storm surge is expected.

Two special cases were run with tidal forcing at the offshore boundary for Events E15 (B37) and E48 (B9) to support community-scale model calibration and validation, described in detail in Sections 7.3 and 7.4.In cases where astronomical tidal forcing was required to support community-scale model calibration and validation, the regional model was forced using the global TPXO database and its regional and local variants from the Oregon State University (Egbert & Erofeeva, 2002). The TELEMAC modelling software contains features to support integration of the TPXO database with hydrodynamic simulation (Ata, 2018).

6.3 Model Calibration

A model sensitivity and calibration exercise was conducted to ensure that the regional model can be used to simulate storm surge with reasonable accuracy. The regional storm surge model was calibrated by adjusting wind drag formulation/coefficients and bed friction coefficients and comparing simulated storm surges to residuals obtained from the analysis of measured water levels.

There are various wind drag formulations/coefficients that can be used to characterize the transfer of wind momentum to the sea surface in hydrodynamic models. Using Event E4 (B3) as a basis for investigation, two wind drag formulations with drag coefficients varying as a function of wind speed were tested: Wu (1980, 1982) and Flather (1976). Event E4 (B3) occurred during ice-free conditions. A constant wind drag coefficient (TELEMAC-2D default setting) was also investigated. The simulated storm surges during Event E4 (B3) at the Escuminac gauge resulting from the different wind drag formulations/coefficients were compared to one another. The model predicted a wide range of storm surge values, varying with different wind drag formulations. Modelled peak storm surge ranged from 1.9m (using Flather (1976)) to 1.2m (using Wu (1980, 1982)). The Flather wind drag formulation resulted in over-prediction of the peak storm surge but captured the temporal evolution and duration of the storm surge event reasonably well. The other two wind drag parameterizations under-predicted both the peak of the storm surge and the duration of the storm surge event. The Flather wind drag equation was used throughout the model calibration exercise and all of the model simulations.

The Flather wind drag formulation includes a wind drag coefficient that varies as a function of wind speed. The wind drag parameterization in the model was calibrated by adjusting drag coefficients within the three wind speed threshold ranges captured by Flather, and comparing the simulated storm surges to measured water level residuals. Model predictions of peak storm surges were quite sensitive to adjustments in the drag coefficient, resulting in a discrepancy of approximately 0.4m between the highest and lowest predicted surge.

Again, using Event E4 (B3) as a basis for investigation, the impact of model to bottom roughness on simulated results was investigated. Five different roughness configurations were applied, with Strickler roughness coefficient (S) varying in the range of S=10 to S=40m$^{1/3}$/s. The simulated peak storm surge for Event E4 (B3) changed by less than 0.08m (4.8%) across the range of roughness configurations investigated and therefore the model was deemed insensitive to roughness.

During the model calibration, roughness and wind drag were iteratively adjusted and the model output was compared to the measured water level residuals at the Escuminac and Belledune gauges for two selected storm events: Event E4 (B3) and Event E23 (B38). During Event E23 (B38) sea ice was present close to the New Brunswick shore; however, a portion of the Gulf of Saint Lawrence west of the island of Newfoundland was ice free. In the final calibrated model, a Flather wind drag formulation was applied with wind drag coefficient (a_{wind}) varying within the range 0.565x10^{-3} and 4.394x10^{-}3 (Ata, 2018), and a spatially uniform bed roughness of S=40m$^{1/3}$/s was applied throughout the domain except for the ocean floor between the island of Newfoundland and the mainland, where a bed roughness of S=10m$^{1/3}$/s was applied.

The storm surges simulated using the calibrated model for Event E4 (B3) and Event E23 (B38) are plotted against the measured storm surge data from the Escuminac tide gauge in Figure 12 and Figure 13, respectively. The maximum modelled storm surge matches the measured data quite well for both calibrated events, with an over-prediction of the peak surge of approximately 2% (Event E4 (B3)) and 4% (Event E23 (B38)). While there are discrepancies between the modelled and measured storm surges both leading up and following the peak surge, the model was able to capture the general trend of the storm surge for both events.

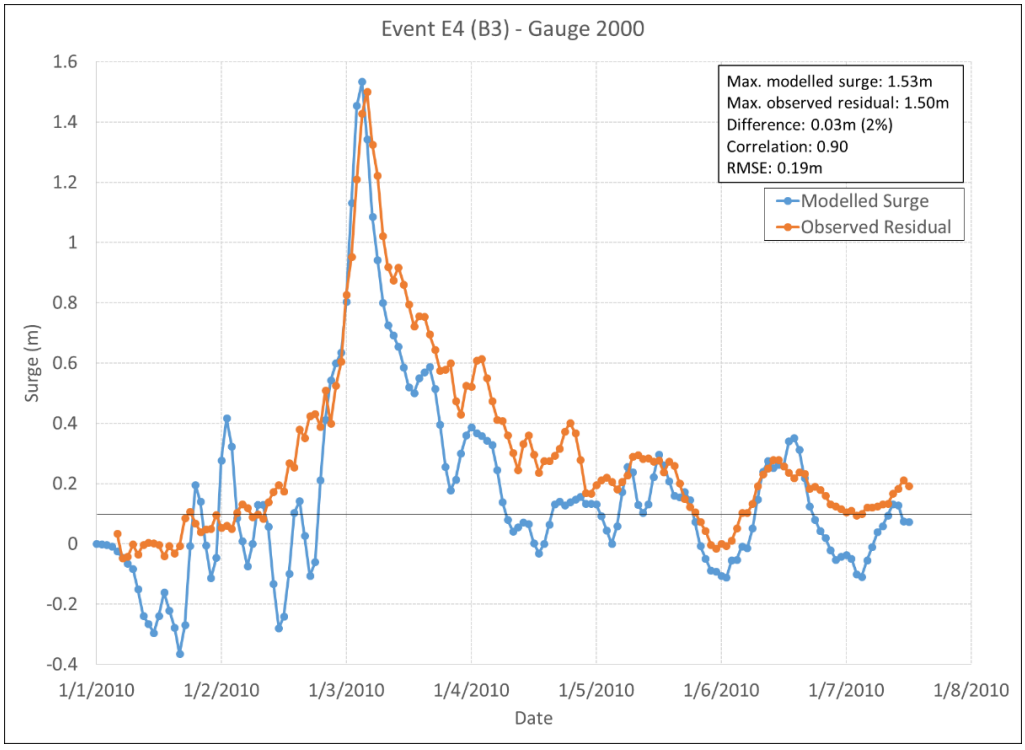

Figure 12. Final calibration results for Event E4 (B3) at the Escuminac gauge.

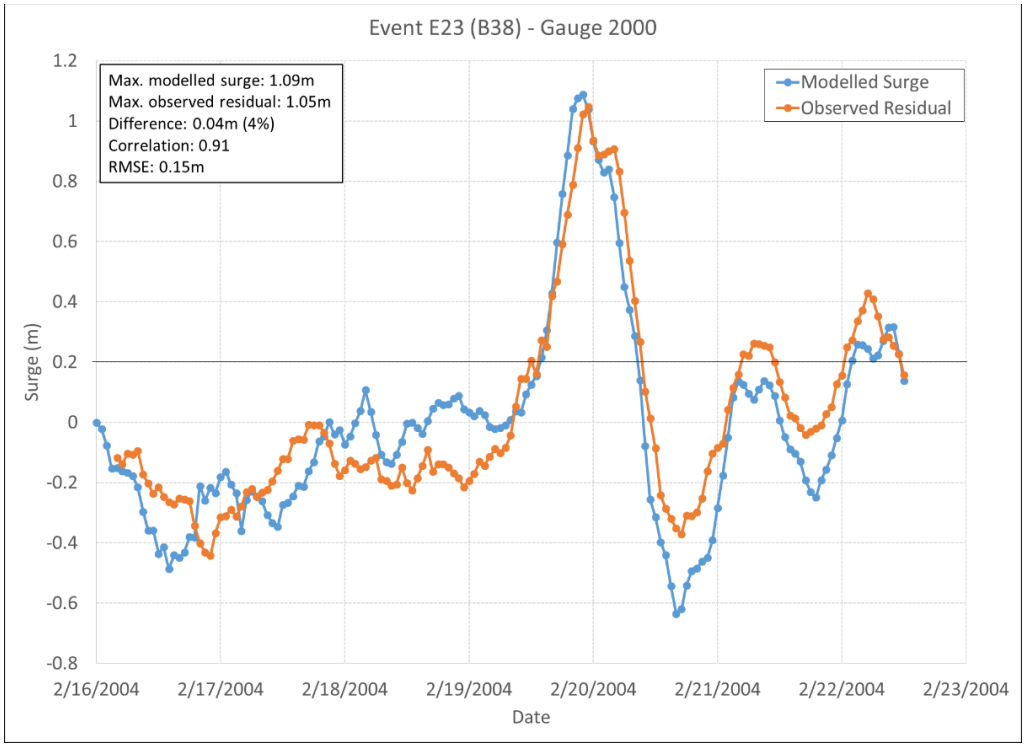

Figure 13. Final calibration results for Event E23 (B38) at the Escuminac gauge.

Comparisons between the modelled and measured surge at the Belledune gauge are presented in Figure 14 and Figure 15 for Event E4 (B3) and Event E23 (B38), respectively. Similar to the model results at the Escuminac gauge, the model was able to reproduce the maximum storm surge with reasonable accuracy; an under-prediction of 4% for Event E4 (B3) and an under-prediction of 11% for Event E23 (B38) was observed. The discrepancies between the modelled and measured surge both before and after the peak storm surge are also seen at the Belledune gauge. Despite these discrepancies, the calibration results were deemed satisfactory as the model is able to simulate both the magnitude and duration of the maximum storm surge, which are the primary factors contributing to storm surge-driven flood hazards.

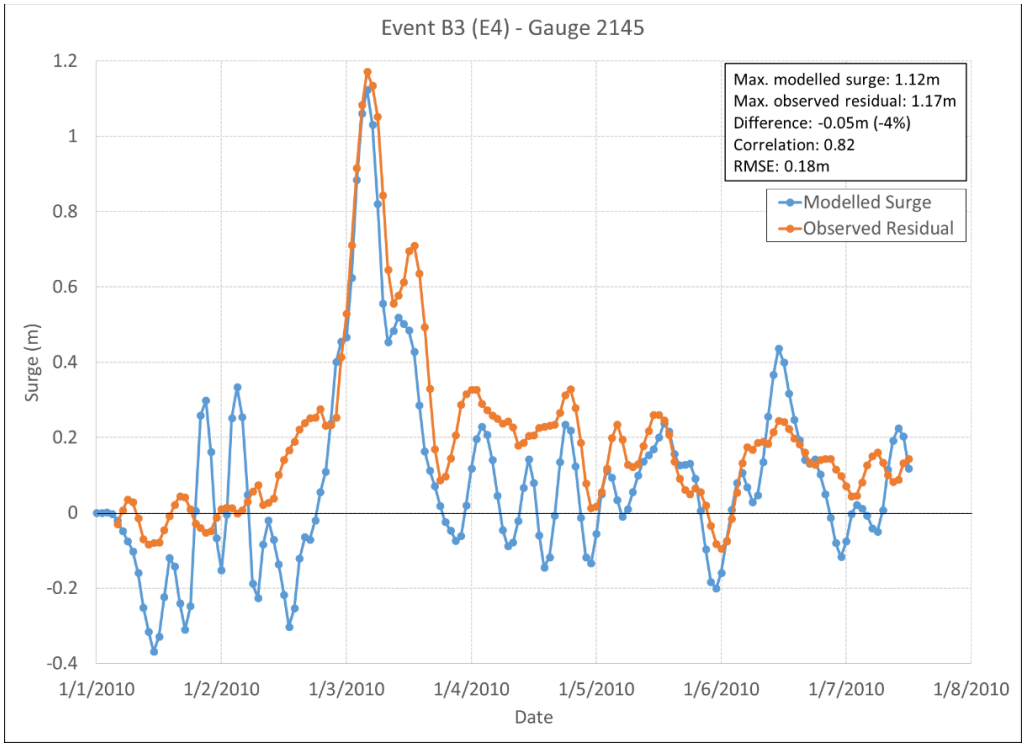

Figure 14. Final calibration results for Event B3 (E4) at the Belledune gauge.

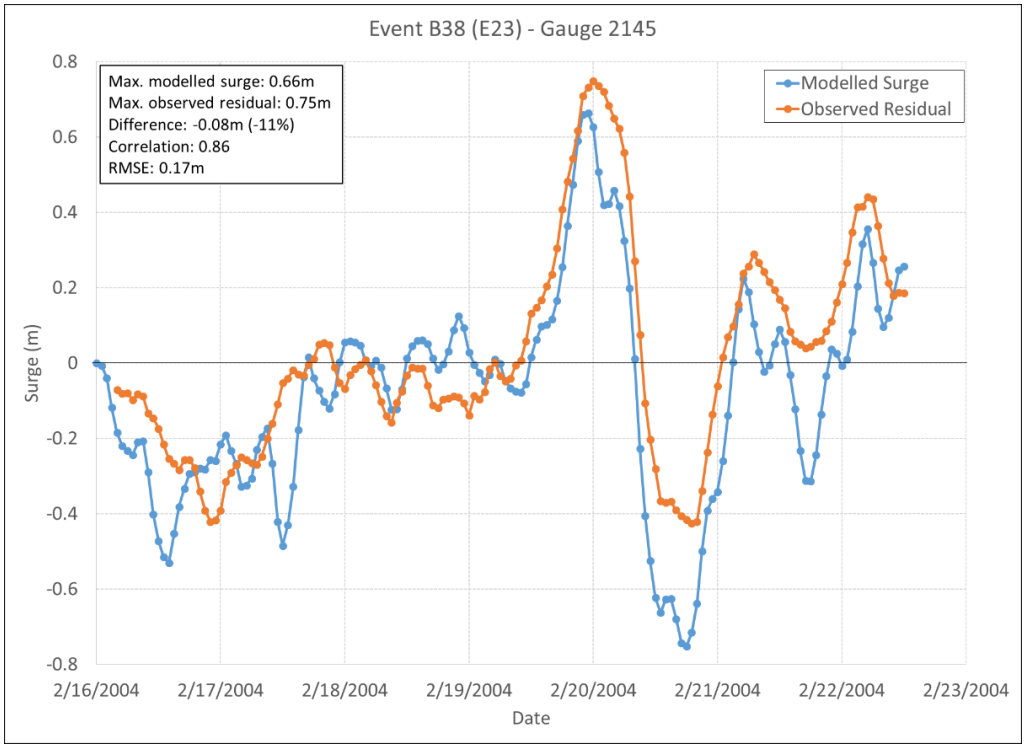

Figure 15. Final calibration results for Event B38 (E23) at the Belledune gauge.

6.4 Model Validation

Following calibration, the regional storm surge model was used to simulate 44 of the 50 largest positive storm surge events identified from the Escuminac gauge record. Six of the top 50 recorded storm surge events occurred prior to 1979, pre-dating the available ERA5 wind and atmospheric pressure data at the time of analysis, and thus were not simulated. Modelled peak storm surge values were compared against observed peak water level residuals to validate model performance. Atmospheric pressure and wind data from the ERA5 reanalysis were used to force the model. Each simulation spanned a 7 day period (including approximately 3 days before and after the occurrence of the peak storm surge) and took approximately 1.5 hours of computation time using 10 processors.

The modelled peak storm surge values for each event are summarized in Table 2. For comparison, Table 2 also includes the observed peak residual (assumed representative of storm surge) along with the difference between the predicted and observed values, the $RMSE$ (calculated using Equation 1), and the correlation coefficient (calculated using Equation 2). Differences between modelled peak storm surges and observed peak residuals exceeding ±15% are highlighted in yellow (model under-prediction) and blue (model over-prediction). The calibrated model was able to predict the peak storm surge to within 15% of the measured peak surge for more than half of the events. However, there was considerable variability in the model's skill in capturing peak storm surges for the remaining events, resulting in an R^2 (coefficient of determination) value of 0.403 when peak modelled storm surges for all 44 events were plotted against measured peak residuals (Figure 17). Of the 44 events presented in Table 2, 20 were either under-predicted (highlighted in yellow) or over-predicted (highlighted in blue) by 15%.

Table 2. Modelled peak storm surge compared to measured peak storm surge for 44 of the largest 50 events. Yellow highlight indicates >15% under-prediction of surge, blue highlight indicates >15% over-prediction of surge.

Event	Modelled Maximum Surge (m)	Measured Maximum Surge (m)	% Difference	RMSE (m)	Correlation Coeff.
Event_E1	1.31	1.61	-19	0.14	0.94
Event_E3	1.33	1.51	-12	0.14	0.95
Event_E4	1.53	1.50	2	0.19	0.90
Event_E5	1.32	1.49	-12	0.16	0.90
Event_E6	1.13	1.45	-22	0.33	0.86
Event_E7	1.28	1.43	-10	0.14	0.94
Event_E9	1.55	1.28	21	0.18	0.94
Event_E10	1.08	1.25	-14	0.19	0.87
Event_E11	0.91	1.21	-24	0.24	0.90
Event_E12	1.13	1.20	-6	0.14	0.94
Event_E13	1.38	1.20	15	0.10	0.97
Event_E15	0.95	1.16	-18	0.29	0.84
Event_E16	1.07	1.13	-6	0.11	0.96
Event_E17	1.30	1.09	20	0.12	0.95
Event_E18	0.74	1.08	-31	0.20	0.88
Event_E19	1.16	1.07	9	0.14	0.96
Event_E20	0.77	1.06	-28	0.25	0.25
Event_E21	0.77	1.06	-27	0.15	0.93
Event_E22	0.97	1.06	-8	0.18	0.92
Event_E23	1.09	1.05	4	0.15	0.91
Event_E25	1.03	1.05	-1	0.16	0.88
Event_E26	1.35	1.03	31	0.18	0.94
Event_E27	1.09	1.03	6	0.14	0.92
Event_E28	1.01	1.01	0	0.16	0.94
Event_E29	1.11	1.00	11	0.19	0.88
Event_E30	0.95	0.99	-4	0.13	0.92
Event_E31	0.92	0.99	-8	0.17	0.87
Event_E33	0.71	0.98	-28	0.15	0.84
Event_E34	1.02	0.98	4	0.16	0.87
Event_E35	0.90	0.98	-9	0.15	0.93
Event_E36	0.69	0.98	-29	0.25	0.83
Event_E37	1.29	0.98	32	0.19	0.93
Event_E38	1.19	0.97	22	0.25	0.83
Event_E40	0.99	0.95	4	0.19	0.93
Event_E41	0.69	0.95	-27	0.12	0.94
Event_E42	0.76	0.94	-20	0.12	0.91
Event_E43	0.91	0.94	-3	0.10	0.96
Event_E44	0.91	0.94	-3	0.15	0.89
Event_E45	0.92	0.93	-2	0.10	0.94
Event_E46	0.93	0.92	0	0.21	0.81
Event_E47	0.62	0.92	-33	0.23	0.86
Event_E48	1.08	0.92	18	0.09	0.92
Event_E49	0.84	0.91	-8	0.16	0.91
Event_E50	0.72	0.90	-21	0.09	0.93

6.4.1 Influence of Waves and Sea Ice

Possible reasons underlying the low regional model skill in predicting peak water level residuals for some events were investigated. It was discerned that the model tended to under-predict peak water level residuals for events coinciding with sustained, strong winds from the east or north-east, where significant wave setup might be expected on the Acadian Peninsula considering open water fetch lengths. By contrast, the model tended to over-predict the peak water level residuals when storms coincided with significant sea ice cover in the Gulf of Saint Lawrence. An investigation of the potential contributions from wave set-up to water levels on the Acadian Peninsula and attenuation of storm surges by sea ice in the Gulf of Saint Lawrence is described by Provan et al. (2022) and summarized here.

Analysis of the ERA5 wind data used to drive the storm surge model revealed that all events where the model under-predicted the maximum surge coincided with sustained, strong winds from the east or north-east (i.e. directed onshore toward the Escuminac gauge – see Figure 2). Winds from these directions blow over relatively long fetches of 400-500km in the Gulf of Saint Lawrence towards the Acadian Peninsula and Northumberland Strait and, therefore, likely generate significant wave set-up on northern New Brunswick shores. Wave effects are not captured by the storm surge model, which simulates wind and barometric (atmospheric pressure) influences on water levels only. Therefore, it was hypothesized that the differences between modelled peak storm surges and observed peak residuals for these events could be explained, in part, by the omission of wave effects in the model. To investigate this hypothesis, a numerical wave model was developed to simulate wave conditions for the 13 under-predicted events in the Gulf of Saint Lawrence, and the results were used to estimate contributions to total water levels by wave setup. The model was based on TOMAWAC, a third generation spectral wave model, which is part of the TELEMAC modelling system (Benoit et al., 1996). The details of the model setup are described in Provan et al. (2022). The TOMAWAC model results for Event E1 are displayed in Figure 16, and indicate a peak significant wave height of approximately 6.5m within the Gulf of Saint Lawrence, and the highest waves in the nearshore region immediately adjacent to the Escuminac gauge. Using the simulated wave parameters as input, wave set-up was estimated using three different formulae: Ji et al. (2018), Stockdon et al. (2006), and Goda (2000). For Event E1, wave set-up estimates were 0.39m, 0.11m and 0.78m, respectively. Although the variability of the wave set-up estimates illustrates some uncertainty, the range encompasses, and the median value is reasonably close to, the difference of 0.3m between the modelled peak storm surge (1.31m) and the measured peak water level residual (1.61m) for this event. The modelled surge for the 13 under-predicted events were corrected by simulating wave conditions using the TOMAWAC model and adding wave setup estimates calculated using the Ji et al. (2018) formula. The results following correction for wave setup and ice impacts (discussed later in this Section) are shown in Figure 17. This analysis demonstrates the circumstances under which wave setup can impact water levels in the Gulf of Saint Lawrence and the Acadian Peninsula.

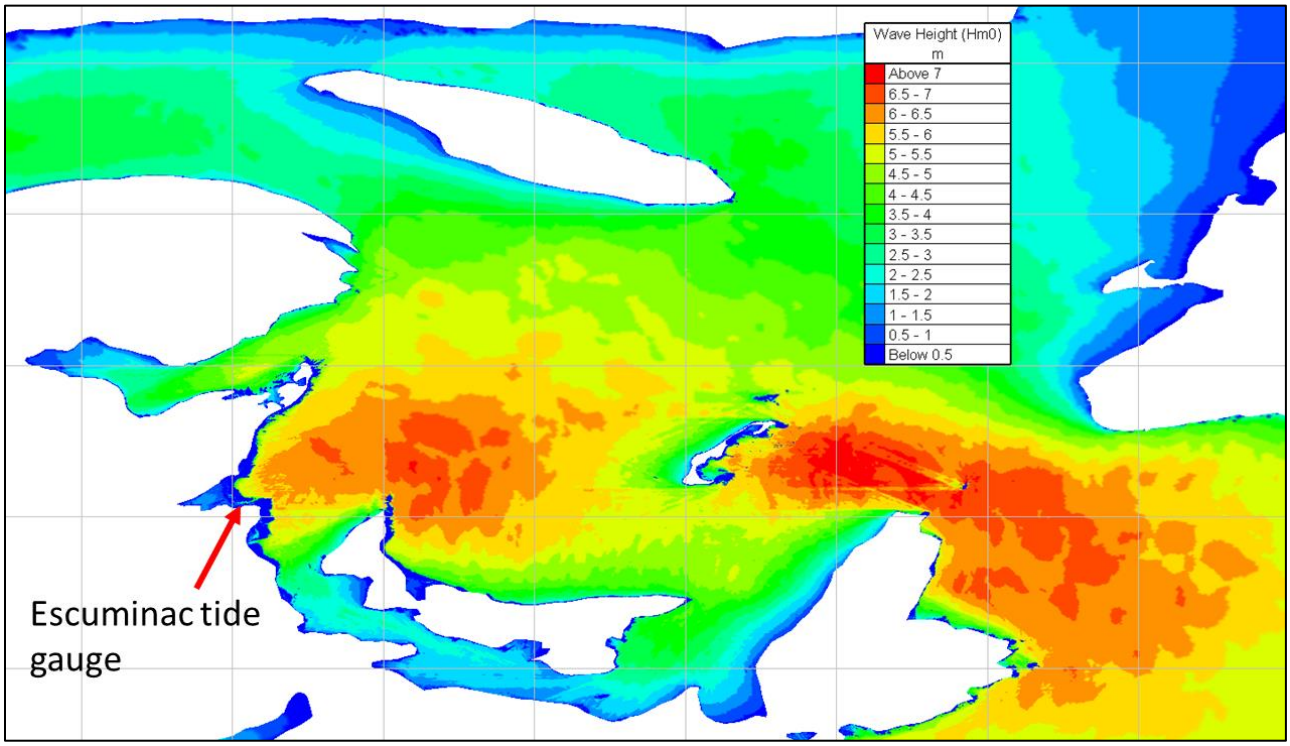

Figure 16. Modelled wave height within the Gulf of St. Lawrence leading up to the peak storm surge in Event E1.

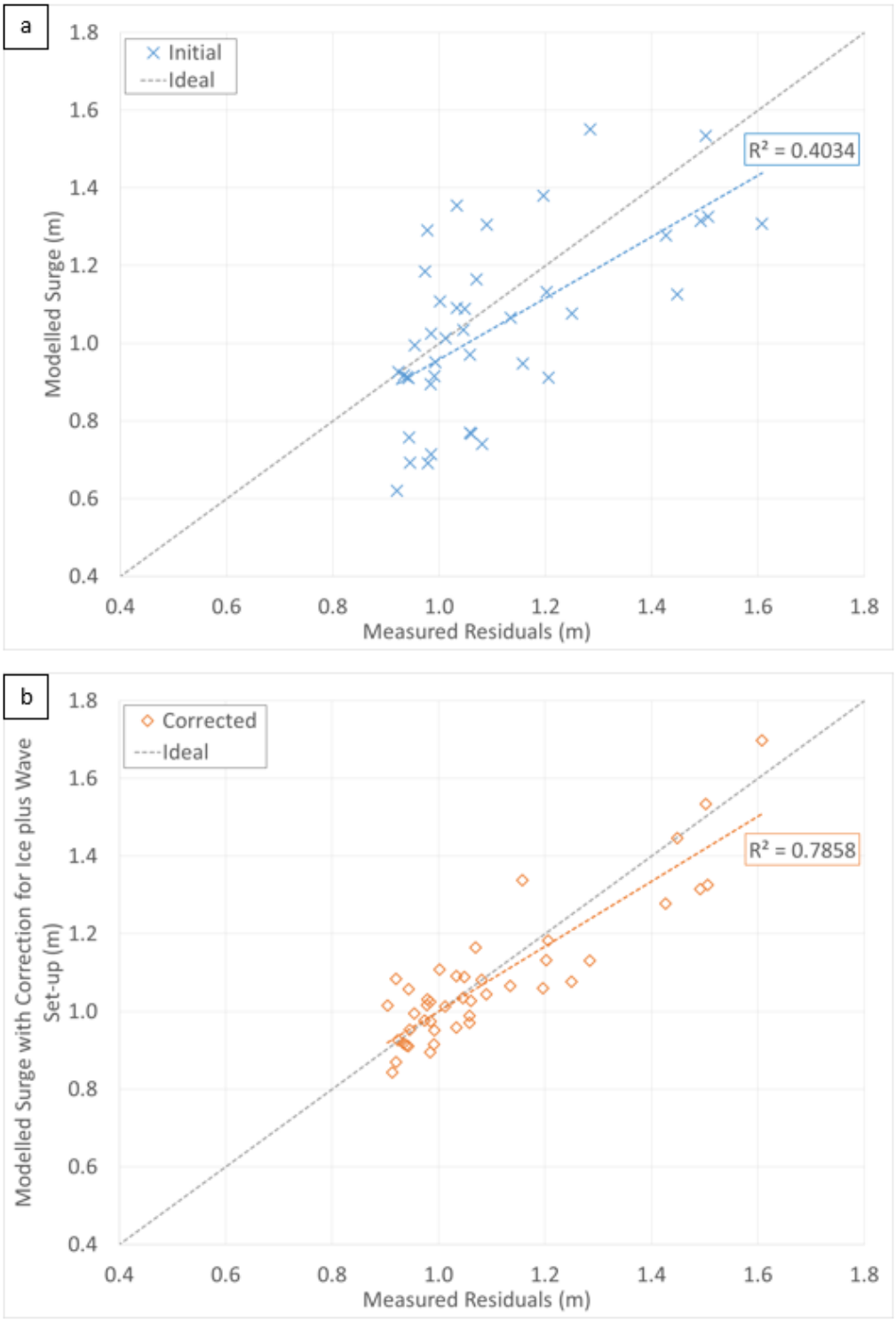

Figure 17. Measured residuals at the Escuminac gauge compared to (a) modelled surge without corrections for ice and wave set-up and (b) modelled surge with correction for ice plus wave set-up.

The seven storm surge events for which the model over-predicted the peak water level residual occurred during winter months (December to March), when there is potential for sea ice to be present within the Gulf of Saint Lawrence. Historical weekly ice concentration charts (Canadian Ice Service, 2019) were inspected and it was found that six of the seven over-predicted events coincided with significant ice cover throughout the Gulf (all except for Event E48 (B9)). An example ice chart coinciding with Event E26 (B15) (March 27, 2014) is presented in Figure 18, and shows ice concentrations exceeding 90% over the majority of the Gulf to the south of Île d'Anticosti. It is worth noting that seven other events (E7, E20, E23, E28, E34, E35, and E44) coincided with ice cover; modelled peak surge for all of these events, except for event E20, agreed well with measured peak water level residuals (discrepancy within 15%) without any correction for ice impacts. As indicated in Table 2, the model under-predicted the peak water level residual for Event E20, despite significant ice cover.

Birnbaum and Lüpkes (2002) and Garbrecht et al. (2002) showed that low ice concentrations amplify wind set-up, owing to the increased surface roughness and form drag induced by ice floes, which increases wind momentum transfer to the sea surface. However, high concentrations of ice, such as those occurring within the Gulf of Saint Lawrence in winter, can act as a barrier between the wind and the water. The ice barrier reduces the wind drag acting on the water (Birnbaum & Lüpkes, 2002) and the corresponding wind set-up, effectively attenuating storm surges. This fits with an explanation that the storm surge model over-predicts water level residuals during periods of significant ice cover in the Gulf of Saint Lawrence, as the attenuating effects of ice cover were not initially included in the model.

To investigate the impacts of sea ice on winter storm surges, the following equations developed by Joyce et al. (2019), which account for the contributions of varying sea ice concentrations (IC) on the overall drag (C_D) acting on the water surface, were implemented in the regional model:

$$C_D = (1 - IC)C_{D-w} + (IC)C_{D-is} + C_{D-if} \quad (3)$$

where C_{D-W} is the calibrated air-sea drag coefficient for open water conditions ($C_D = C_{D-W}$ during ice-free conditions), C_{D-is} is the contribution due to ice skin drag, which was set to a constant value of 0.0015 (Lüpkes et al., 2012), and C_{D-if} is the contribution due to ice form drag which is calculated from:

$$C_{D-if} = 4C_{D-if,max}(IC)(1 - IC) \quad (4)$$

where $C_{D-if,max}$ is set to 0.0025, which is the maximum value of C_{D-if} that occurs at a 50% ice concentration (Joyce et al., 2019).

The six storms that coincided with significant sea ice, and for which the model over-predicted peak water level residual, were simulated again using the modified wind drag formulation. Alteration of wind drag based on sea ice conditions improved agreement between the measured water level residuals and simulated winter storm surges (see Figure 17). Altogether, incorporating impacts of wave setup and sea ice into the regional modelling improved the coefficient of determination from 0.4034 to 0.7858. Further details regarding implementation of sea ice in the regional model, and results, are provided in Provan et al. (2022).

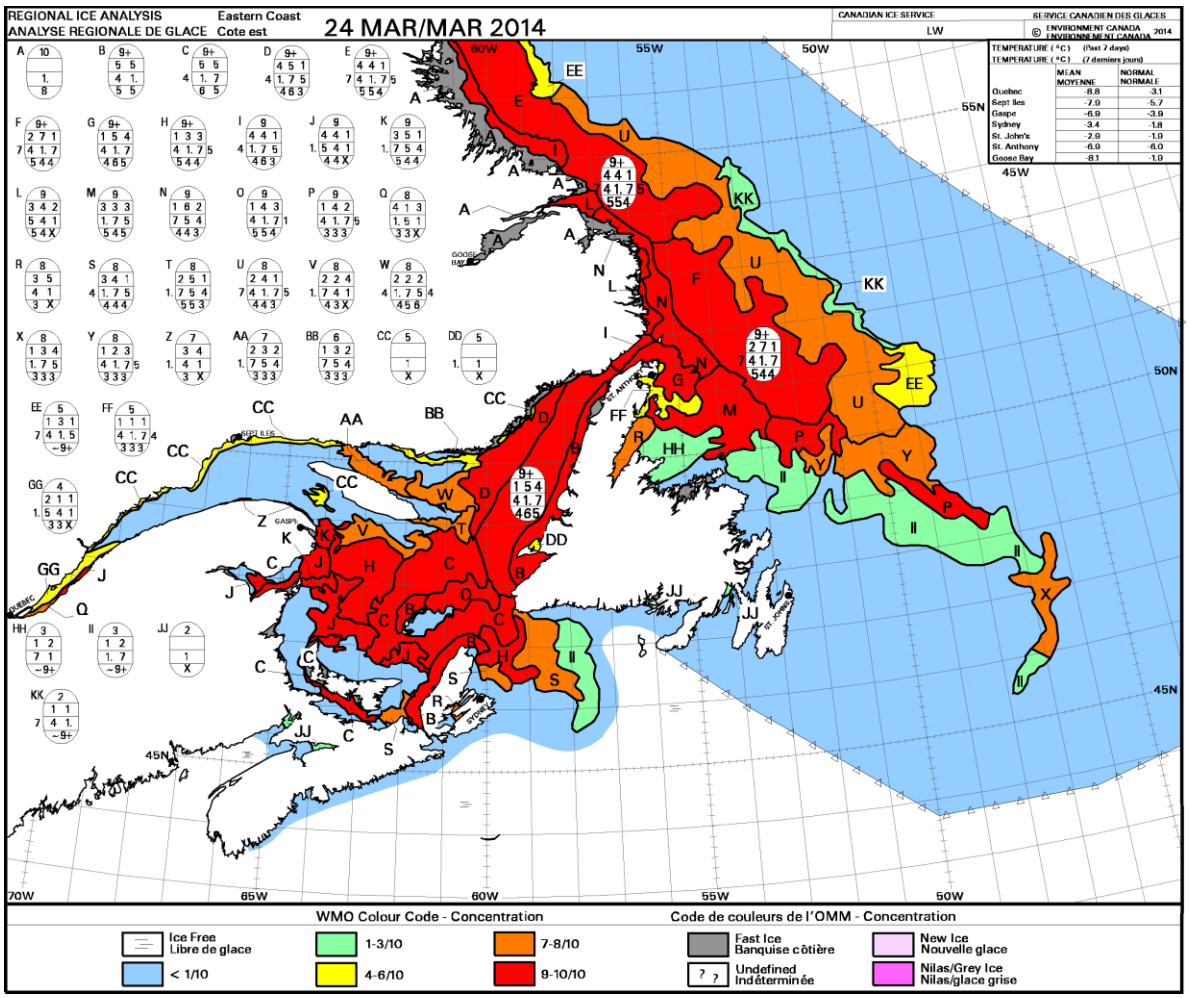

Figure 18. Ice concentration chart coinciding with Event E26 (B35) (Canadian Ice Service, 2019).

The demonstrated influence of sea ice in attenuating storm surges in the region poses a potential concern for coastal flood and erosion risk management and coastal infrastructure resilience, as projections indicate that ice cover and ice season durations within the Gulf of Saint Lawrence will decline over the 21st century due to climate change (Greenan et al., 2018). Therefore, even if the frequency and intensity of storms were to remain stationary in the future, it is possible that future winter storms will produce higher peak storm surges when there is less (or no) ice cover to attenuate storm surges, and when low ice concentrations may exacerbate peak surges.

7 Community-Scale Model Development

A community-scale model was developed to support detailed simulation of storm surge-driven flood hazard and inundation in the seven communities of interest.

7.1 Model Setup

7.1.1 Model Mesh

Similar to the regional model, the community-scale hydrodynamic (flood hazard) model computations were performed on an unstructured triangular mesh. The model domain (Figure 19) encompasses the Acadian Peninsula region, extending from the north coast of New Bandon Parish, eastward to Miscou Island, and southward to Tracadie-Sheila. The model domain extends approximately 20-30km from the north coast of the Acadian Peninsula into Chaleur Bay, and approximately 30km from the south-east coast of the Acadian Peninsula into the Gulf of Saint Lawrence.

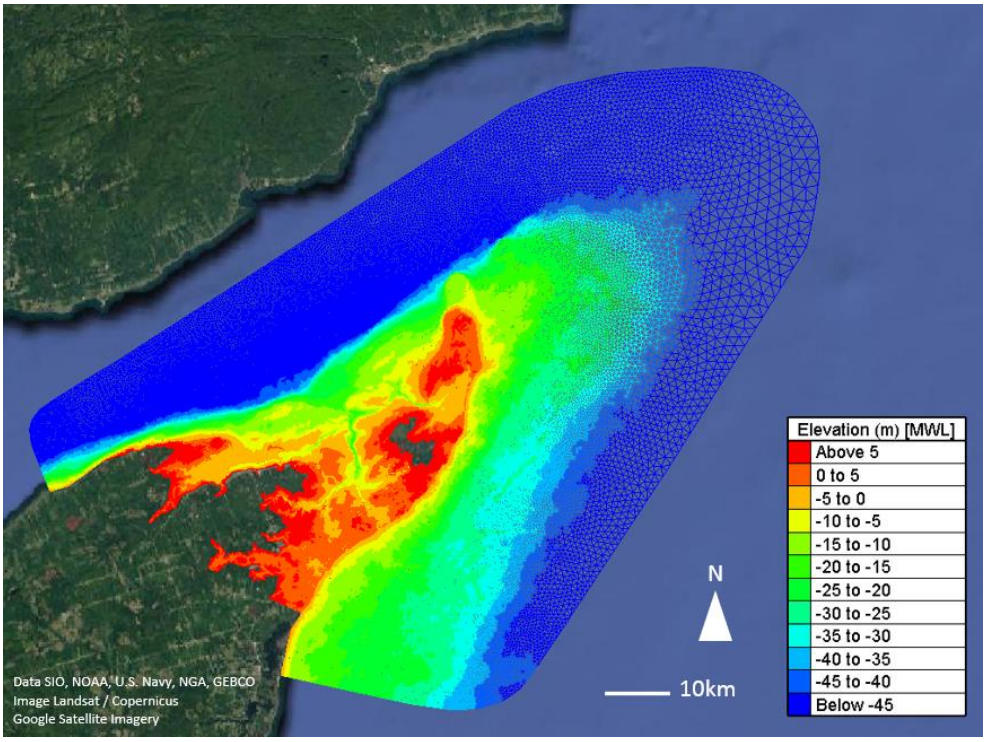

Figure 19. Community-scale model mesh and year-2018 elevation data referenced to MWL.

Similar to the regional model, the community-scale model mesh was generated using Blue Kenue software (Barton, 2019; Canadian Hydraulics Centre, 2011). The mesh resolution at the offshore boundary was designed to closely resemble the resolution of the regional model mesh to minimize interpolation error when applying regional model simulation results as boundary condition input to the community-scale model. The spatial resolution of the offshore boundary ranged from approximately 250m (characteristic triangular element edge length) in Chaleur Bay to 2000m in the Gulf of Saint Lawrence. To resolve overland flooding pathways and floodplain features, characteristic mesh element edge lengths of 10m were adopted in the vicinity of the seven communities of interest as shown in Figure 20. Land areas exceeding 10m in elevation (referenced to CGVD2013) were excluded from the mesh to alleviate computational effort, as it was unrealistic to expect these areas to be inundated by coastal flooding, even under extreme future sea-level rise scenarios; for reference, Daigle (2017) suggests that even the most extreme coastal flood events, with sea level rise projections to year-2100, are not likely to produce water levels exceeding 4.0m CGVD2013 in the Acadian Peninsula.

As mentioned in Section 4.2, a hydro-enforced DEM was provided, which includes special alteration of elevation data in the vicinity of culverts and drainage features. In order to ensure that the fine-detail drainage features are reflected in the model mesh, a 5m-resolution was specified in the vicinity of culverts and drainage features, and the mesh was "snapped" onto these features. This is visible in Figure 21 which shows a portion of the community-scale model mesh near Rue Principale in the Village of Le Goulet. Altogether, the community-scale model mesh consisted of approximately 940,000 computational nodes.

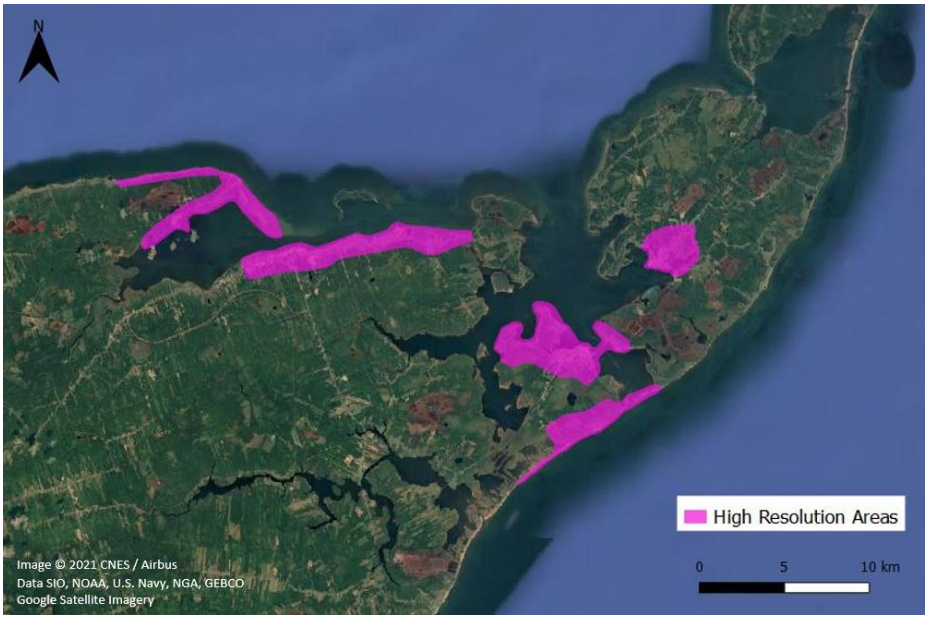

Figure 20. Areas modelled with high spatial resolution (10m-resolution)

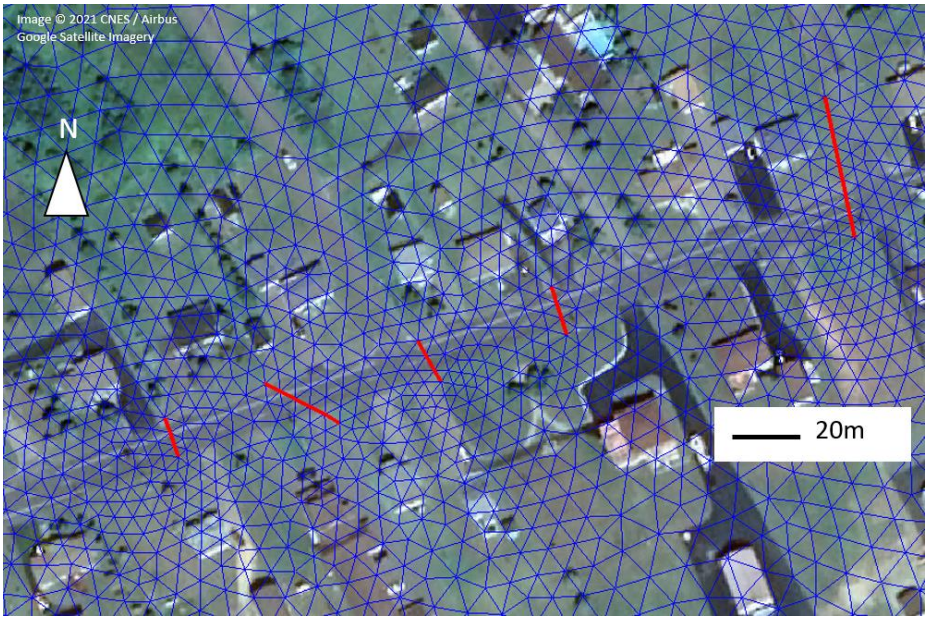

Figure 21. Community-scale model mesh near Rue Principale in the Village of Le Goulet. Culverts are shown in red.

7.1.2 Model Elevations

In general, the model topography and bathymetry was based on the following datasets, as described in Sections 4.1 and 4.2:

- Best-available bathymetry acquired directly from CHS (Canadian Hydrographic Service, 2020) or from the CHS-NONNA dataset (Canadian Hydrographic Service, 2019)
- The 1m-resolution, hydro-enforced DEM reflecting year-2018 ground elevations, where available (acquired directly from Government of New Brunswick)
- The 1m-resolution DEM (not hydro-enforced) reflecting year-2018 ground elevations (Government of New Brunswick, 2019a)
- Sub-meter-resolution LiDAR point data reflecting year-2018 ground elevations (Government of New Brunswick, 2019d)

An exception involved the replacement of some topography data with older historical data in dynamic or altered shore regions, when simulating historical events as part of the model calibration and validation process described in Sections 7.3 and 7.4.

The hydro-enforced DEM encompasses a large portion of the coastal geography of the Acadian Peninsula, including all seven communities of interest. The non-hydro-enforced DEM was used to fill in sections far inland from the coast that were not covered by the hydro-enforced DEM. The LiDAR point data were used to fill in nearshore areas that were not captured well by the available DEMs or the CHS bathymetry. Figure 22 and Figure 23 illustrate the topography and bathymetry data used in the community-scale model, respectively. For the calibration and validation process (discussed in detail in Sections 7.3 and 7.4), historical digital elevation data reflecting 2009 ground elevations were used in place of the more-recent data reflecting 2018 ground elevations in the vicinity of Le Goulet.

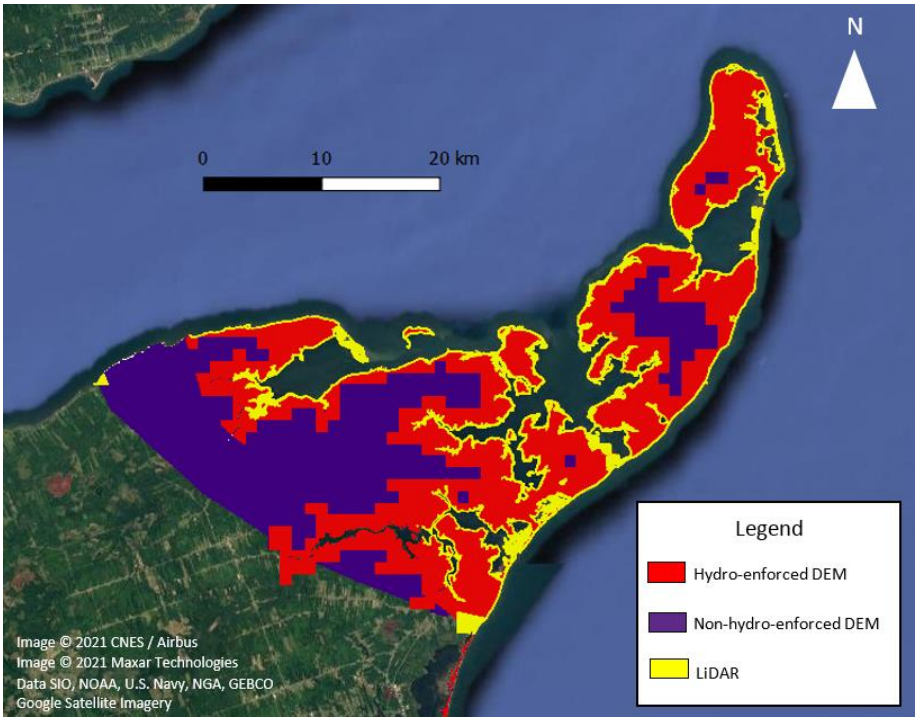

Figure 22. Topography data used in community-scale model.

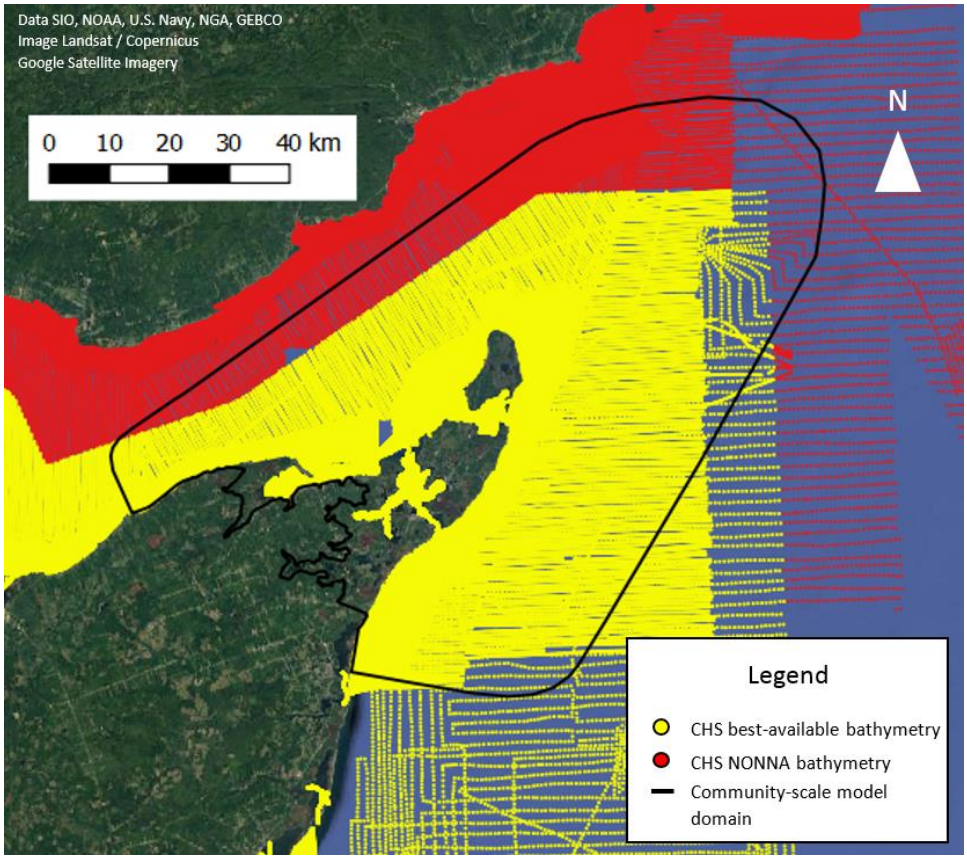

Figure 23. Bathymetry data used in community-scale model.

7.1.3 Building Footprints

As described in Section 4.7, building and infrastructure footprints were provided by Government of New Brunswick. Buildings and other structures can impact the hydrodynamics by exerting drag force on incident flows. There are several methods to incorporate the impacts of buildings and structures into numerical hydrodynamic models. The most intensive and computationally expensive methods often involve building-scale adjustment of the computational mesh, where each individual building or structure is explicitly represented either as a "hole" in the computational mesh, or as an elevated "block" (Schubert & Sanders, 2012). For building-scale methods to be feasible, the computational mesh must have sufficient resolution to capture individual buildings, as well as spaces between buildings. Simplified methods often involve implementing zones of additional roughness or drag into the model mesh to simulate the presence of a collection of buildings or structures (e.g. a residential neighbourhood or a collection of industrial buildings) (Schubert & Sanders, 2012).

The community-scale model did not have sufficient resolution to support building-scale implementation of buildings and infrastructure. Rather, the buildings and structures were implemented into the model using a zonal approach similar to the "building porosity" method described by Schubert & Sanders (2012). This was accomplished using the "vertical structures" functionality of TELEMAC-2D which allows users to specify drag elements using the DRAGFO subroutine (Ata, 2018). The user must specify: the geographic area containing the drag elements, the number of drag elements (e.g. buildings) contained in the area, the frontal

width of each drag element, and a drag coefficient. A drag coefficient of 2.0 was assumed for all buildings and structures, which is representative of a square column (White, 2003).

First, polygons or "zones" were manually drawn around collections of similar buildings, building-types, and building footprint areas (e.g. a residential neighborhood containing houses and sheds or a collection of industrial buildings). The number of buildings within each zone were counted to identify the number of drag elements contained in the zone. Average frontal width for each zone (representative of the buildings or structures contained in the zone) was computed as follows:

- The area of each building footprint within a given zone was computed
- A representative frontal width was computed for each building footprint by taking the square root of the area (i.e. assuming each building and structure is a perfect square)
- A representative frontal width was computed for each zone by calculating the average frontal width of the buildings and structures contained within

Buildings and infrastructure outside of the communities of interest were not incorporated into the model. Similarly, buildings and structures that had a ground elevation greater than approximately 4.0m CGVD2013 (comparable to the extreme maximum flood elevation estimated by Daigle (2017)) were not incorporated into the model. An example of the drag zones specified in the communities of Shippagan and Pointe-Brûlée is shown in Figure 24.

Figure 24. Example of building drag zones implemented in the communities of Shippagan and Pointe-Brûlée. Building and infrastructure footprints are outlined in black, purple polygons indicate drag zones, and the yellow line indicates the elevation contour coinciding with 4m CGVD2013.

7.1.4 Special Considerations for the December 6, 2010 and December 21, 2010 Storm Surge Events

Beginning in 2013, the village of Le Goulet undertook an initiative to restore the coastal dune system in an effort to limit erosion and mitigate coastal flooding caused by storm surges (Hébert & Aubé, 2015). The project consisted of the installation of sand retention structures as well artificial reconstruction of the dune system. Consequently, the coastline of Le Goulet has undergone significant alteration since the two calibration storms which occurred in December 2010. To facilitate realistic comparison between modelled results and the calibration data (see Section 4.9 and 4.10), digital elevation data representative of year-2009 were used in place of the 2018 data in the vicinity of Le Goulet during model calibration and validation. The 2018 elevation data were used elsewhere, as the modern elevation data did not appear to differ greatly from the historic elevation data; the 2018 elevation data also provide the added advantage of more-realistic, hydro-enforced drainage.

7.2 Model Boundary Conditions

Spatially and temporally varying water levels were prescribed at the offshore boundary of the community-scale coastal flood hazard model, based on output from the regional model. Modelled hourly water levels acquired from the regional model were mapped onto the offshore boundary of the community-scale model to drive community-scale simulations. As such, the water level elevation along the community-scale model boundary fluctuates spatially and temporally, according to the regional model results in the vicinity of the community-scale model boundary. Inverse distance weighting was used to interpolate hourly values onto the community-scale model boundary nodes based on values acquired from the three closest regional model nodes; the process is illustrated in Figure 25. Similar to the regional model, community-scale simulations were also forced by the ERA5 wind and atmospheric pressure data described in Section 4.3.3.

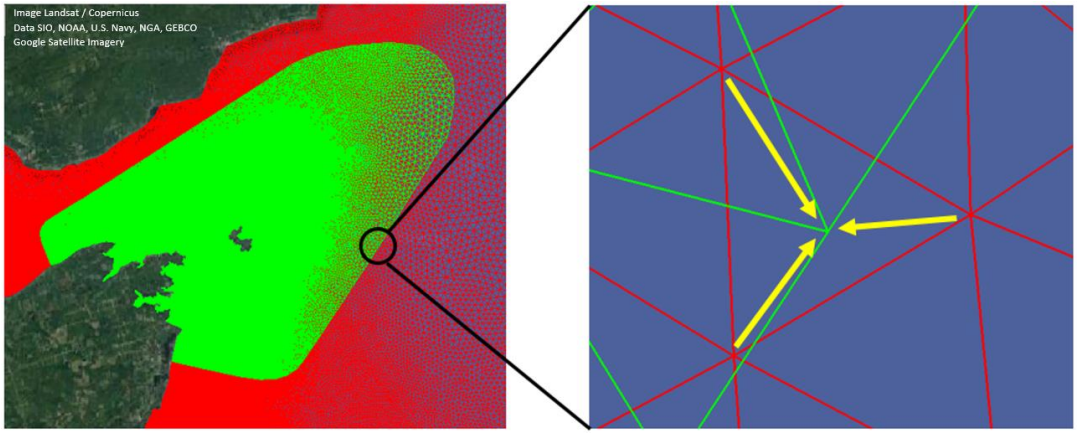

Figure 25. Defining community-scale model boundary conditions. Hourly water level results from the regional model mesh (red) are mapped onto the boundary nodes of the community-scale model mesh (green) using inverse distance weighting interpolation.

Historical events that were simulated to support model calibration (see Section 7.3) included both tides and storm surges to enhance the realism of the modelled results and facilitate comparison with high water level observations. For these historical events, tidal fluctuations were integrated into the regional-scale modelling via the TPXO database, and regional model results were mapped onto the offshore boundary of the community-scale model.

7.3 Model Calibration

The following sections (Sections 7.3, and 7.3.1 through 7.3.3) describe, in detail, calibration work that is largely adapted from Ferguson et al. (2022). Model performance was calibrated using high water level indicators that were surveyed following two major storm surge events that occurred on December 6, 2010 and December 21, 2010 (Events E48 (B9) and E15 (B37), respectively). The survey data were provided to NRC-OCRE by the survey leads, Dominique Bérubé and Marc Desrosiers, from Government of New Brunswick (see Section 4.9). Surveyed elevations were converted to CGVD2013 using the GPS·H tool (Government of Canada, 2021) to support comparison with the model; model simulations were run using elevations referenced to MWL, but results could be easily transformed to CGVD2013. It is worth noting that other researchers have used debris observations to support analyses related to coastal flooding (Harper et al., 1988; Jardine et al., 2021; Kim et al., 2021; MacLeod & Dallimore, 2021; Melton et al., 2010); notably, Didier et al. (2015) used debris surveys coinciding with the December 6th, 2010 event (i.e. the same event investigated in this study) as a metric to assess model skill in locations immediately north of the Acadian Peninsula on the north coast of Chaleur Bay.

7.3.1 Calibration Approach

Similar to the regional model, the community-scale model was calibrated through adjustment of the model roughness and wind drag formulation/coefficients until satisfactory results were achieved with regard to both water surface elevation and flood water extent. Initial estimates for land roughness were based on land cover data acquired from GeoNB (Section 4.6) and typical roughness values cited from literature (Chin, 2013; Houghtalen et al., 2010). Consistent with the regional model, a uniform roughness of S=40m$^{1/3}$/s was specified for offshore areas. Table 3 lists the initial estimates for land roughness. The initial estimate for wind drag formulation/coefficients was based on the optimal wind drag formulation/coefficients identified for the regional model (Section 6.3).

Table 3. Initial Estimates for Land Roughness

Land Cover	Manning Coefficient (s/m$^{1/3}$)	Strickler Coefficient (m$^{1/3}$/s)
Wetland	0.07	14
Forest	0.1	10
Non-Forest - No Vegetation	0.015	67
Non-Forest - Grasses, Crops, or Other	0.033	30
Non-Forest - Shrubs	0.05	20
Non-Forest - Trees	0.1	10

7.3.2 December 2010 Flood Events

It was uncertain whether the June 23 and June 28, 2011 surveys represented high water levels produced by the December 6 or the December 21, 2010 event. A simple modelling exercise was executed to investigate linkage between the survey data and the two storm events.

Both storm events were simulated using the model set up and initial estimations discussed in Section 7.3.1. Comparison of the modelled flood extents from the two simulations suggested that the December 21, 2010 event produced more extensive flooding in the vicinity of the survey data in Pointe-Brûlée in comparison to the December 6, 2010 event (Figure 26). Furthermore, the December 21, 2010 event consistently produced

more extensive flooding in comparison to the December 6, 2010 event in Pointe-Brûlée for all alike model setups discussed in Section 7.3.3. The modelled flood extents for the two storms in the vicinity of the survey data in Bas-Caraquet were nearly identical (Figure 26), likely due to the steep shoreline/bluff at that location. However, in general, the modelled December 21, 2010 event produced slightly more extensive flooding in Bas-Caraquet in comparison to the December 6, 2010 event. This suggests that the June 23 and June 28, 2011 survey data actually represent high water elevations associated with the December 21, 2010 event, particularly in Pointe-Brûlée.

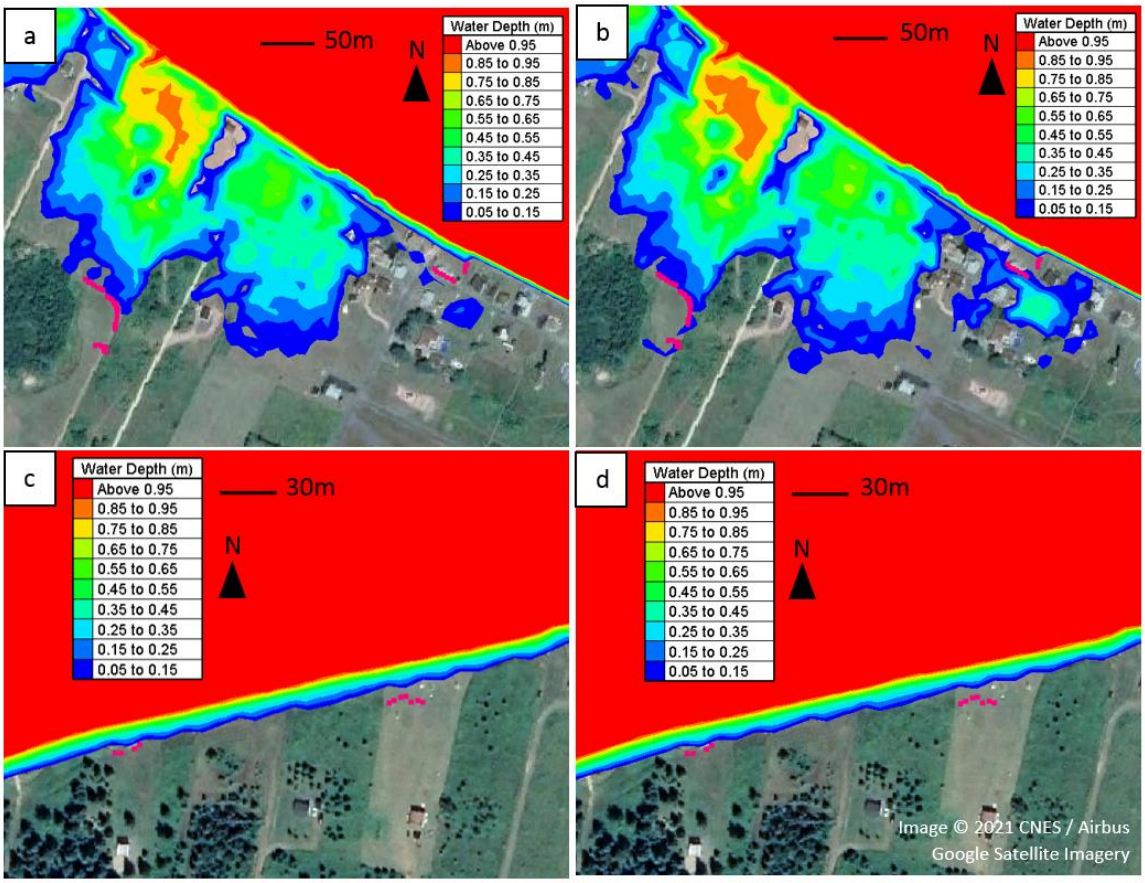

Figure 26. Modelled flood extent based on the initial model setup for the December 6, 2010 event (a and c) and the December 21, 2010 event (b and d), in Pointe-Brûlée (a and b) and Bas-Caraquet (c and d). Survey points are shown in pink.

7.3.3 Comparison with Surveyed High Water Level Indicators

The survey data were collected in 13 locations across the Acadian Peninsula (Figure 27). Prior to the calibration exercise, the surveyed elevations were compared to the ground elevation of the model at the point locations. Table 4 presents a summary of the survey data and comparison against the model ground elevations. As illustrated in Table 4, the ground elevations of the model agree quite well with the surveyed elevations; all but two locations (PB3 and BPP) have discrepancies less than +/- 15cm.

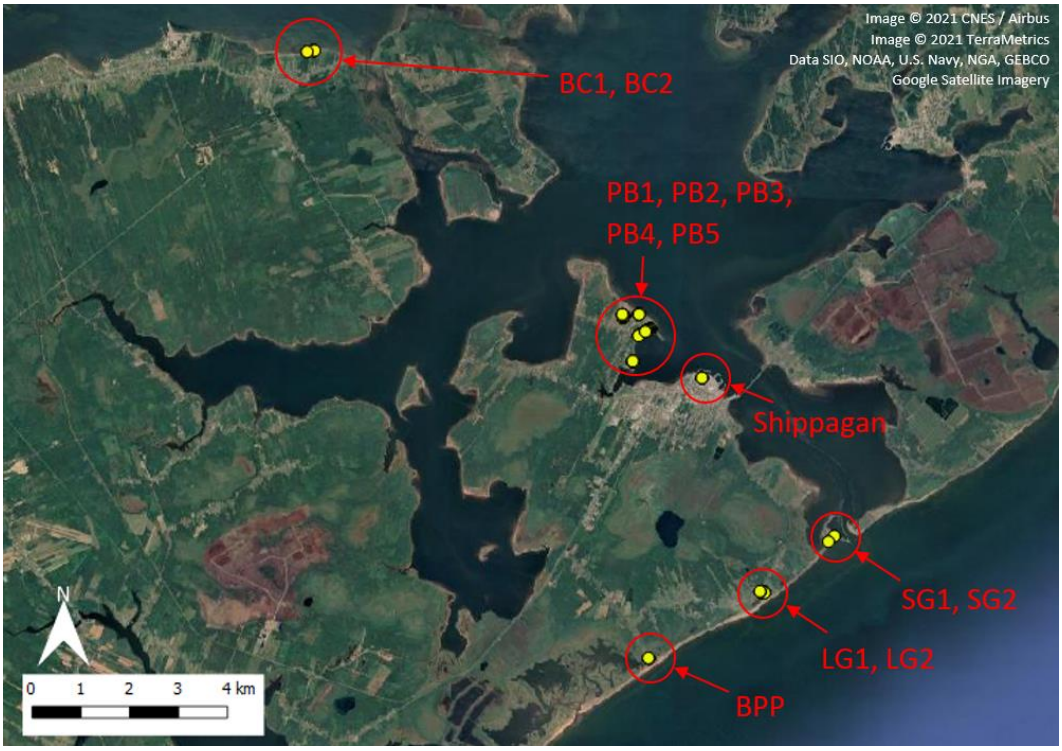

Figure 27. Survey locations. Adapted from Ferguson et al. (2022).

Table 4. Summary of Survey Points

Location	Relevant Event	Number of Survey Points	Average Elevation from Survey (m CGVD2013)	Average Elevation from Model (m CGVD2013)	Discrepancy (m) [Model – Survey]
BPP	Dec 6, 2010	9	1.17	0.64	-0.53
LG1	Dec 6, 2010	6	1.14	1.17	0.03
LG2	Dec 6, 2010	24	1.30	1.19	-0.11
SG1	Dec 6, 2010	2	0.79	0.92	0.14
SG2	Dec 6, 2010	3	1.03	0.97	-0.06
Shippagan	Dec 6, 2010	7	1.09	1.18	0.09
PB1	Dec 21, 2010	45	1.37	1.32	-0.06
PB2	Dec 21, 2010	11	1.41	1.36	-0.06
PB3	Dec 21, 2010	76	1.18	1.54	0.36
PB4	Dec 21, 2010	35	1.17	1.26	0.09
PB5	Dec 21, 2010	16	1.35	1.28	-0.07
BC1	Dec 21, 2010	4	2.23	2.155	-0.08
BC2	Dec 21, 2010	7	2.12	1.98	-0.14

* LG = Le Goulet, SG = Shippagan Gully, PB = Pointe-Brûlée, BC = Bas-Caraquet, BPP = Baie-de-Petit-Pokemouche

Model skill was assessed by comparing modelled flood water elevation and flood water extents for the December 6 and December 21, 2010 events with the surveyed elevations and extents. To support this analysis, an assumption had to be made about the flood depth required to mobilize and deposit the surveyed ocean debris and sea wrack. Furthermore, considering the spatial resolution of the model, as well as the error and uncertainty of the model ground elevations and computational processes, it is impractical to realistically identify areas with very small flood depth from the model results. It was assumed that a flood depth of 5cm was required in order to mobilize and deposit debris and sea wrack, and also represents a suitable lower-threshold from which to extract flood hazard metrics such as depth and flood extent. Therefore, in order to test model skill, surveyed elevations were compared against the ground elevation coinciding with the modelled 5cm flood depth contour for each calibration trial.

For each calibration trial, the 5cm flood depth contour was extracted from the model results in the vicinity of each of the survey point groups (see Table 4). The ground elevation coinciding with each 5cm flood depth contour was then determined. The average ground elevation along each contour was compared against the average elevation of the survey data for each survey point group. In addition, average horizontal distance between survey points and the extracted contour for each survey point group was computed. The standard deviation of the computed distances was also computed for each survey point group. The average horizontal distance values indicate the proximity of the modelled flood extent to the surveyed high water level indicators, whereas the standard deviation values indicate how closely the planar shape of the modelled flood extent matches the shape of the surveyed high water level indicators. The process is illustrated in Figure 28.

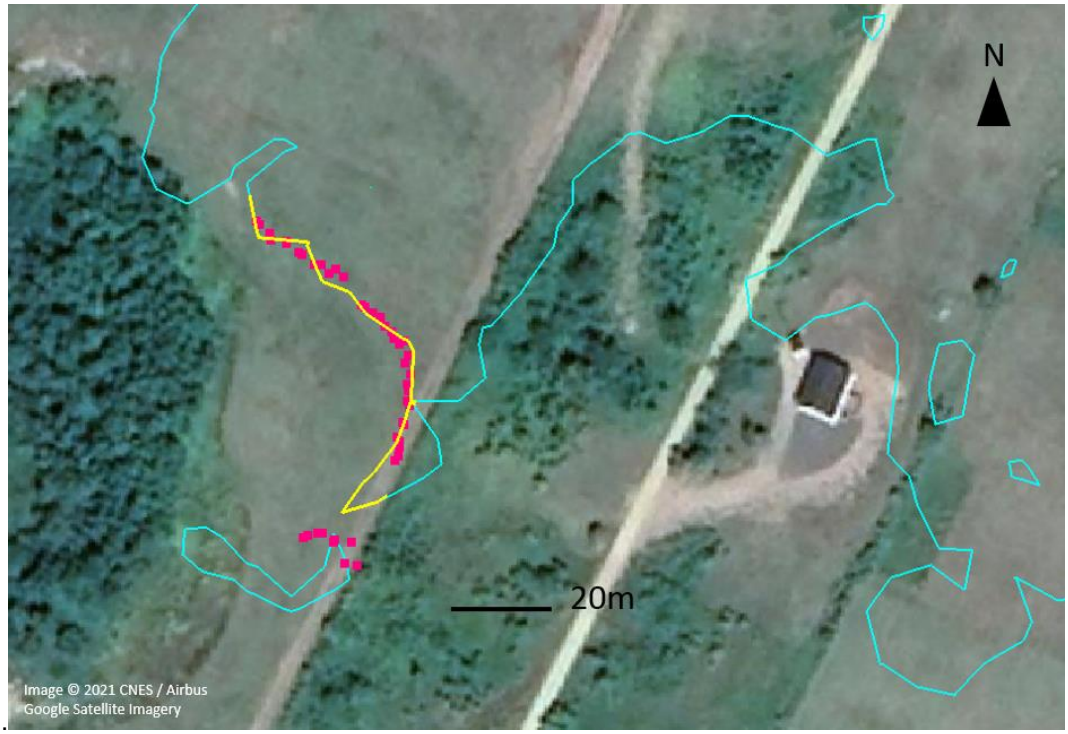

Figure 28. Comparison of modelled results with surveyed point data for location PB1. The modelled 5cm water depth contour is shown in blue. A section of the 5cm water depth contour was isolated (shown in yellow). Ground elevations coinciding with the contour were compared against elevations from the surveyed point data (pink points). Horizontal distances between the modelled flood contour and the survey points were also computed.

Wind drag and land roughness were adjusted, and model results were compared to surveyed high water level indicators. Ultimately, a Flather wind drag formulation was applied with wind drag coefficient (a_{wind}) varying within the range 0.565×10^{-3} and 2.513×10^{-3} (Ata, 2018). The initial estimates for land roughness based on land cover polygons and values from literature (Table 3) were maintained. However, it was observed that the land cover polygons did not adequately capture the shape and extent of the Le Goulet beach. Therefore, a roughness of S=30 $m^{1/3}/s$ was manually specified for the Le Goulet beach; this improved modelled water surface elevations and flood extent in the vicinity of Baie-de-Petit-Pokemouche. The final results of the model calibration are shown in Table 5 and Table 6.

Table 5. Comparison of Modelled Flood Elevations with Survey Data

Location	Relevant Event	Modelled Flood Elevation (m CGVD2013)	Average Elevation from Survey (m CGVD2013)	Error (m) [Model – Survey]
BPP	Dec 6, 2010	1.188	1.174	0.01
LG1	Dec 6, 2010	1.513	1.136	0.38
LG2	Dec 6, 2010	1.668	1.304	0.36
SG1	Dec 6, 2010	1.462	0.788	0.67
SG2	Dec 6, 2010	1.516	1.030	0.49
Shippagan	Dec 6, 2010	1.488	1.092	0.40
PB1	Dec 21, 2010	1.319	1.374	-0.06
PB2	Dec 21, 2010	1.351	1.414	-0.06
PB3	Dec 21, 2010	1.511	1.183	0.33
PB4	Dec 21, 2010	1.456	1.167	0.29
PB5	Dec 21, 2010	1.456	1.351	0.10
BC1	Dec 21, 2010	1.991	2.232	-0.24
BC2	Dec 21, 2010	1.839	2.123	-0.28

* LG = Le Goulet, SG = Shippagan Gully, PB = Pointe-Brûlée, BC = Bas-Caraquet, BPP = Baie-de-Petit-Pokemouche; ** Table adapted from Ferguson et al. (2022)

Average absolute vertical (elevation) error was equal to 0.28m, and $RMSE$ was equal to 0.34m. Discrepancies less than 30cm were observed for 7 of the 13 locations, and discrepancies of 10cm or less were observed for 4 of the 13 locations. The largest discrepancies were observed at the Shippagan Gully (SG) locations. However, it is perhaps expected that the fast and dynamic flows through the gully, and the presence of fine resolution structures, would present challenges to achieving accurate model results. It is also worth noting that although Shippagan Gully was modelled with high (10m) resolution, it is not one of the focus areas of the study.

Average horizontal (flood extent) error was equal to 6.25m, $RMSE$ was equal to 7.16m, and average standard deviation was equal to 2.44m. Except for locations LG1 and LG2, the model was able to reproduce modelled flood extents with sub-mesh-resolution accuracy (i.e. less than 10m discrepancy). At 9 of the 13 locations, observed discrepancy did not exceed 6m.

Table 6. Comparison of Modelled Flood Extents with Survey Data

Location	Relevant Event	Average Distance Between Modelled and Surveyed Flood Extent (m)	Standard Deviation of Distances Between Modelled and Surveyed Flood Extents (m)
BPP	Dec 6, 2010	5.54	0.68
LG1	Dec 6, 2010	11.33	2.30
LG2	Dec 6, 2010	15.43	7.11
SG1	Dec 6, 2010	6.00	1.60
SG2	Dec 6, 2010	4.97	1.66
Shippagan	Dec 6, 2010	6.94	1.11
PB1	Dec 21, 2010	2.20	2.87
PB2	Dec 21, 2010	2.85	2.58
PB3	Dec 21, 2010	4.79	3.31
PB4	Dec 21, 2010	5.45	2.08
PB5	Dec 21, 2010	5.33	3.11
BC1	Dec 21, 2010	2.73	1.19
BC2	Dec 21, 2010	7.64	2.17

* LG = Le Goulet, SG = Shippagan Gully, PB = Pointe-Brûlée, BC = Bas-Caraquet, BPP = Baie-de-Petit-Pokemouche; ** Table adapted from Ferguson et al. (2022)

In general, the model showed better predictive skill when compared against survey points coinciding with the December 21, 2010 event with regard to both water level elevation and flood extent. Consequently, the best predictive skill was observed in the communities of Pointe-Brûlée and Bas-Caraquet. Both horizontal and vertical error may be explained, in part, by wave contributions to observed high-water marks, which were not included in the community-scale modelling; the largest horizontal error was observed in Le Goulet which is exposed to waves propagating from long north-easterly fetches in the Gulf of Saint-Lawrence. Altogether, with consideration of the model resolution, and in light of uncertainties regarding water depth and debris deposition, the observed discrepancies were deemed acceptable. Images showing modelled flood extent alongside surveyed points are shown in Appendix A.

7.4 Model Validation

The following section (Section 7.4) describes, in detail, validation work that is largely adapted from Ferguson et al. (2022). The model was validated by qualitatively comparing simulated flood extents to photographic and video evidence of flooding captured during and after the December 6 and December 21, 2010 events. This information was particularly helpful to assess model skill in areas where survey data were not collected. Several areas across the Acadian Peninsula, referred to as Qualitative Assessment Areas (QAAs), were identified where photographic or video evidence could be used to enhance assessment of model skill. Five QAAs were identified for the December 6, 2010 event based on photographic evidence provided by Dominique Bérubé (Government of New Brunswick), Marc Desrosiers (Government of New Brunswick), and Dr. André Robichaud (University of Moncton). Eight QAAs were identified for the December 21, 2010 event based, again, on photographic evidence provided by Dominique Berubé, Marc Desrosiers, and Dr. André Robichaud, and also based on video evidence uploaded to YouTube (Doucet, 2010). The QAAs are illustrated in Figure 29 and images comparing the modelled flood events to flood observations are provided in Appendix B and C.

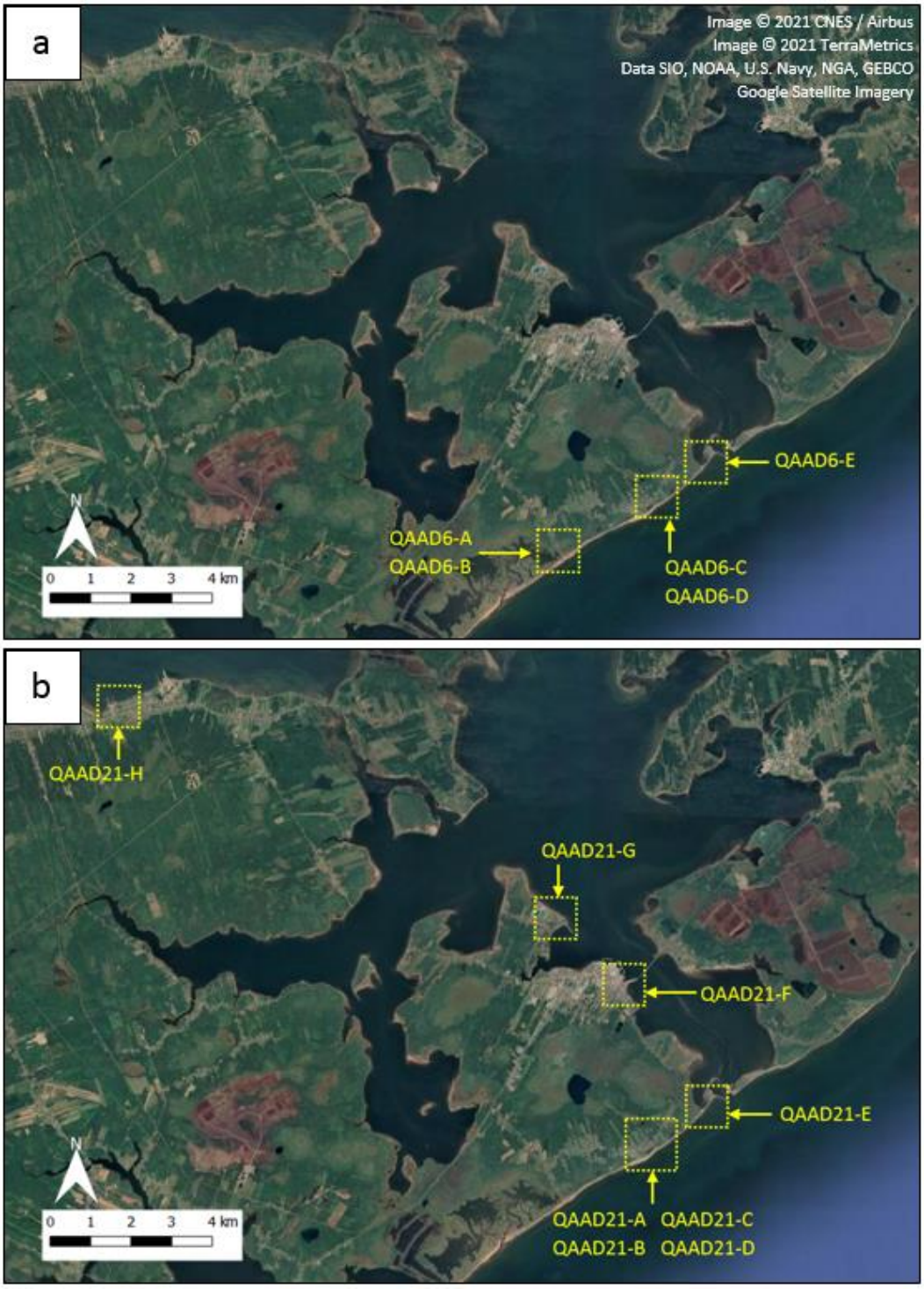

Figure 29. Approximate locations of Qualitative Assessment Areas for (a) the December 6, 2010 event and (b) the December 21, 2010 event. Adapted from Ferguson et al. (2022).

In general, the modelled flood extents agreed well with photographic and video evidence, both with regard to degree of inland extent and the "pattern" or "shape" of the maximum flood contour. However, based on the evidence available, the model under-predicted flood extent in the northeastern portion of Le Goulet for the December 21, 2010 event; referring to locations QAAD21-C and QAAD21-D in Appendix C, it is apparent that the model failed to predict flooding in some areas that were, in fact, exposed to flooding.

7.5 Limitations

Although the communities of Maisonnette, Caraquet, and Lamèque are modelled in high resolution in the community-scale model, it is important to note that no data were available to assess model skill in these communities. Rather, model skill is inferred based on the calibration and validation processes described in Sections 7.2 and 7.3, focused on Bas-Caraquet, Pointe-Brûlée, Shippagan, Shippagan Gully, Le Goulet, and Baie-de-Petit-Pokemouche. Therefore, modelled results in Maisonnette, Caraquet, and Lamèque should be interpreted with caution. Those interpreting model results should also be conscious of uncertainty levels associated with predictions of flood stage and flood extent summarized in Table 5 and Table 6, as well as the resolution of the computational mesh (10m-resolution).

Bathymetric data coverage was quite limited in the shallow, interior bays of the Acadian Peninsula (Figure 30), often necessitating interpolation over large coastal sections. In particular, bathymetric data were quite sparse in the vicinity of Lamèque, including the two bays located north and south of the village, bisected by Rue du Ruisseau and Rue Principale, respectively. Similarly, bathymetric data were quite sparse in the bays immediately west and east of Pointe-Brûlée. Whereas model skill could be assessed in the vicinity of Pointe-Brûlee, data were not available to assess model skill in the vicinity of Lamèque. Therefore, in light of scarcity of both calibration and bathymetric data, caution should be exercised when interpreting model results in Lamèque.

It should be noted that wave effects, coastal erosion, and ice impacts were not incorporated into the community-scale modelling described in this report.

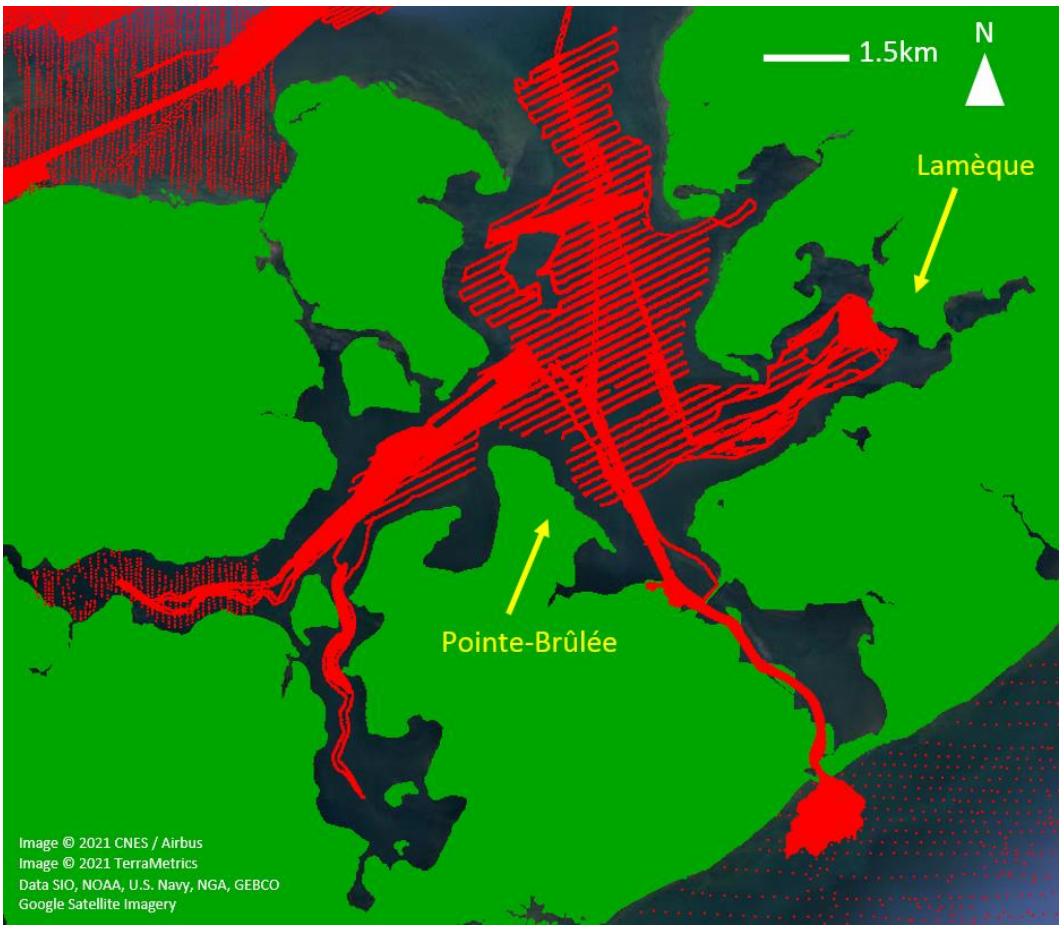

Figure 30. Available elevation data in the interior bays of the Acadian Peninsula. Topographic data points are shown in green (appear as a solid surface owing to the density of the data) and bathymetric data points are shown in red.

8 Hazard Event Development

A series of synthetic storm surge hazard events were developed to support risk-based analyses, based on an analysis of the tide gauge records. The analysis was comprised of two parts. First, peak storm surge values near the Acadian Peninsula were compared with water level residuals near the Escuminac and Belledune tide gauges to evaluate spatial autocorrelation (Section 8.1), as the basis for identifying which gauge to select as being representative of storm surges on the Acadian Peninsula. Second, statistical methods were applied to estimate annual exceedance probabilities (AEPs) for extreme water levels associated with storm surges (Section 8.2).

8.1 Tide Gauge Selection

Long-term tide gauge records are not available in the vicinity of the Acadian Peninsula, posing a challenge to direct estimation of extreme value statistics from measured water level data. The two closest tide gauges that have a substantial period of record include the Escuminac tide gauge and the Belledune tide gauge. As described in Section 4.3.1, the Escuminac gauge contains water level records from 1973 to present (~47 years) and the Belledune gauge contains water level measurements from 1999 to present (~20 years).

The two gauges are approximately equidistant from the Acadian Peninsula. As mentioned in Section 8, the data records used to support statistical analyses and hazard event development were truncated at September 13, 2019.

Environment Canada (2006) cautions that the distribution of storm surges and tides across the Gulf of Saint Lawrence varies considerably across the region. Therefore, a brief analysis was conducted to determine if one of the gauges is more-closely linked to the water levels experienced by the Acadian Peninsula during extreme events. The 51 largest storm surge events (those listed in Table 1 plus Hurricane Dorian) were identified for the Escuminac and Belledune tide gauges. Of the 51 identified events for each gauge, those that occurred after 1979 and did not coincide with significant ice cover or a post-tropical cyclone were simulated using the regional model. In total, 29 out of 51 events were simulated for the Escuminac guage and 22 out of 51 events were simulated for the Belledune gauge. Modelled peak storm surge (from the regional model) in the vicinity of Le Goulet, Shippagan, and Caraquet were compared to peak residuals recorded at the gauges. Modelled peak storm surge in the vicinity of Le Goulet, Shippagan, and Caraquet were also compared to modelled peak storm surge near the Escuminac and Belledune gauges. The results are shown in Figure 31 and Figure 32.

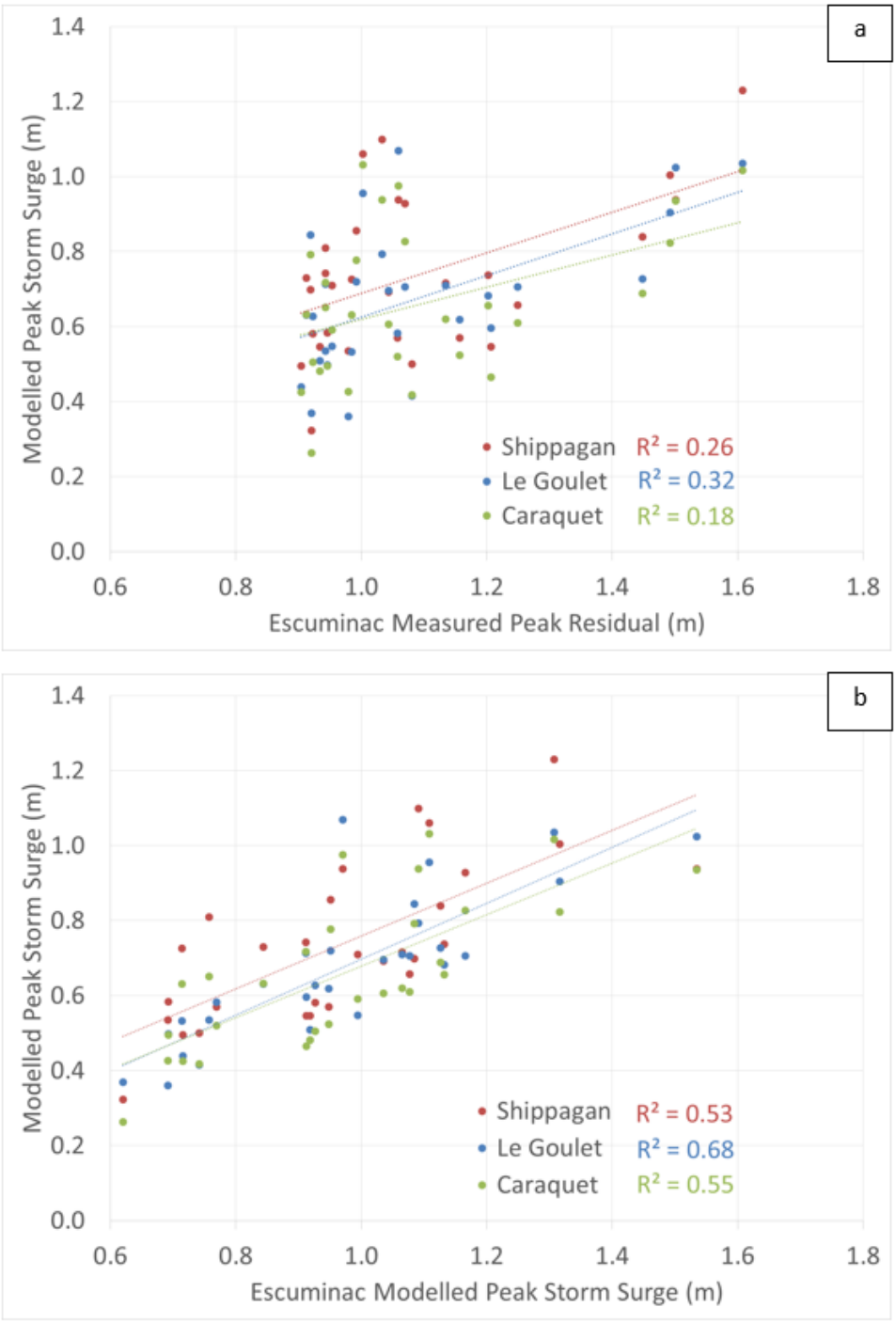

Figure 31. Relationship between modelled peak storm surge in the Acadian Peninsula versus measured peak residual (a) and modelled peak storm surge (b) at the Escuminac tide gauge.

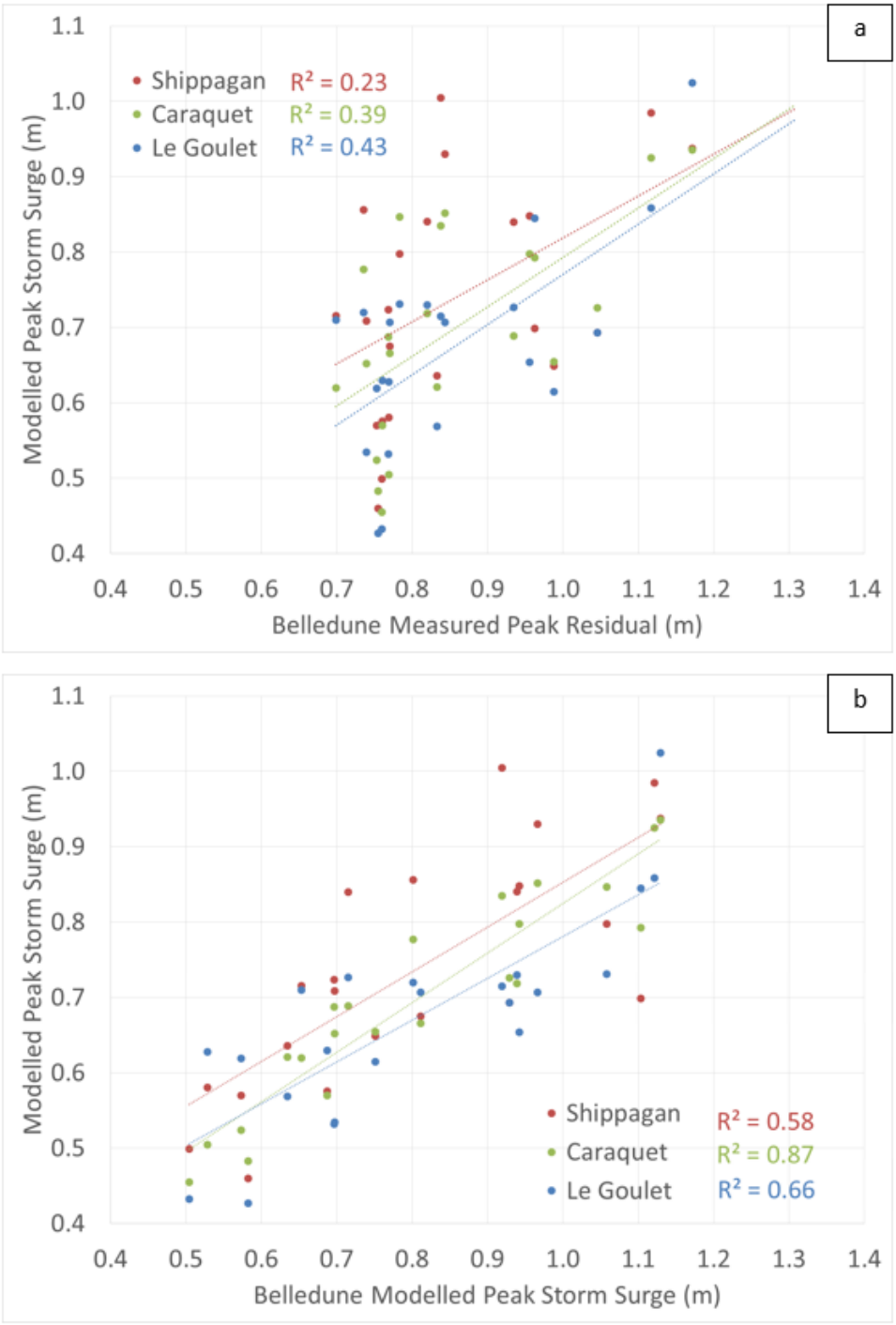

Figure 32. Relationship between modelled peak storm surge in the Acadian Peninsula versus measured peak residual (a) and modelled peak storm surge (b) at the Belledune tide gauge.

The computed coefficients of determination (R^2) suggest that there is a stronger autocorrelation between peak storm surges on the Acadian Peninsula and residuals at the Belledune tide gauge during extreme events. Comparing modelled results to measured data, peak residual magnitudes at the Belledune tide gauge explain 23-43% (R^2=0.23-0.43) of the variation in peak surge magnitudes experienced by the Acadian Peninsula, whereas the Escuminac tide gauge explains only 18-32% (R^2=0.18-0.32) of the variation. Therefore, the Belledune tide gauge record was selected as a basis for extreme value analyses to determine annual exceedance probabilities associated with different storm surge event magnitudes. It should be noted that modelled values presented in Figure 31 and Figure 32 represent storm surge only; no effort was made to incorporate wave set up into the modelling, nor was effort made to identify and remove events that may have produced large wave setup in the vicinity of the tide gauges. Wave effects could account for some of the data scatter shown in Figure 31a and Figure 32a, particularly for storms that produced large wave setup near the Escuminac or Belledune gauge. Comparing modelled results in the Acadian Peninsula to modelled results near the tide gauges, the coefficients of determination improve to 0.58-0.87 and 0.53-0.68 for Belledune and Escuminac, respectively.

Although the Escuminac gauge has a longer data record, it is worth noting that the gauge was not operational during the January 21, 2000 storm surge event which is the largest event recorded on the Belledune gauge, is widely regarded as one of the most significant events in the region, and is often selected as a benchmark reference for hazard assessment (Environment Canada, 2006; Robichaud et al., 2011). This lends further support to using the Belledune gauge to support extreme value analyses, as large event observations are crucial in shaping the tail of probability distribution fits to the data and, consequently, the return values assigned to low annual exceedance probability events.

8.2 Statistical Analysis of Tide Gauge Data

Because there are many combinations of tides, storm surge, and other contributing factors that influence coastal water levels, it is often challenging to establish representative storm events (Murphy et al., 2020). Some practitioners choose to adopt a conservative approach where representative storm surge events are modelled in combination with a characteristic high tide reference plane such as Higher High Water Large Tide (HHWLT) or Higher High Water Mean Tide (HHWMT) (Daigle, 2017; Fine & Thomson, 2021). Other methods aim to address, more-explicitly, the joint probability of the multiple contributing factors (Pugh & Vassie, 1980).

Several methods were used to estimate AEPs for extreme water levels caused by storm surge. Results were compared and assessed to produce final AEP estimates to support risk-based assessment of storm surge hazard in the Acadian Peninsula.

Fundamental to extreme value statistics is the assumption that the observed set of values, or the population sample, used to compute statistical metrics is derived by sampling from a homogeneous parent distribution such that values are independent and identically distributed (FEMA, 2016; Mazas & Hamm, 2011). A large majority of the largest storm surge events identified in the Escuminac and Belledune gauge records are associated with extratropical, winter storms (Section 4.3.3). Although, post-tropical cyclones (e.g. the remnants of hurricane storms) can pass through Gulf of Saint Lawrence with sufficient energy to drive large storm surges, they are responsible for only a small proportion of the largest surge events. Arguably, the extratropical winter storm events and post-tropical cyclone events that impact the Canadian Atlantic do not belong to the same parent distribution, owing to differences in origin and seasonality. There are also relatively few post-tropical storm-generated storm surges in the historical record, which makes it challenging

to develop reliable extreme value probability distributions for such events. In this study, post-tropical hurricane events were removed from the tide gauge records to focus only on extratropical winter storms, the main drivers of storm surge in the area of interest. Consequently, post-tropical cyclone events were not incorporated into the statistical analyses presented in the following chapters, unless otherwise stated.

8.2.1 Peaks-Over-Threshold Extreme Value Statistics

8.2.1.1 Storm Surges

A stationary extreme value analysis was applied to elucidate AEPs for storm surges at the Belledune tide gauge based on measured residuals (i.e. measured water levels minus the theoretical tide). Following procedures described in WAFO Group (2011) and Mazas and Hamm (2011), the residuals were analyzed using a peaks-over-threshold (POT) approach. The residuals were linearly detrended to remove the non-stationary contribution of relative sea-level rise. Detrended residuals were then declustered using a 48-hour minimum inter-event duration to isolate event maxima. An iterative process was used to identify a threshold for which declustered exceedances were well-described by the Generalized Pareto Distribution (GPD). A threshold of 0.68m was selected and 58 storm surge events were identified. Considering the period of record of the Belledune tide gauge, this equates to approximately 3 storm surge events per year of record, which is within the range recommended by Mazus and Hamm (2011). A GPD was fitted to the 58 storm surge events using methods from WAFO Group (2011) and was used to estimate storm surge magnitudes associated with key AEPs. The results of the analysis are shown in Figure 33.

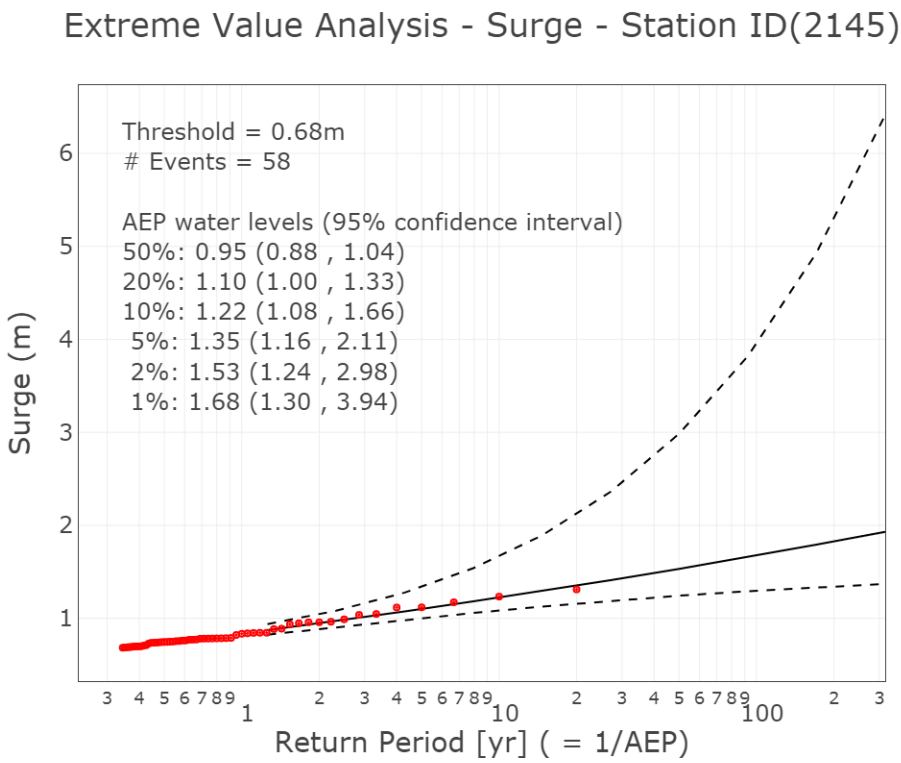

Figure 33. GPD fit to peak storm surge values recorded at the Belledune tide gauge and resulting storm surge estimates for key AEPs.

As discussed in Section 8.2, storm surges associated with post-tropical cyclones/hurricanes were excluded from the statistical analysis (Figure 33). Thirty-three post-tropical cyclones/occurred within the timespan of the Belledune gauge record; 3 events were missed by the gauge and the remaining 30 events were manually removed from the gauge record. To examine the sensitivity of the extreme value analysis to excluding these events from the sample dataset, the analysis was repeated, this time including post-tropical cyclone/hurricane events. Best fit return values for AEPs greater than 10% (i.e. smaller, more-common events) were unaltered (to within 2 decimal places) by the inclusion of the post-tropical cyclone/hurricane events. The best fit return value estimates for the 1% AEP increased by less than 2%. Thus, the inclusion or omission of post-tropical cyclones/hurricanes has a negligible impact on storm surge AEPs or return values estimates for AEPs lower than 1%. The results of this analysis are shown in Figure 34.

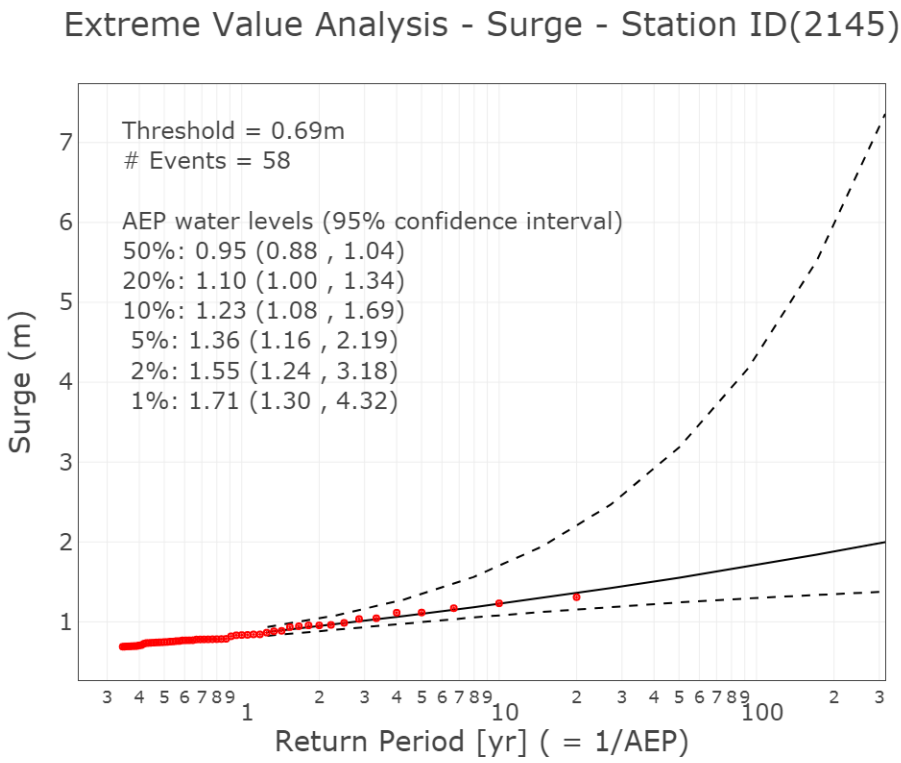

Figure 34. GPD fit to peak storm surge values recorded at the Belledune tide gauge, including post-tropical cyclone/hurricane events, and resulting storm surge estimates for key AEP events.

8.2.1.2 Water Levels

The POT statistical analysis described in Section 8.2.1.1 was repeated for total water levels recorded at the Belledune tide gauge, as opposed to the non-tidal residuals. Therefore, this analysis accounts for contributions from astronomical tides as well as residuals caused by storm surges and other contributing factors. Again, tropical cyclones/hurricane events were not included in the analysis. The results are shown in Figure 35 and water levels are referenced to MWL.

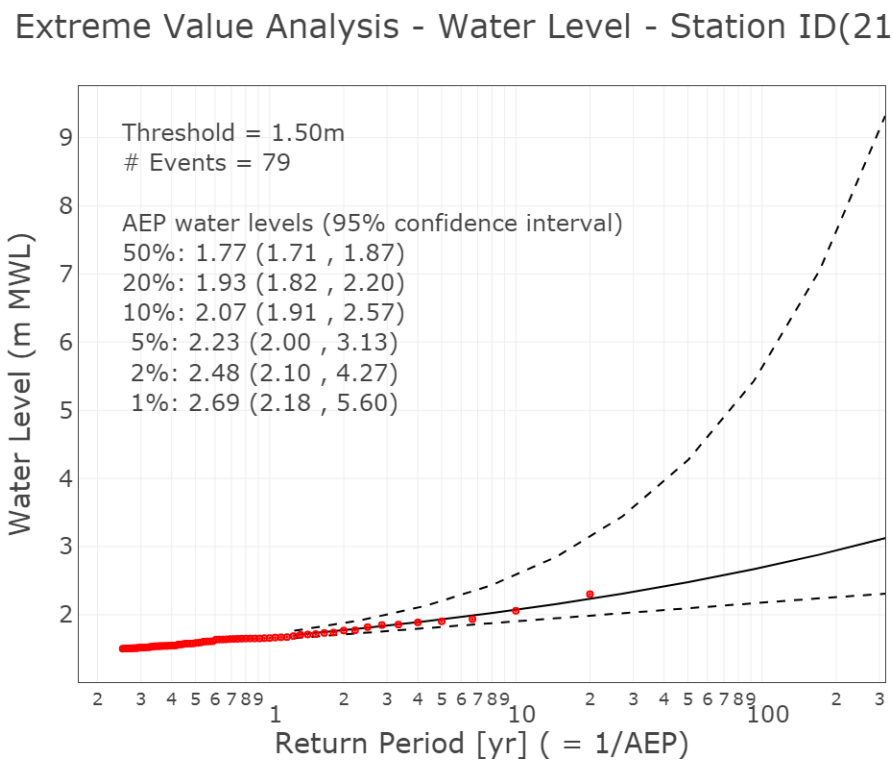

Figure 35. GPD fit to peak water levels recorded at the Belledune tide gauge and resulting estimates for key AEP events. Water levels are referenced to MWL.

8.2.2 Joint Probability of Tides and Storm Surge

Joint probability of tides and storm surge was investigated using methods presented by Pugh and Vassie (1980). In summary, the methods assume that tidal stage and storm surge are statistically independent from one another. Independent probability distribution functions are derived for the tidal stage and storm surge components, and the two functions are multiplied to establish probabilities associated with various water levels.

Following the methods presented by Pugh and Vassie (1980), dependence between storm surge and tidal stage at the Belledune gauge was investigated by plotting the standard deviation of residuals observed at the tide gauge versus the theoretical tidal stage computed using harmonic analysis (Figure 36). Each point represents the standard deviation of residuals observed at a given tidal stage. Only a small dependence was observed between storm surge and tidal stage at the Belledune gauge, with slightly larger residuals occurring at lower tidal stages. The two right-most points in Figure 36 are believed to be outliers and can be explained by a very small sample size of residuals coinciding with tidal stages within the range of 1.4m to 1.5m MWL; the standard deviation values associated with these two points represent 201 and 15 observations, respectively, out of a total of 164,209. For reference, the highest astronomical tide at the Belledune gauge is equal to 1.48m MWL. Based on this analysis, storm surge and tidal stage were assumed to be practically independent from one another at the Belledune gauge.

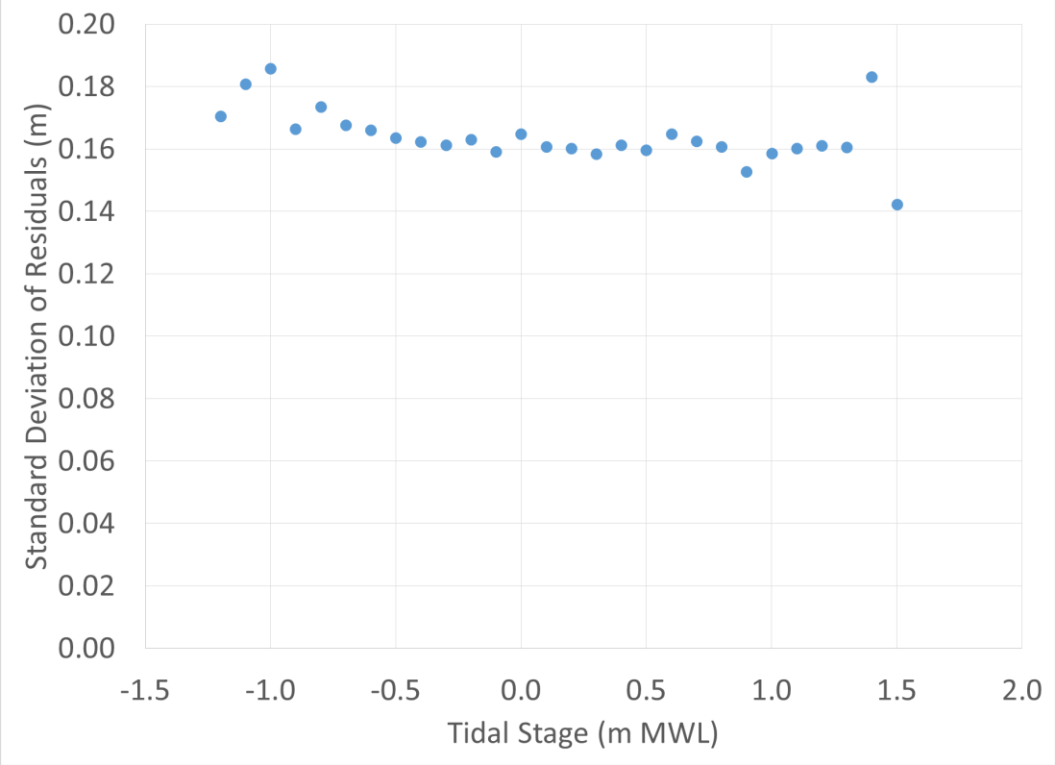

Figure 36. Relationship between standard deviation of residuals and tidal stage at the Belledune tide gauge.

The joint probability methods proposed by Pugh and Vassie (1980) require the practitioner to sort tidal stage values and residuals using a specified "bin" size. Sensitivity testing indicated that 0.1m bin sizes provided a good compromise between sample size and estimate precision. Smaller bin sizes did not significantly change the resulting estimates. Figure 37 shows the probability distribution of residuals and tidal stage values parcelled into 0.1m bins, respectively. The resulting AEP values for extreme water levels are shown in Table 7 and Figure 38.

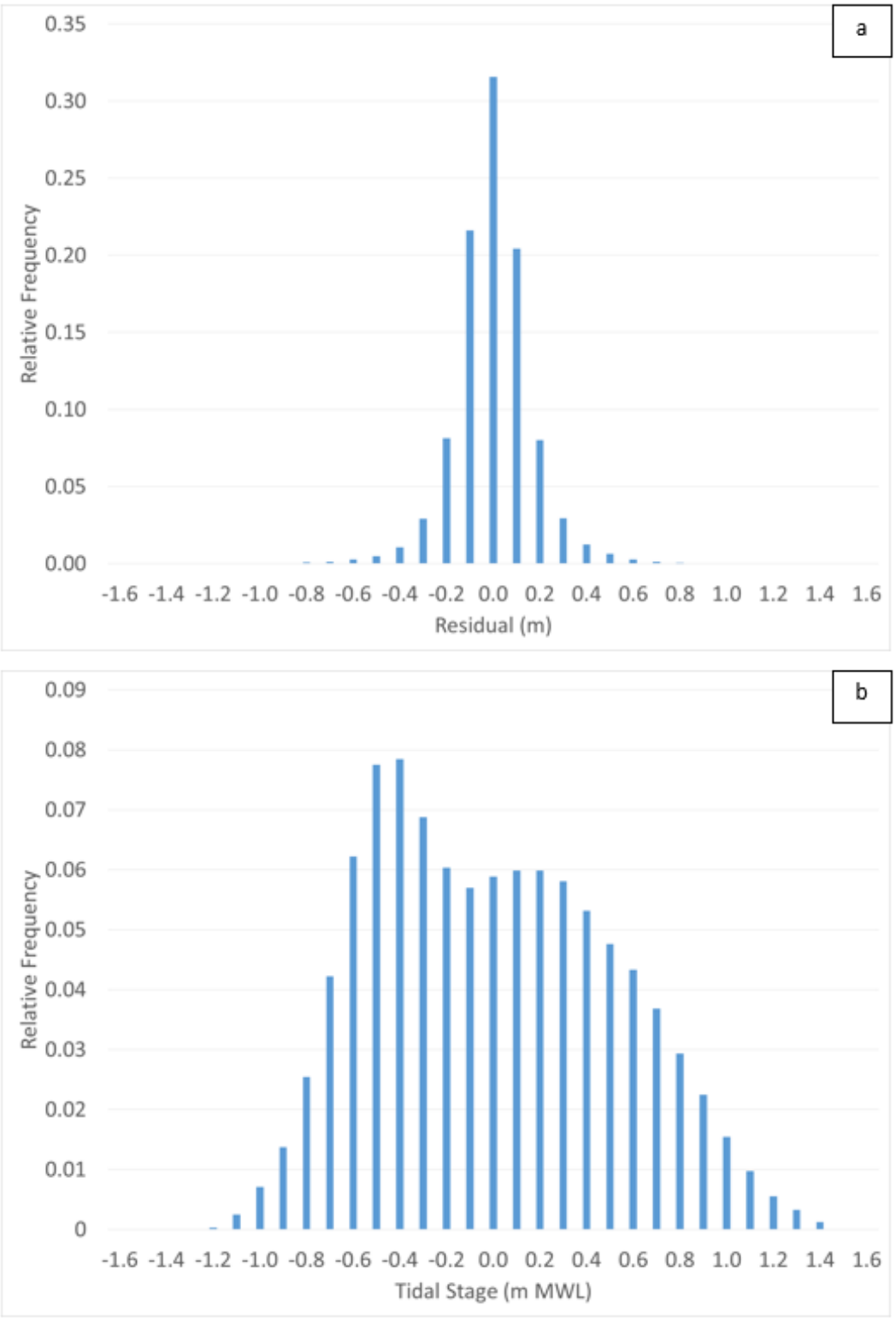

Figure 37. Probability distribution of residuals (a) and tidal stage (b) at the Belledune tide gauge.

Table 7. Annual Exceedance Probabilities for Water Levels Based on Joint Probability of Storm Surges and Tides

AEP	Water Level (m MWL)
50%	1.77
20%	1.91
10%	2.01
5%	2.10
2%	2.20
1%	2.27

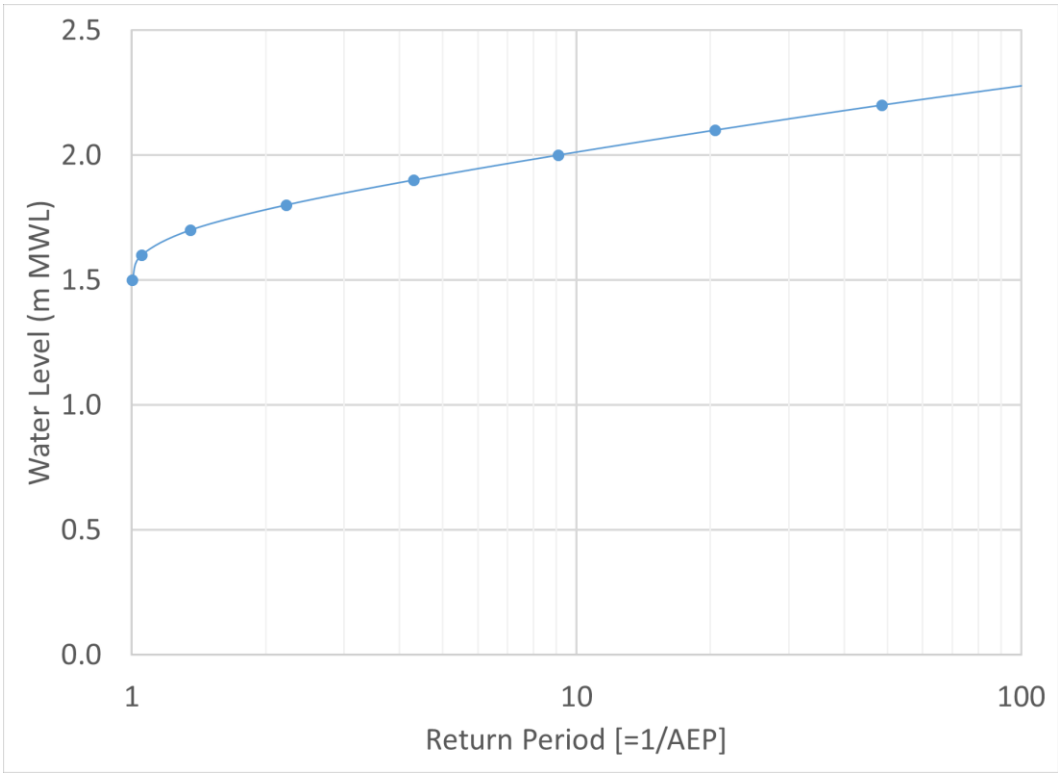

Figure 38. Plot of annual exceedance probabilities for water levels based on joint probability of storm surges and tides.

The joint probability process was repeated using methods presented by Pugh and Vassie (1980) to decluster residuals to avoid "double-counting" single storm surge events. Basically, the method assumes that the hourly time series of residuals are 1-dependant, such that each residual depends on the value preceding it. For events with AEP exceeding 2% (i.e. events that are smaller and more frequent than the 2% AEP event), the computed values were smaller than, but did not differ greatly from, those computed without the assumption of 1-dependance. Without accounting for 1-dependance, the extreme water level estimates for the 50%, 20%, 10%, and 5% AEP events exceeded those computed assuming 1-dependance by 0.04, 0.08, 0.11, and 0.12m, respectively.

8.3 Comparison with Previous Studies

Estimated storm surge return values at the Belledune tide gauge for various AEPs (discussed in Section 8.2) were compared with values estimated by Daigle (2017) for regions adjacent to the Belledune tide gauge. Daigle (2017) estimated extreme sea levels and storm surge for various Zones across the Province of New Brunswick based on values derived from a 40-year hindcast of storm surges in the Northwest Atlantic (Bernier, 2005; Environment Canada, 2006). Table 8 shows a comparison between the storm surge AEP estimates based on the POT statistical analysis of the Belledune gauge residuals, and the estimates by Daigle (2017) for Zone 1 and 2 (the Belledune gauge is located near the border between Zone 1 and Zone 2).

Table 8. Comparison of Storm Surge AEP Estimates

AEP	A. Storm Surge estimates based on analysis of Belledune gauge residuals (m)	B. Storm Surge estimates by Daigle (2017) for Zone1 and Zone 2 – Restigouche County to Grande-Anse, NB (m)	Difference [A - B] (m)
50%	0.95	0.70	0.25
20%	1.10	0.85	0.25
10%	1.22	0.97	0.25
5%	1.35	1.06*	0.29
4%	1.38*	1.11	0.27
2%	1.53	1.23	0.30
1%	1.68	1.34	0.34

* Linearly interpolated between return values for adjacent AEPs

As illustrated in Table 8, computed storm surge AEP estimates based on the analysis of the Belledune gauge records are larger than those estimated by Daigle (2017) for Zone 1 and Zone 2. A brief review of the hindcast model, which Daigle (2017) used as a basis for storm surge estimates, was conducted to further investigate this discrepancy. Storm surge return values estimates from the analysis of Belledune gauge residuals are approximately 30cm higher than values estimated by Daigle (2017) for adjacent regions. Available literature on the hindcast model does not explicitly discuss model performance near the Belledune gauge. However, the authors do assess the skill of the hindcast model at the Escuminac gauge. The observed difference is consistent with the approximately 30cm under-prediction of storm surge elevations by the hindcast model (reported near the Escuminac gauge) on which Daigle's (2017) estimates are based.

The HHWLT estimated from predicted tides at the Belledune gauge (1.44m MWL / 1.18 CGVD2013) is consistent with Daigle's (2017) estimates for Zone 1 (1.4m CGVD2013) and Zone 2 (0.9m CGVD2013). A HHWMT of 0.89m MWL (0.63m CGVD2013) was estimated from predicted tides at the Belledune gauge. Table 9 shows a comparison between the water level estimates from this study versus values proposed by Daigle (2017) based on statistical analysis of storm surge.Table 10 shows water level estimates based on statistical analysis of water level measurements and joint-probability of surges and tides.

Table 9. Storm Surge AEP Estimates plus Characteristic Tidal Planes

AEP	Belledune Tide Gauge Analysis		Daigle (2017) for Zone 1 [Surge + HHWLT] (m)	Daigle (2017) for Zone 2 [Surge + HHWLT] (m)
	Water Level [Storm Surge + HHWMT] (m)	Water Level [Storm Surge + HHWLT] (m)		
50%	1.84	2.39	2.36	1.86
20%	1.99	2.54	2.51	2.01
10%	2.11	2.66	2.63	2.13
5%	2.24	2.79	2.72*	2.22*
4%	2.27*	2.82*	2.77	2.27
2%	2.42	2.97	2.89	2.39
1%	2.57	3.12	3.00	2.50

* Values are linearly interpolated between adjacent return values

Table 10. Water Level AEP estimates (all values referenced to MWL)

AEP	Water Level (from extreme value analysis of records)	Water Level (from joint probability analysis of tides and surge)
50%	1.77	1.77
20%	1.93	1.91
10%	2.07	2.01
5%	2.23	2.10
4%	2.27*	2.12*
2%	2.48	2.20
1%	2.69	2.27

* Values are linearly interpolated between adjacent return values

As illustrated in Table 9 and Table 10, the water level estimates derived by adding storm surge to HHWMT and the estimates derived from the POT statistical analysis of water levels are quite close (average absolute and percent discrepancy of 0.05m and 2.33%, respectively). Of course, computed values based on HHWLT are 0.55m greater than those based on HHWMT (i.e. the difference between the two characteristic tidal planes). When compared to values proposed by Daigle (2017), computed values based on surge plus HHWMT, surge plus HHWLT, and POT analysis of water levels produced average absolute discrepancies of 0.24m, 0.30m, and 0.24m, respectively, and average percent discrepancies of 10.10%, 12.38%, and 10.24%, respectively. Values proposed by Daigle (2017) fell in between computed values based on HHWMT and HHWLT.

HHWMT represents the average of the higher high water tides observed each lunar day over period of 19 years (Forrester, 1983). Conversely, HHWLT is a more-extreme metric representing the average of the highest high waters encountered each year over a period of 19 years (Forrester, 1983). Water levels estimated from statistical analysis of storm surge plus HHWMT were similar to water levels estimated from statistical analysis of total water level records ($RMSE$=0.06m). Conversely, water levels estimated from statistical analysis of storm surge plus HHWLT exceeded those computed from statistical analysis of total water levels ($RMSE$=0.55m). This suggests that HHWMT is a more representative characteristic tidal

elevation than HHWLT when using simplified (additive) approaches to determine water level return values for this region.

The water level estimates derived from the joint probability analysis produced similar estimates to those derived by adding storm surge to HHWMT and those derived from the POT analysis of water levels for smaller AEP events. When compared to the joint-probability method, computed values based on surge plus HHWMT and POT analysis of water levels produced average absolute differences of 0.15m and 0.15m, respectively, and average percent differences of 7.12% and 6.97%, respectively. Eliminating events with AEPs lower than 5% (i.e. events that are larger and less frequent than the 5% AEP event), the average differences improved to 0.10m and 0.05m (4.88% and 2.56%), respectively.

8.4 Hazard Events

Six return value estimates for water level, each with a unique AEP spanning a range from 50% to 1%, were selected for subsequent hazard modelling. This ensured that a range of event magnitudes and likelihoods were captured in the hazard assessment so that results could be used to inform future risk assessment. In order to provide realistic, but somewhat conservative, estimates for extreme water levels, the estimates derived by adding storm surge and HHWMT and the estimates derived from the POT statistical analysis of water levels were adopted. The greater of the two estimates for each AEP were used as a basis for the hazard modelling. Table 11 presents the final estimates for extreme storm surges and water levels in the vicinity of the Belledune gauge for this study.

Table 11. Extreme Storm Surge and Water Level Estimates at the Belledune Tide gauge

AEP	Storm Surge (m)	Water Level (m MWL)
50%	0.95	1.84
20%	1.10	1.99
10%	1.22	2.11
5%	1.35	2.24
2%	1.53	2.48
1%	1.68	2.69

The present-day hazard events developed in this study are representative of a time frame spanning year-1999 to 2019 (i.e. the range of the tide gauge data from which the estimates were derived). As an approximate median, it may be assumed that the present-day hazard event estimates in this study represent an approximately year-2010 condition.

9 Synthetic Storm Surge Simulations

A total of 24 synthetic storm surge events were simulated using the calibrated and validated community-scale model described in Section 7, to represent events with defined AEPs. Six of the hazard events reflect storm surge hazard during present-day conditions, each with a unique likelihood (or AEP) conforming to those shown in Table 11. The remaining 18 hazard events reflect storm surge hazards at future time horizons, incorporating the effects of relative sea-level rise. All 24 simulations were conducted using digital elevation data (bathymetry and topography) representative of year-2018.

9.1 Scaling Storm Events

The six simulations for present-day events were conducted assuming a base tidal stage of 0.9m MWL, representative of HHWMT at the Belledune tide gauge.

The January 21, 2000 event was selected as the basis for generating synthetic wind and atmospheric pressure fields because it produced the largest observed water level residual at the Belledune gauge. Furthermore, the January 21, 2000 event is widely regarded as one of the most significant events in the region, and is often selected as a benchmark reference for hazard assessment (Environment Canada, 2006; Robichaud et al., 2011). It should be noted, however, that the January 21, 2000 event coincided with sea-ice conditions, which are not incorporated into the regional or community-scale synthetic storm surge simulations.

Using the January 21, 2000 event as a foundation, wind speeds were iteratively adjusted until the regional model produced peak water levels in the vicinity of the Belledune tide gauge coinciding with those listed in Table 11. Once suitable regional simulations were achieved for the six storm surge hazard events, modelling was conducted at the community-scale to simulate coastal flooding in the Acadian Peninsula.

9.2 Modelling Relative Sea-Level Rise

Each synthetic storm surge event, with AEPs as listed in Table 11, was simulated under three future relative sea-level rise scenarios, as described in Section 4.8. Relative sea-level rise was integrated into the model by adjusting the model bathymetry and topography. For the future sea-level rise events, the wind and atmospheric pressure forcings applied for the synthetic storm surge events were identical to those for the present-day sea-level events described in Section 9.1. This approach assumes no changes in extreme value probability distributions of wind and atmospheric pressure over the time horizons associated with the sea-level rise scenarios. As reported in Greenan et al. (2018), significant trends in winds and storminess have not be found for most marine areas of Canada owing, in part, to limited data and natural variability. Evidence indicates a modest projected decrease in future wind speeds in Atlantic Canada; however, the findings are reported with low-confidence.

9.3 Results

The results of the hydrodynamic modelling provide information regarding flood extent, flood depths, and flow velocities. Furthermore, the results provide information regarding spatial and temporal variation (i.e. movement of flood water over the land during the storm surge event and the duration of flooding). Appendices D through F contain figures summarizing model results, including:

- Flood hazard under present-day conditions (Appendix D)
- Flood hazard under future conditions accounting for potential sea-level rise (Appendix E)
- Flow-induced hazard under present-day conditions and future conditions accounting for potential sea-level rise (Appendix F)

The peak values shown in Appendix D, E, and F indicate maximum values encountered over the duration of the simulations, excluding the first 24 hours of simulation time which were discarded (i.e. model spin-up). All synthetic event simulations were initiated approximately 3 days prior to the peak surge. Similar to the calibration process described in Section 7.3, it was assumed that a flood depth of 5cm represented a

suitable lower-threshold from which to extract flood hazard metrics such as depth and flood extent. Therefore peak flood depths less than 5cm were disregarded when evaluating flood hazard.

9.3.1 Present-Day Flood Hazard

9.3.1.1 Maisonnette

Results show that some buildings and infrastructure become exposed to flood hazards during common storm surge events with AEPs of 50% and 20%. However, exposure to flood hazards is restricted to buildings abutting the coast. For larger and rarer events (AEP<10%), model results indicate flooding over Route 303, westward (and in the vicinity) of the intersection with Route 320 (Figure 39), along with more-extensive flooding of coastal infrastructure. In addition, model results for the 1% AEP storm surge event indicate flooding over Route 303 east of the intersection with Chemin Olivier.

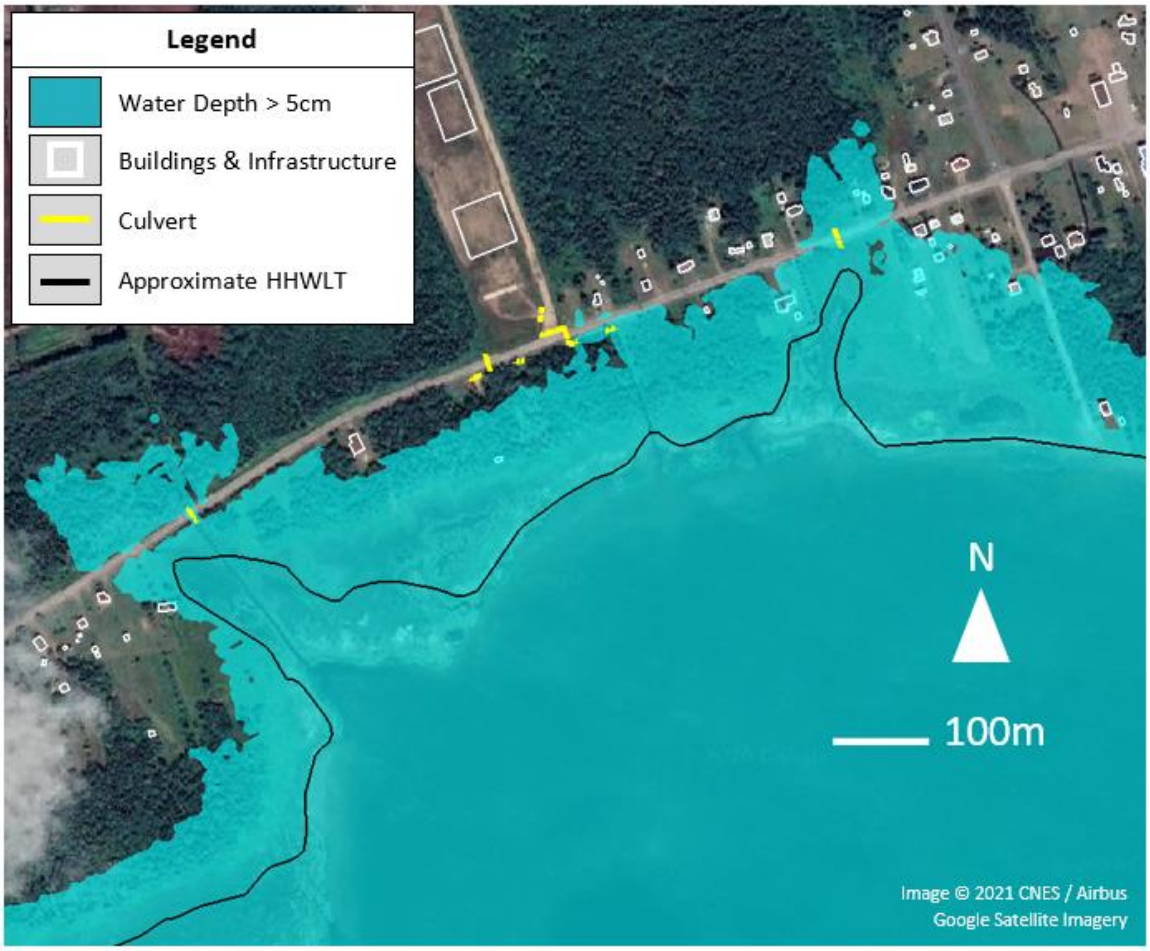

Figure 39. Flood hazard caused by the 10% AEP event in Maisonnette near Route 303 west of the intersection with Route 320.

9.3.1.2 Caraquet

Model results indicate that coastal infrastructure in Caraquet is generally not exposed to storm surge-driven flood hazards for events smaller, and more-common, than the 10% AEP event. Model results indicate that buildings and infrastructure are exposed to flood hazards for events with AEPs less than or equal to 10%. However, exposure to flood hazards is localized to the eastern portion of the Caraquet Port as well as Route 145 eastward of the intersection with Rue de la Saline.

Figure 40. Flood hazard caused by the 1% AEP event in Caraquet near Route 145 eastward of the intersection with Rue de la Saline.

9.3.1.3 Bas-Caraquet

Model results indicate that common events, such as the 50% AEP event, cause flooding over Route 145 east of Bas-Caraquet near the causeway/bridge-crossing (Figure 41). The results for the 50% AEP event also indicate that infrastructure are exposed to flood hazards near the Route 145 causeway/bridge-crossing as well as the Bas-Caraquet Marina. The results for larger and rarer events indicate that infrastructure abutting the coast are exposed to flood hazards. The results for the 2% and 1% AEP events indicate flooding in the vicinity of the low-lying wetland in the middle of the community.

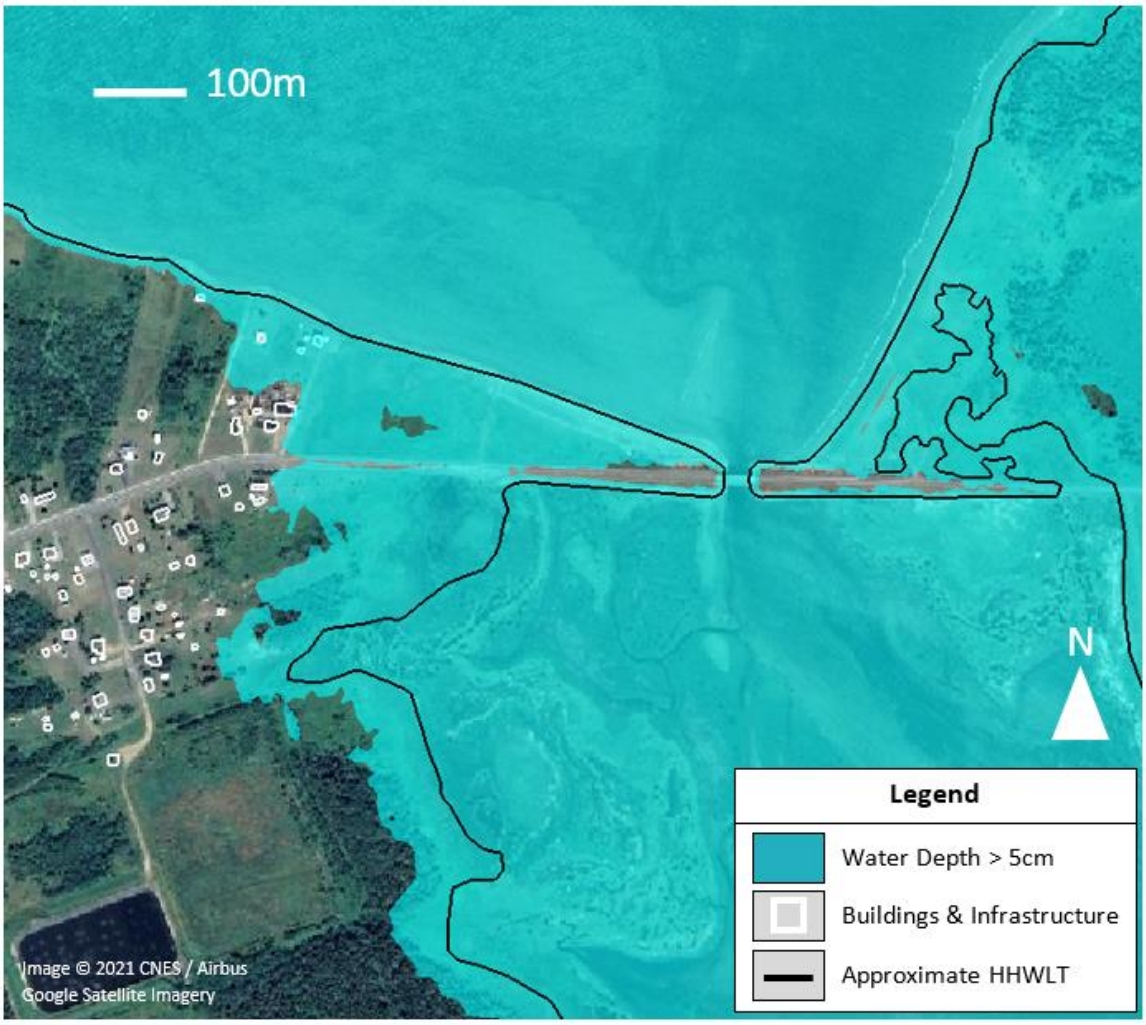

Figure 41. Flood hazard caused by the 50% AEP event near the Route 145 causeway/bridge-crossing on the east side of Bas-Caraquet.

9.3.1.4 Shippagan and Pointe-Brûlée

Model results for the 50% AEP event indicate flooding in the south-eastern portion of Shippagan, including flooding over the causeway connecting Shippagan to Savoy Landing, and Boulevard J.D. Gauthier southeastward of the intersection with Rue 17. The same event appears to produce extensive flooding in Pointe-Brûlée, exposing infrastructure on the west, north and east coast of the peninsula to flood hazard. For larger and rarer events (AEP<50%), the model results indicate flooding of: portions of northwestern Shippagan abutting the coast; areas southward of Boulevard J.D. Gauthier between the intersections with Rue Mallet and Rue Audet; and Rue Pointe-Brûlée near the intersection with Boulevard J.D. Gauthier. Model results indicate that Boulevard J.D. Gauthier is exposed to flood hazard between the intersections with Rue Mallet and Rue Audet for events equal to, and larger than, the 10% AEP event (Figure 42). Flooding over Boulevard J.D. Gauthier in central Shippagan is observed for modelled events equal to, and larger than, the 2% AEP event.

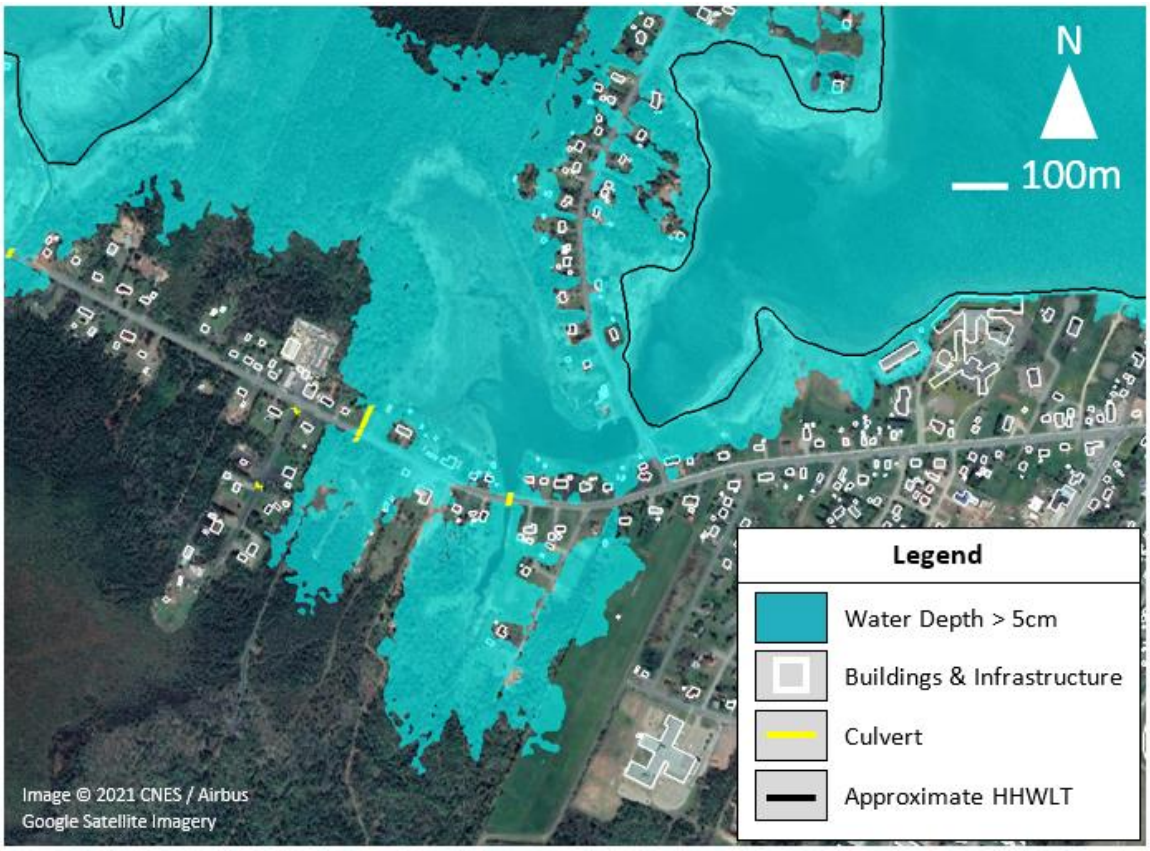

Figure 42. Flood hazard caused by the 10% AEP event near the intersection of Rue Pointe-Brûlée and Boulevard J.D. Gauthier. Flooding is observed over Boulevard J.D. Gauthier between the intersections with Rue Mallet and Rue Audet.

9.3.1.5 Le Goulet

Model results for the 50% AEP event indicate flooding in Le Goulet, particularly for areas located closest to the coast (i.e. areas seaward of Rue Principale and Avenue Du Portage). For larger and rarer events (AEP<50%), the model results indicate more extensive flooding; buildings and infrastructure landward of Rue Principale and Avenue Du Portage become exposed to flood water. Model results for the 20% AEP event indicate flooding of Rue Principale in the eastern portion of the community, eastward of the intersection with Rue Acadie. Model results for the 10% AEP event indicate flooding of Avenue Du Portage in the western portion of the community. Model results for the 2% and 1% AEP events indicate extensive flooding of Rue Principale and Avenue Du Portage (Figure 43).

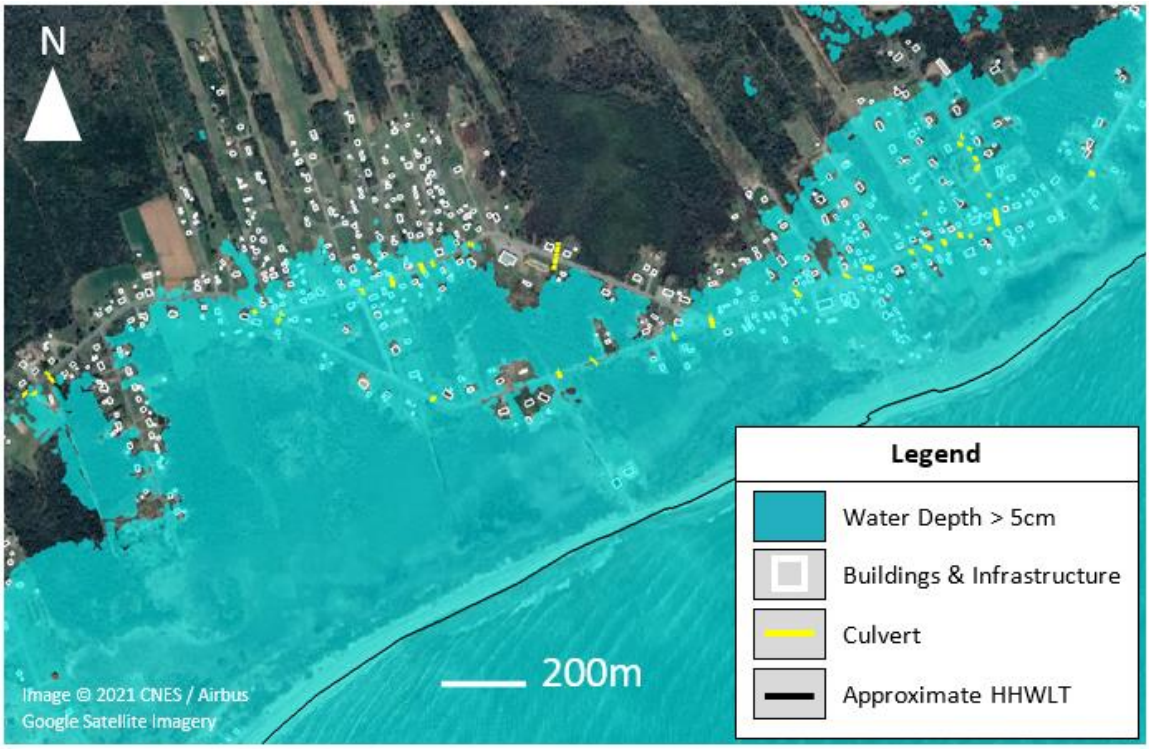

Figure 43. Flood hazard caused by the 1% AEP event in Le Goulet.

9.3.1.6 Lamèque

Model results for the 50% AEP event indicate generally low flood hazard in Lamèque, aside from some localized flooding near the port and the southern extent of Rue du Pêcheur where it meets the coast. Model results for the 10% AEP event indicate more extensive flooding near the port and Rue du Pêcheur, as well as some exposure to flood hazard for buildings adjacent to Route 313 in the northwestern portion of the community. Model results for the 2% and 1% AEP events indicate exposure to flood hazard for buildings adjacent to Route 113 in the eastern portion of the community and flooding of the Route 313 causeway connecting Lamèque to Pointe-Alexandre.

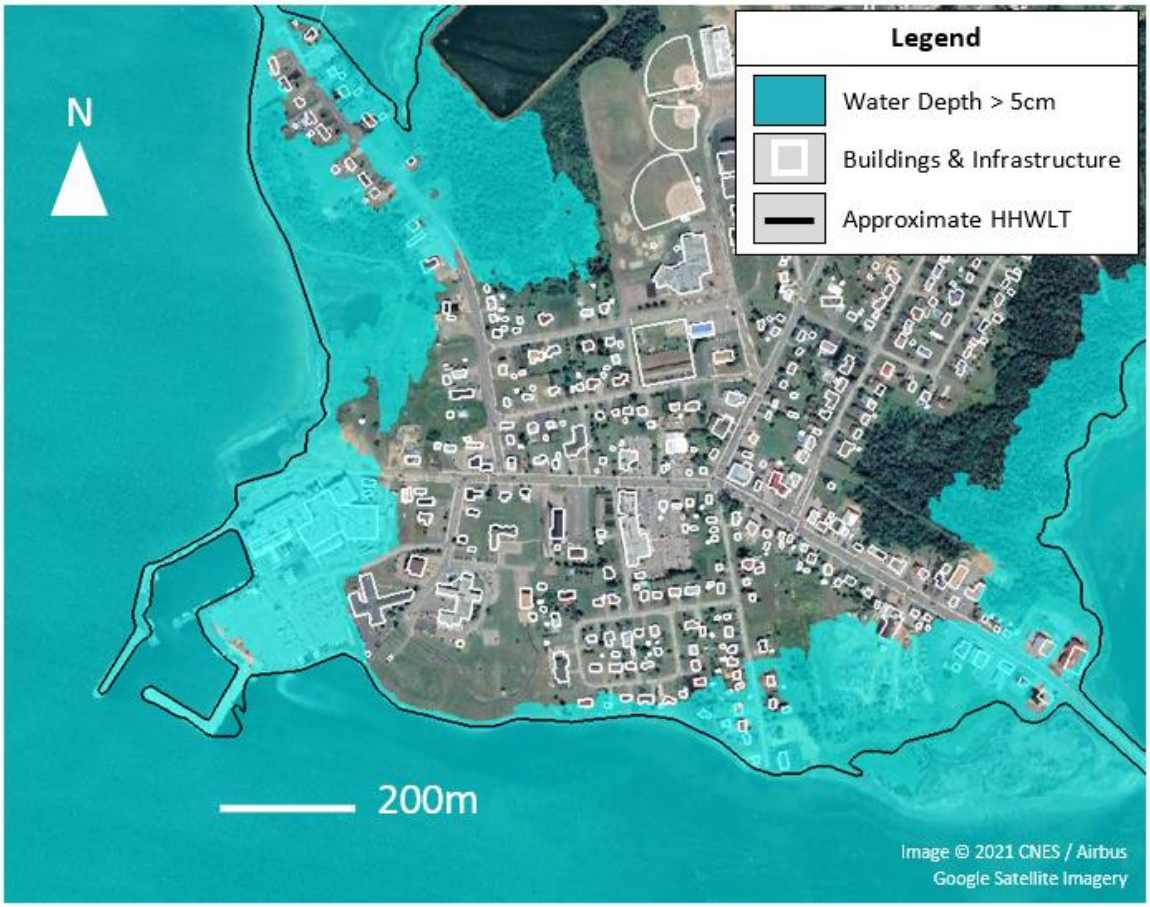

Figure 44. Flood hazard caused by the 1% AEP event in Lamèque.

9.3.2 Future Flood Hazard Accounting for Sea-Level Rise

The severity of simulated flood hazards (as represented by inundation extents, peak water depths, and flow velocities) for future sea level events exceeded the severity observed for the corresponding present-day sea level events. A comparison of maximum flood extents produced by future events and present-day events (discussed in Section 9.3.1) was conducted based on qualitative, visual observation of model results. Table 12 indicates future and present-day events that produced similar flood extents.

Table 12. Present-Day and Future Flood Hazard Events that Produced similar Flooding

Community	Water Level AEP (Present-Day Event)	Water Level AEP Resulting in Comparable Maximum Flood Extent under Future Sea Level Scenarios		
		0.5m GSLR	1.0m GSLR	2.0 m GSLR
Maisonnette	50%	-	-	-
	20%	-	-	-
	10%	-	-	-
	5%	50%	-	-
	2%	20%	-	-
	1%	10%	-	-
Caraquet	50%	-	-	-
	20%	-	-	-
	10%	-	-	-
	5%	50%	-	-
	2%	20%	-	-
	1%	10%	50%	-
Bas-Caraquet	50%	-	-	-
	20%	-	-	-
	10%	-	-	-
	5%	50%	-	-
	2%	20%	-	-
	1%	10%	50%	-
Shippagan and Point-Bûlée	50%	-	-	-
	20%	-	-	-
	10%	-	-	-
	5%	-	-	-
	2%	20%	-	-
	1%	10%	50%	-
Le Goulet	50%	-	-	-
	20%	-	-	-
	10%	-	-	-
	5%	-	-	-
	2%	50%	-	-
	1%	10%	-	-
Lamèque	50%	-	-	-
	20%	-	-	-
	10%	-	-	-
	5%	-	-	-
	2%	50%	-	-
	1%	10%	50%	-

* Dashes (-) indicate conditions where flooding associated with the 50% AEP event (and larger) for a given GSLR condition exceeded flooding observed for the associated present-day event.

As indicated in Table 12, the highest AEP flood hazard event investigated in this study for the 0.5m future global sea-level rise scenario (50% AEP – 0.5m GSLR) produced more flooding than the present-day 10% AEP event in all locations. Modelled maximum flood extents for the present-day 5% AEP event were comparable to a future 50% AEP accounting for 0.5m of GSLR in Maisonnette, Caraquet, and Bas-Caraquet. Modelled maximum flood extents for the present-day 2% AEP event were comparable to a future 20% AEP event accounting for 0.5m of GSLR in Maisonnete, Caraquet, Bas-Caraquet, Shippagan, and Pointe-Brûlée. In Le Goulet and Lamèque, modelled maximum flood extents for the present-day 2% AEP event were comparable to a future 50% AEP event accounting for 0.5m of GSLR. In all of the communities included in this study, modelled maximum flood extents for the present-day 1% AEP event were comparable to a future 10% AEP event accounting for 0.5m of GLSR. In Caraquet, Bas-Caraquet, Shippagan, Pointe-Brûlée, and Lamèque, modelled maximum flood extents for the present-day 1% AEP event were also comparable to a future 50% AEP event accounting for 1.0m of GSLR.

9.3.3 Flow Hazard

Model results were compared to flow hazard metrics pertaining to pedestrian safety and building damage. Cox et al. (2010) present criteria for pedestrian safety (i.e. thresholds for stability) as a function of depth-velocity product (DV). In their report, safety criteria are presented for three groups: infants, small children, and frail/older persons; children; and adults. FEMA (2021) present criteria for structural damage as a function of momentum flux (depth multiplied by velocity-squared, or DV^2) for various building construction types. It is important to note that the criteria presented by FEMA (2021) are intended to support analyses for tsunami generated flow. However, the criteria were adopted to support analyses in this study where flows are generated by storm surge. Additionally, it should be noted that wave effects were not included in the hazard modelling, which could induce additional hazard.

9.3.3.1 Pedestrian Safety

The following list summarizes safety criteria from Cox et al. (2010):

- Infants, small children, and frail/older persons:
  - DV > $0m^2/s$: Extreme Hazard
- Children:
  - $0m^2/s$ < DV < $0.4\ m^2/s$: Low Hazard
  - $0.4m^2/s$ < DV <$0.6m^2/s$: Significant Hazard
  - DV > $0.6m^2/s$: Extreme Hazard
- Adults:
  - $0m^2/s$ < DV < $0.6m^2/s$: Low Hazard
  - $0.6m^2/s$ < DV < $0.8m^2/s$: Moderate Hazard
  - $0.8m^2/s$ < DV < $1.2m^2/s$: Significant Hazard
  - DV > $1.2m^2/s$: Extreme Hazard

Maximum depth-velocity product values were extracted from model results for the present-day 1% AEP event and compared to the above-listed criteria to interpret potential flow-induced hazard. In general, model results indicate that flow-induced hazard to able-bodied adults and older children is quite low in the communities included in this study. In most locations, depth-velocity product did not exceed $0.4m^2/s$, representing low hazard to children and adults, albeit, an extreme hazard to infants, small children, and frail/older persons. It is worth noting that any depth-velocity product exceeding $0m^2/s$ represents an extreme hazard to infants, small children, and frail/older persons. It is important to note that wave effects were not included in the hazard modelling, which could induce additional hazard to stability.

Model results indicate three locations where flows may exceed “low hazard” for adult stability for the tested present-day events: the Route 145 causeway/bridge-crossing on the east side of Bas-Caraquet (Figure 45), the Route 113 causeway connecting Shippagan to Savoy Landing and the Route 313 causeway connecting Lamèque to Pointe-Alexandre. Maximum depth-velocity product values for these three locations are shown in detail in Appendix F for each present-day event. When interpreting results shown in Appendix F, it is important to note that depth-velocity product values shown in the vicinity of bridge crossings or culverts indicate the depth-velocity product of flow under the bridge crossing or through the culvert, and not the depth-velocity product of flow over the road.

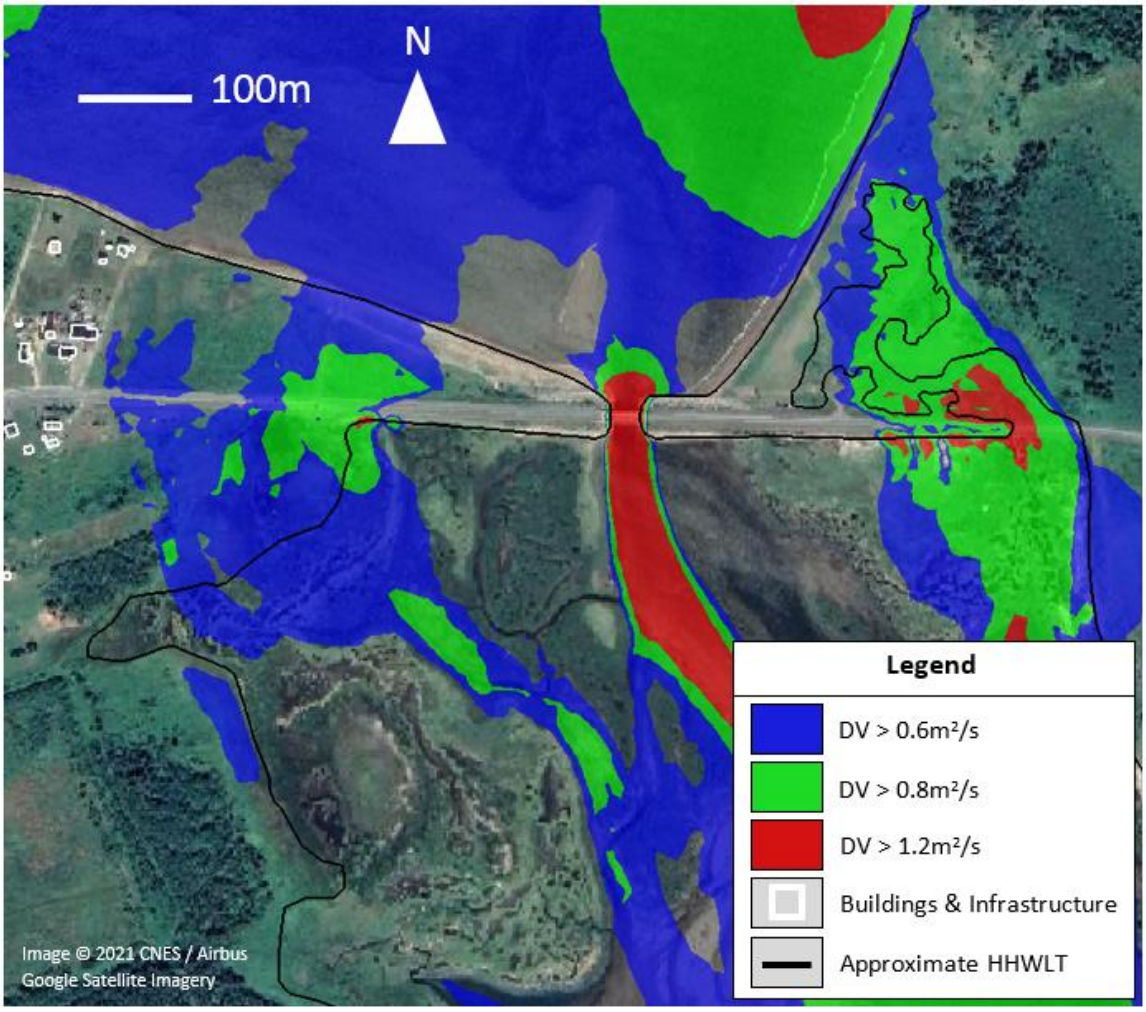

Figure 45. Depth-velocity product for the 1% AEP event near the Route 145 causeway/bridge-crossing on the east side of Bas-Caraquet.

9.3.3.2 Structural Damages

Adopting pre-code seismic design criteria (i.e. the most-conservative design criteria) from FEMA (2021), flows that generate momentum flux exceeding $7.0 m^3/s^2$ and $0.45 m^3/s^2$ have potential to cause structural damage to wood-frame buildings and mobile homes, respectively.

Maximum momentum flux values were extracted from modelled results for the present-day 1% AEP event and the future 1% AEP event accounting for 2.0m GSLR. The present-day 1% AEP event did not produce momentum flux exceeding $7.0m^3/s^2$ at any community investigated in this study. The future 1% AEP event accounting for 2.0m GSLR produced momentum flux exceeding $7.0m^3/s^2$ at only one location, over the causeway connecting Shippagan and Savoy Landing. Therefore, model results suggest that present-day and future storm surge events likely do not produce flows capable of flow-induced structural damage to wood-frame buildings. This, of course, should not be confused with damages associated with flood depth, exposure to flood water, or exposure to waves (not included in the hazard modelling).

The present-day 1% AEP event produced momentum flux exceeding $0.45m^3/s^2$ in three locations: the Route 145 causeway/bridge-crossing on the east side of Bas-Caraquet (Figure 46), the Route 113 causeway connecting Shippagan to Savoy Landing, and the Route 313 causeway connecting Lamèque to Pointe-Alexandre. The future 1% AEP event accounting for 2.0m GSLR produced momentum flux exceeding $0.45m^3/s^2$ in portions of Pointe-Brûlée, Shippagan, Le Goulet, and Lamèque. These results are shown in Appendix F. Therefore, model results suggest that, under present-day sea level conditions, the simulated storm surge-driven overland flooding does not produce flows capable of flow-induced structural damage to mobile homes (except for some localized areas mentioned above). However, flow-induced damage to mobile homes may be possible under future conditions.

Figure 46. Momentum flux exceeding $0.45m^3/s^2$ for the 1% AEP event near the Route 113 causeway connecting Shippagan to Savoy Landing.

10 Discussion

10.1 Comparison with Bathtub Modelling

Peak flood extents estimated from numerical hydrodynamic modelling were compared with bathtub modelling results (see Section 3) presented by Robichaud, et al. (2011) and Aubé at al. (2016).

10.1.1 Le Goulet

Robichaud et al. (2011) show a map indicating flood extent coinciding with a 2.4m (CGVD28) water surface elevation. They estimate that the flood stage is representative of a 100-year (1% AEP) storm surge event in year-2000 or a 50-year (2% AEP) storm surge event in year-2025. Therefore, the flood map developed by Robichaud et al. (2011) was compared to the present-day 1% AEP and 2% AEP hazard events modelled in this study. Figure 47 shows a comparison between the flood map produced by Robichaud et al. (2011) and the peak flood extents estimated from the community-scale model. It is important to note that the inundation extent shown by Robichaud et al. (2011) uses topography representative of a year-2009 condition, whereas the synthetic event simulations in this study use topography representative of year-2018.

As illustrated in Figure 47, the flood extent estimated by Robichaud et al. (2011) closely matches the modelled flood extent for the 2% AEP event. The modelled flood extent for the 1% AEP event exceeds the flood extent proposed by Robichaud et al. (2011); however, this is expected owing to the differences in representative year.

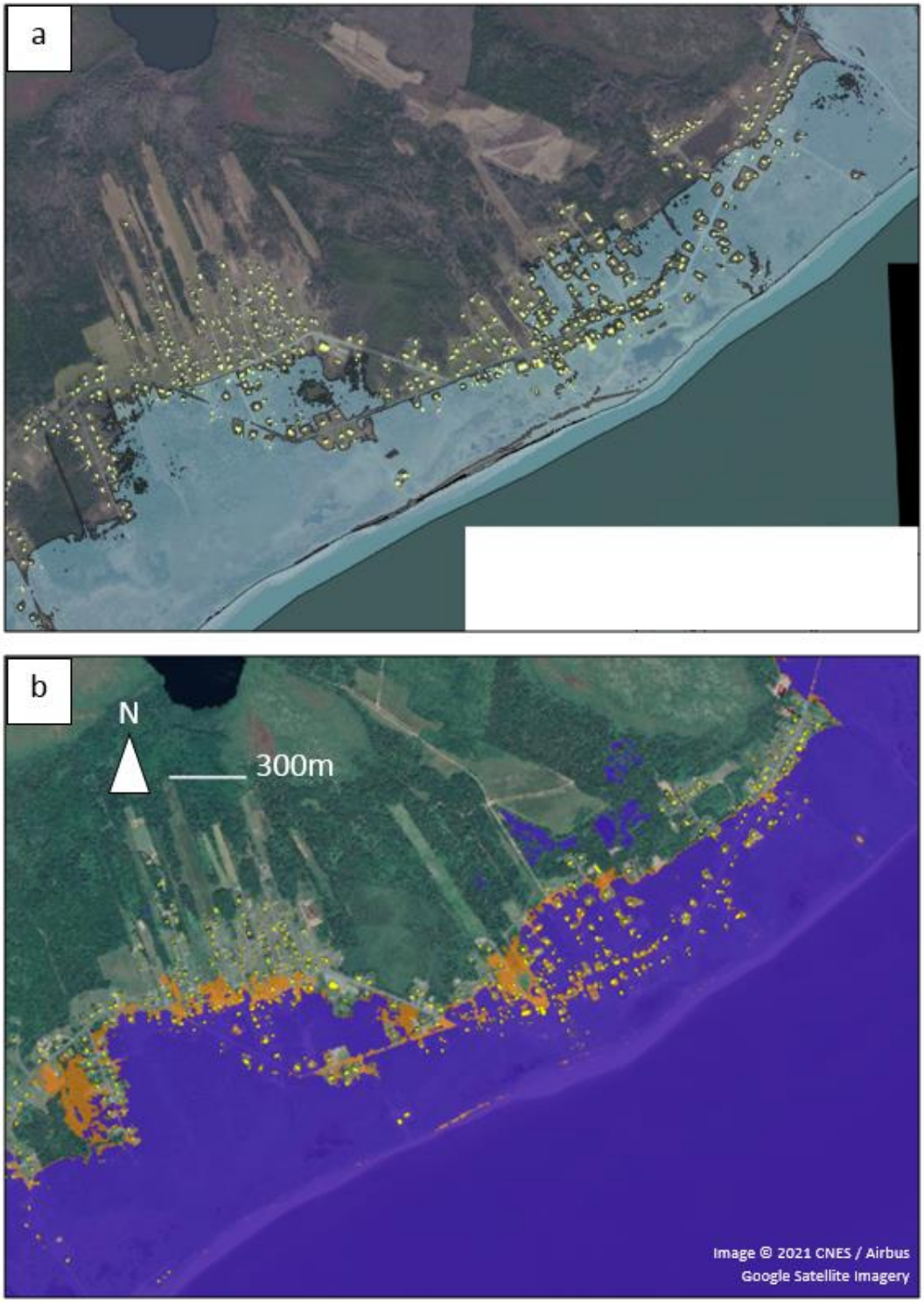

Figure 47. Comparison of flood extents estimated from (a) bathtub modelling conducted by Robichaud et al. (2011) and (b) numerical hydrodynamic modelling in Le Goulet. The area shaded in blue in (a) indicates the flood extent estimated for a 100-year (1% AEP) event in year-2000 or a 50-year (2% AEP) event in year-2025. The area shaded in purple in (b) indicates the flood extent of a 2% AEP event during approximately present-day conditions, and the area shaded in orange indicates the flood extent of a 1% AEP event during approximately present-day conditions.

10.1.2 Shippagan

Robichaud et al. (2011) show a flood map indicating flood extent coinciding with a 2.4m (CGVD28) water surface elevation for Shippagan. They estimate that the flood stage is representative of a 10-year (10% AEP) storm surge event in year-2000 or a 5-year (20% AEP) storm surge event in year-2025. Therefore, the flood map developed by Robichaud et al. (2011) was compared to the present-day 10% AEP and 20% AEP hazard events modelled in this study. Figure 48 shows a comparison between the flood map produced by Robichaud et al. (2011) and the peak flood extents estimated from the community scale model.

The 10% AEP flood extent estimated by Robichaud et al. (2011) using the bathtub modelling approach lies somewhere between the hydrodynamically modelled flood extents for the 10% AEP and 20% AEP events in the eastern portion of Shippagan. Along Rue Pointe-Brûlée (in the western portion of Shippagan), the flood extent estimated by Robichaud et al. (2011) closely resembles the hydrodynamically modelled flood extent for the 20% AEP event, and is exceeded by the dynamically modelled flood extent for the 10% AEP event. However, the flood extent estimated by Robichaud et al. (2011) is more-aligned with the dynamically modelled flood extent for the 10% AEP event for areas in the western portion of Shippagan south of Boulevard J.D. Gauthier.

The hydrodynamically modelled flood extents for the 10% AEP and 20% AEP events both exceed the extent proposed by Robichaud et al. (2011) in a small area west of the marina. This can perhaps be explained by differences in resolution between the bathtub modelling and the hydrodynamic modelling. Bathtub modelling is less computationally demanding than hydrodynamic modelling, and is therefore more conducive to fine-resolution investigation of flood depths and flood extents. Including fine-resolution features such as sea-walls and other structures is quite straightforward in bathtub modelling, but can be very taxing on computational demand for hydrodynamic modelling. Robichaud et al. (2011) were able to model inundation while maintaining fine-resolution elevation details. However, the hydrodynamic modelling in this study was conducted using a 10-m resolution computational mesh causing some fine-detail features to be artificially “smoothed-out” in the model domain. At the location in question, there is a boardwalk and some structural reinforcement along the coastline. It is speculated that the overestimation of flooding produced by the hydrodynamic model is caused by an artificial “smoothing” of these structural features in the model domain. Therefore, for this specific location and situation, the bathtub modelling approach likely provides a better estimate for flood extent compared to the hydrodynamic modelling approach. However, the bathtub modelling does not allow for spatial and temporal flood propagation, flow velocity (and flow hazard metrics), and flood durations to be assessed.

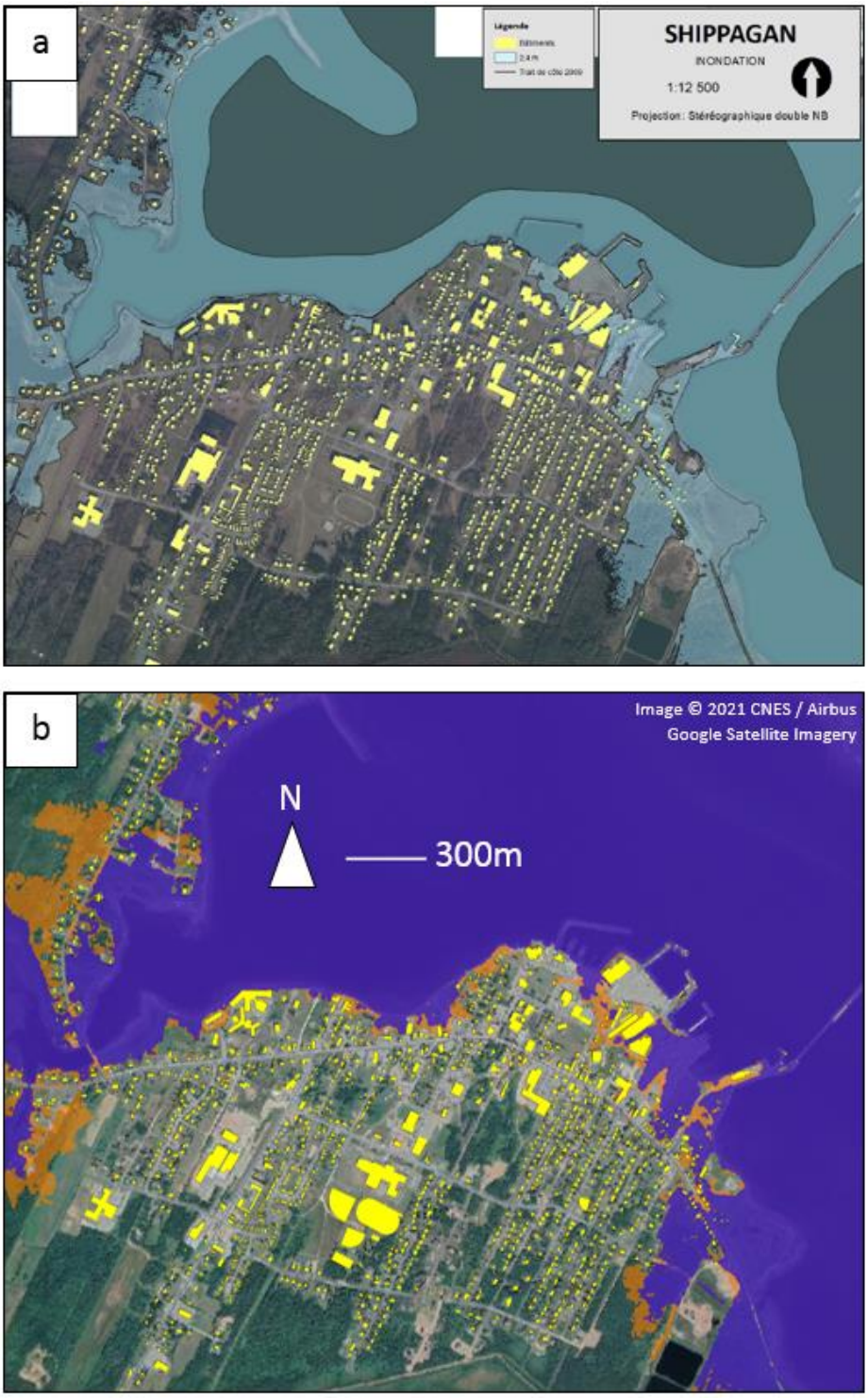

Figure 48. Comparison of flood extents estimated from (a) bathtub modelling conducted by Robichaud et al. (2011) and (b) numerical hydrodynamic modelling in Shippagan. The area shaded in blue in (a) indicates the flood extent estimated for a 10-year (10% AEP) event in year-2000 or a 5-year (20% AEP) event in year-2025. The area shaded in purple in (b) indicates the flood extent of a 20% AEP event during approximately present-day conditions, and the area shaded in orange indicates the flood extent of a 10% AEP event during approximately present-day conditions.

10.1.3 Bas-Caraquet

Robichaud et al. (2011) show a flood map indicating flood extent coinciding with a 2.4m (CGVD28) water surface elevation for Bas-Caraquet. They estimate that the flood stage is representative of a 10-year (10% AEP) storm surge event in year-2000 or a 5-year (20% AEP) storm surge event in year-2025. Therefore, the flood map developed by Robichaud et al. (2011) was compared to the present-day 10% AEP and 20% AEP hazard events modelled in this study (Figure 49). Robichaud et al. (2011) also show flood extent coinciding with a 3.3m (CGVD28) flood stage. Robichaud et al. (2011) indicate that this flood stage is representative of a 50-year (2% AEP) storm surge event in year-2085 or a 10-year (10% AEP) storm surge event in year-2100. However, the origin of the relative sea-level rise estimates used in Robichaud et al. (2011) differed from those used in this study, so no attempt was made to compare hydrodynamic model results with the 3.3m flood stage. The relative sea-level rise estimates used in Robichaud et al. (2011) were based on the Fourth Assessment Report (AR4) of the IPCC (Daigle, 2011; IPCC, 2007) and the relative sea-level rise estimates used in this study were based on IPPC AR5. In general, the bathtub modelling results agreed well with the hydrodynamic modelling results in Bas-Caraquet. Therefore, the hydrodynamic modelling and bathtub modelling approaches appear to be similarly well-suited to estimate flood extent. However, again, the bathtub modelling does not allow for spatial and temporal flood propagation, flow velocity (and flow hazard metrics), and flood durations to be assessed.

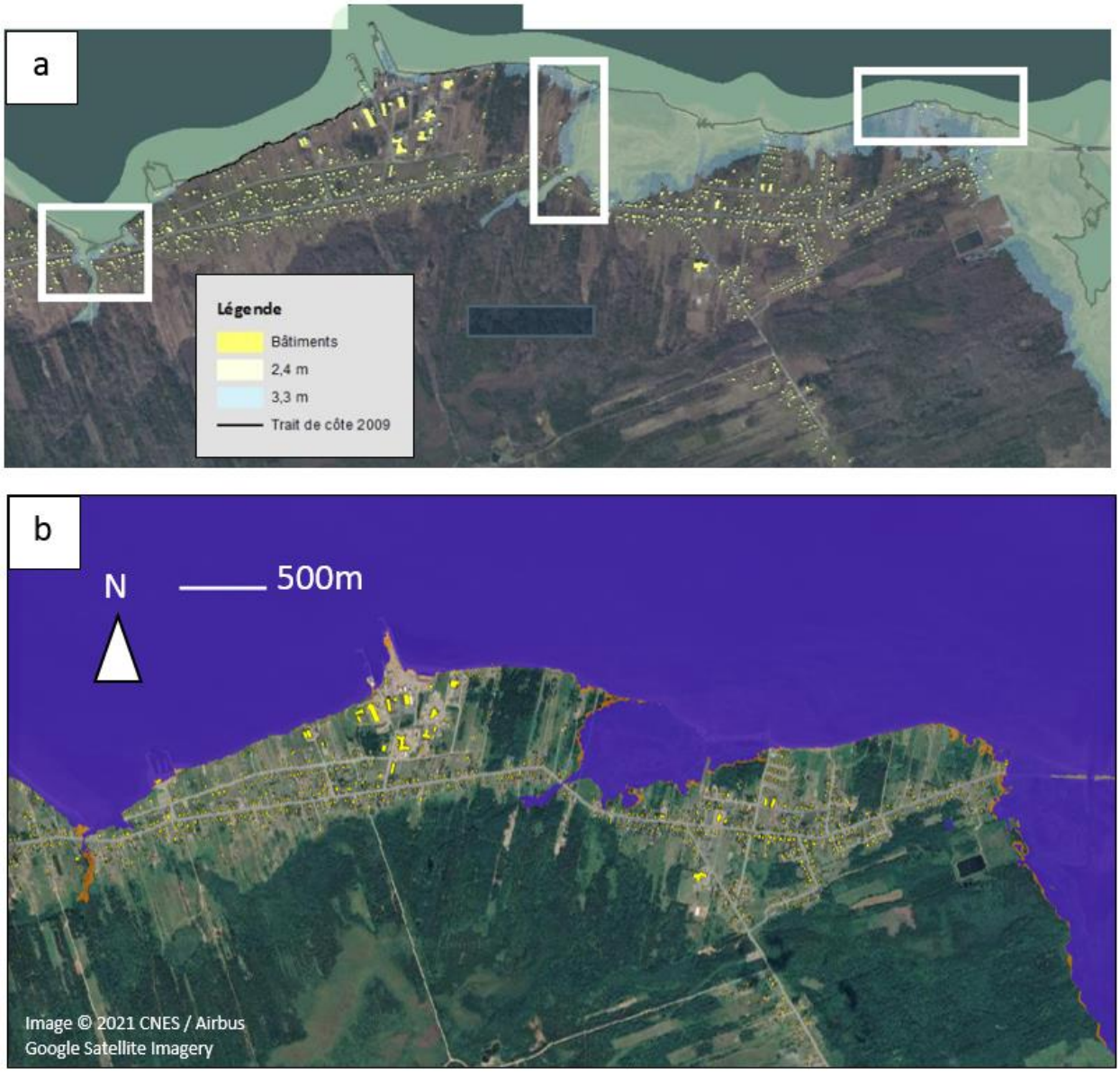

Figure 49. Comparison of flood extents estimated from (a) bathtub modelling conducted by Robichaud et al. (2011) and (b) numerical hydrodynamic modelling in Bas-Caraquet. The area shaded in beige in (a) indicates the flood extent estimated for a 10-year (10% AEP) event in year-2000 or a 5-year (20% AEP) event in year-2025. The area shaded in purple in (b) indicates the flood extent of a 20% AEP event during approximately present-day conditions, and the area shaded in orange indicates the flood extent of a 10% AEP event during approximately present-day conditions.

10.1.4 Maisonnette

Aubé et al. (2016) show a flood map indicating the flood extent coinciding with a 3.0m, 3.3m, and 3.5m (CGVD28) water surface elevation for Maisonnette. They indicate that the 3.0m flood stage is representative of a 50-year (2% AEP) storm surge event in year-2030, and is also similar to a 100-year (1% AEP) storm surge event in year-2010. They indicate that the 3.5m flood stage is representative of a 50-year (2% AEP) storm surge in year-2100. Relative sea-level rise estimates in Aubé et al. (2016) were based on IPPC AR5. Therefore, the flood map developed by Aubé et al. (2016) was compared to the present-day 1% AEP hazard event and also to the 2% AEP hazard event accounting for 1.0m of global sea-level rise (representative of the upper 95% percentile estimate for sea-level rise in year-2100, assuming a high-emissions scenario). Figure 50 shows a comparison between the flood map produced by Aubé et al. (2016) and the peak flood extents estimated from the community scale model.

In general, the bathtub modelling results for the 100-year (1% AEP) event in year-2010 agreed well with the hydrodynamic modelling results for the present-day 1% AEP event. The hydrodynamic modelling results for the 2% AEP event accounting for 1.0m GSLR were similar to the bathtub modelling results representing the 50-year (2% AEP) event for year-2100 in the eastern portion of Maisonnette along Route 303. Elsewhere, hydrodynamic modelling results for the 2% AEP event accounting for 1.0m GLSR produced more-extensive flooding compared to the bathtub modelling results representing the 50-year (2% AEP) event for year-2100.

Comparing events indicative of present-day, the hydrodynamic modelling and bathtub modelling approaches appear to be similarly well-suited to estimate flood extent. There was less agreement between the bathtub and hydrodynamically modelled events under future sea-level scenarios, which may be explained by differences in the sea-level rise projections used in the analyses. As stated, both the bathtub and hydrodynamic modelling approaches used sea-level rise estimates based on IPPC AR5 (Church et al., 2013). More specifically, the future sea level event shown in Figure 50b (modelled in this study) represents 1.0m of GLSL which is representative of the upper 95% percentile estimate for sea-level rise in year-2100, assuming a high-emissions scenario. The details associated with the year-2100 sea level rise estimates from Aube et al. (2016) (based on Daigle (2014)) are not described. Therefore, it is possible that the sea-level rise estimates incorporated into the hydrodynamic modelling and the bathtub modelling differ from one another.

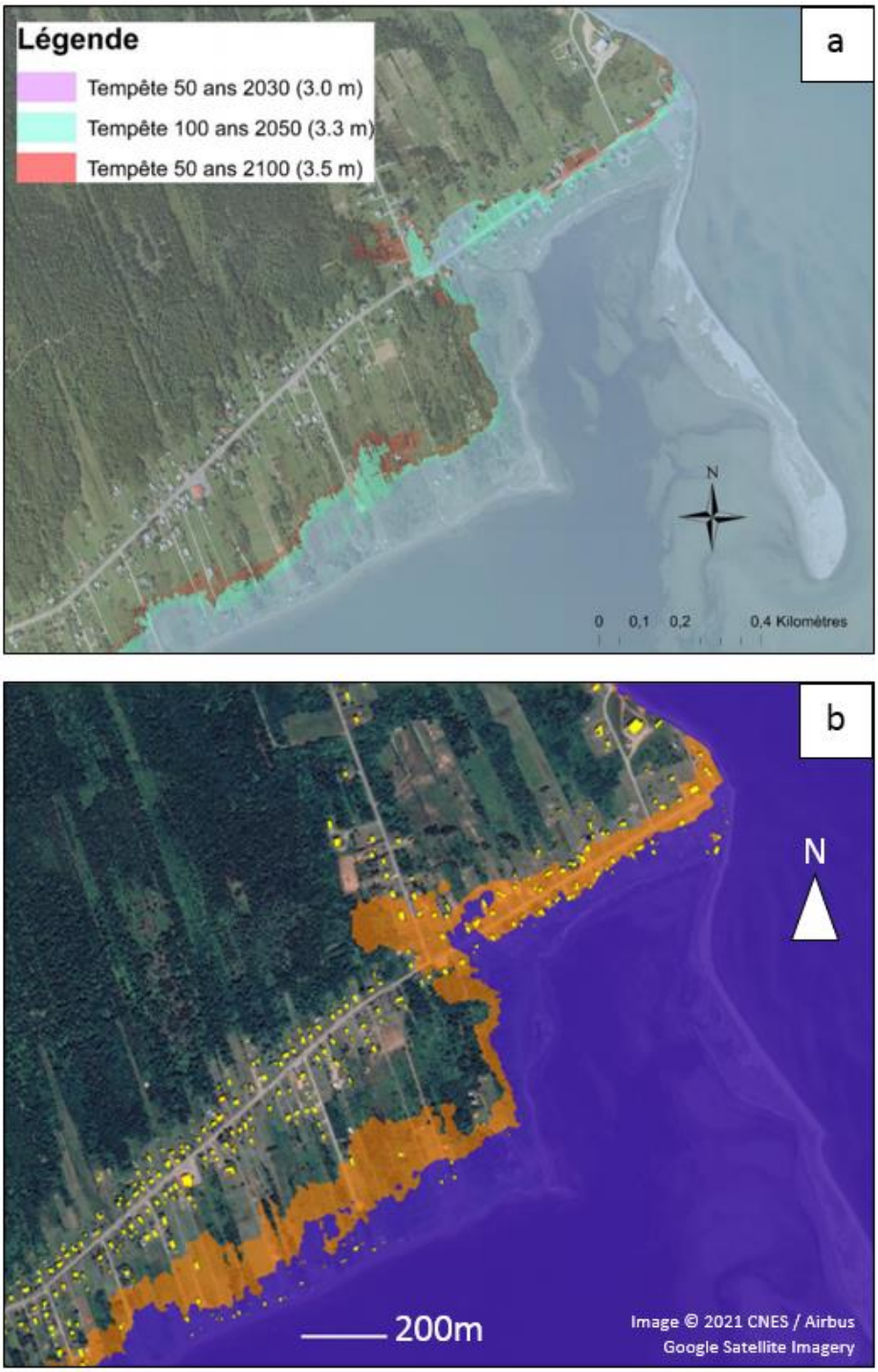

Figure 50. Comparison of flood extents estimated from (a) bathtub modelling conducted by Aubé et al. (2016) and (b) numerical hydrodynamic modelling in Maisonnette. The area shaded in purple in (a) indicates the flood extent estimated for a 50-year (2% AEP) event in year-2030 or a 100-year (1% AEP) event in year-2010. The area shaded in red indicates the flood extent estimated for a 50-year (2% AEP) event in year-2100. The area shaded in purple in (b) indicates the flood extent of a 1% AEP event during approximately present-day conditions, and the area shaded in orange indicates the flood extent of a 2% AEP event in accounting for 1.0m GSLR.

10.1.5 Synthesis

In general, hydrodynamically modelled flood extents for storm surge events in this study agreed well with bathtub modelling completed in other studies for comparable event likelihoods. The synthetic events developed and hydrodynamically modelled in this study were designed based on specific elevation criteria (Table 11). Likewise, the bathtub modelled events were designed based on elevation criteria. The difference, of course, is that the water surface elevations in the bathtub modelled events are based on a static value assigned by the modeller, whereas the water surface elevations in the hydrodynamically modelled events are developed from simulated wind and barometric set-up. Because flood extent is a function of water surface elevation and ground elevation, it is perhaps unsurprising that the two modelling approaches produced similar flood extents for comparable events. It is worth noting that the differences between the bathtub and hydrodynamically modelled flood extents (although, generally-small) may also be caused, in part, by differences in the hazard event development (i.e. the statistical and water level analyses that are used to inform model forcing).

The comparisons conducted in this study suggest that bathtub modelling and hydrodynamic modelling are similarly well-suited to estimate maximum flood extent, and by extension, maximum flood depths. In fact, bathtub modelling may actually be better-suited to estimate maximum flood extent and flood depths in the vicinity of fine-resolution features and abrupt elevation changes, as apparent from the comparison presented for Shippagan in Section 10.1.2, or where dynamic interactions of floodwater with floodplain features are not important in controlling maximum flood extents. It is also worth noting that bathtub modelling is less computationally demanding than hydrodynamic modelling. However, unlike hydrodynamic modelling, bathtub modelling does not allow for assessment of spatial and temporal flood propagation, flow velocity (and flow hazard metrics), and flood durations. This information may be of importance to support future risk assessments, land use planning, mitigation and adaptation strategies, and decision making.

10.2 Data Considerations for the Acadian Peninsula

One of the overarching challenges in assessing flood hazard for the Acadian Peninsula was scarcity of pertinent data resources. Specifically, scarcity of proximate, long-term water level records and historical flood observations hindered assessment of model skill and introduced uncertainty into hazard event estimation.

The closest tide gauge stations with sufficiently long periods of record to support extreme value statistical analyses and model skill assessment were located quite far from the Acadian Peninsula. The Escuminac and Belledune gauges were located approximately 75km and 85km away from Shippagan, respectively. Environment Canada (2006) cautions that the distribution of storm surges and tides across the Gulf of Saint Lawrence varies considerably across the region. Therefore, an analysis of water level residuals was conducted to evaluate spatial autocorrelations between the Acadian Peninsula and the two gauges (Section 8.1), and ultimately to identify which gauge was more suitable to inform hazard event development. Hazard events were designed under the assumption that event likelihood at the Belledune gauge reflects event likelihood at the Acadian Peninsula (i.e. a storm event that produces water levels with a 1% AEP at the Belledune gauge also produces water levels with a 1% AEP at the Acadian Peninsula). A more robust assessment would use local water level records to support statistical analyses and inform hazard event development; however, local, long-term water level records were not available.

Lack of local, long-term water level records also hindered assessment of model skill for both the regional and community-scale model. The regional model was calibrated and validated based on observations from

the Escuminac and Belledune tide gauges. However, modelled storm surge in the regional model could not be evaluated in the vicinity of the Acadian Peninsula owing to lack of data. Similarly, tide gauge data were not available to support community-scale model calibration; the community-scale model domain did not encompass the Escuminac or Belledune gauges. Rather, the community-scale model was calibrated and validated based on high water level indicators and photographic and video evidence of flooding linked to the December 6 and December 21, 2010 coastal flood events (Sections 7.3 and 7.4). Additional observations associated with other historic flood events could enable a more robust assessment of community-scale model skill.

10.3 Current and Future Storm Surge-Driven Flood Hazard

Section 9.3 and Appendices D, E, and F provide a detailed summary of storm surge-driven flood hazard under present-day sea levels and future sea-levels accounting or potential sea-level rise. As described in Section 9.3.2, results indicate that potential sea-level rise will exacerbate storm surge-driven flood hazards in the Acadian Peninsula. The findings summarized in Table 12 indicate that sea-level rise will increase the likelihood of extreme water levels. In all of the communities included in this study, modelled maximum flood extents for the present-day 1% AEP event were comparable to a future 10% AEP event accounting for 0.5m of GLSR. Furthermore, findings form the regional model validation analysis (Section 6.4) indicated that sea ice is capable of attenuating storm surges in the region. Projections indicate that ice cover and ice season durations within the Gulf of Saint Lawrence will decline over the 21st century due to climate change (Greenan et al., 2018). Combined, the impacts of sea level rise and diminished sea ice pose a potential concern for the Acadian Peninsula. Even if the frequency and intensity of storms were to remain stationary in the future, results indicate that future storm events will produce larger storm surges and greater flood hazard on the Acadian Peninsula.

11 Conclusions and Future Work

This report summarizes the development of numerical hydrodynamic models to support assessment of storm surge flood hazard in the Acadian Peninsula. The regional storm surge model covers much of Canada's Atlantic coast and continental shelf and is large enough to capture storm surges generated by synoptic meteorological forcing. Regional model skill was assessed using data available from tide gauge records. Impacts of wave setup and sea ice were investigated at the regional-scale. Results indicated that wave setup can contribute to elevated water levels near the Escuminac gauge for events coinciding with sustained, strong winds from the east and north-east, and that sea ice cover can attenuate storm surges in the region. Methods to incorporate impacts of sea-ice into hydrodynamic modelling of storm surge were explored and applied with good success, resulting in an improvement in model skill; these results provide a foundation for potential future research focused on the evolution of coastal flood hazard in the Gulf of Saint Lawrence in the context of diminishing sea-ice under future climate change scenarios.

The community-scale flood hazard model, focused on the Acadian Peninsula, is nested within the regional model and contains sufficient resolution and detail to simulate flood hazard in several Acadian Peninsula communities including Maisonnette, Caraquet, Bas-Caraquet, Pointe-Brûlée, Shippagan, Le Goulet, and Lamèque. Owing to a scarcity of tide gauge records in the vicinity of the Acadian Peninsula, non-conventional methods were explored to support assessment of model skill and calibration. The community-scale model was calibrated using surveyed high water-level indicators provided by Government of New Brunswick. Model skill was validated based on photographic and video evidence of flooding.

A number of statistical methods were explored to investigate the likelihood and magnitude of storm surge hazards in the Acadian Peninsula including, univariate extreme value analyses of storm surge and water levels, and multivariate methods that incorporate the joint-probability of tides and storm surge. Six present-day storm surge hazard events were developed based on data available from the Belledune tide gauge. An additional 18 storm surge hazard events were developed, representing future conditions under three different relative sea-level rise scenarios.

Each of the 24 storm surge hazard events were modelled at the regional and community-scales. Images illustrating peak flood depths, flood extents, and flow-induced hazard in each of the seven Acadian Peninsula communities were produced.

The hydrodynamic modelling presented in this report will support risk-based assessment in the seven Acadian Peninsula communities of interest. The results will be used to identify infrastructure and other assets exposed to, and impacted by, coastal flooding. Future analyses by project partners will focus on assessment of damages and community impacts to inform coastal flood hazard mitigation.

12 Acknowledgements

This work was funded as part of the Coastal Flood Mitigation Canada project by Defence Research and Development Canada through the Canadian Safety and Security Program, with support from the National Research Council of Canada. The authors thank those listed below for their helpful contributions to the research:

- **Guidance and project coordination:** Nicky Hastings, Julie Van de Valk, and Jackie Yip
- **Local knowledge and data contribution:** André Robichaud, Dominique Bérubé, Marc Desrosiers, Robert Capozi, Reid McLean, Cindie Hébert, and Maxime Doucet
- **Hosting and coordination of community workshop:** Valorēs
- **Translation and presentation of community workshop materials:** David Didier
- **NRC and Ocean Program support:** Marie-Chantal Ross, Andrew Cornett, and Maryse Proulx

This study relied on data provided by the Canadian Hydrographic Service (CHS), pursuant to CHS MOU No. 2020-0206-1260-NRCC and CHS MOU No. 2021-0805-1260-NRCC. The incorporation of data sourced from CHS in this study shall not be construed as constituting an endorsement by CHS of this study. The products produced in this study do not meet the requirements of the *Charts and Nautical Publications Regulations, 1995* or the *Navigation Safety Regulations, 2020* under the *Canada Shipping Act, 2001*. Official charts and publications, corrected and up-to-date, must be used to meet the requirements of those regulations.

References

Anderson, T. R., Fletcher, C. H., Barbee, M. M., Romine, B. M., Lemmo, S., & Delevaux, J. M. S. (2018). Modeling multiple sea level rise stresses reveals up to twice the land at risk compared to strictly passive flooding methods. *Scientific Reports*, *8*, 14. https://doi.org/10.1038/s41598-018-32658-x

Ata, R. (2018). *Telemac2d User Manual Version v8p0*.

Aubé, M., Hébert, C., & Simard, I. (2016). *Analyse des risques d'inondation et d'érosion dans les régions de Grande-Anse, Maisonnette, Bertrand et Caraquet*. Institut de recherche sur les zones côtières inc. & Geomediatix innovations inc.

Aucelli, P. P. C., Di Paola, G., Incontri, P., Rizzo, A., Vilardo, G., Benassai, G., Buonocore, B., & Pappone, G. (2017). Coastal inundation risk assessment due to subsidence and sea level rise in a Mediterranean alluvial plain (Volturno coastal plain – southern Italy). *Estuarine, Coastal and Shelf Science*, *198*, 597–609. https://doi.org/10.1016/j.ecss.2016.06.017

Barnard, P. L., van Ormondt, M., Erikson, L. H., Eshleman, J., Hapke, C., Ruggiero, P., Adams, P. N., & Foxgrover, A. C. (2014). Development of the Coastal Storm Modeling System (CoSMoS) for predicting the impact of storms on high-energy, active-margin coasts. *Natural Hazards*, *74*, 1095–1125.

Barton, A. J. (2019). Blue Kenue enhancements from 2014 to 2019. *26th Annual Telemac-Mascaret Users Conference*.

Benoit, M., Marcos, F., & Becq, F. (1996). Development of a third generation shallow-water wave model with unstructured spatial meshing. *Proceedings of the 25th International Conference on Coastal Engineering*, 465–478.

Bernier, N. (2005). *Annual and Seasonal Extreme Sea Levels in the Northwest Atlantic: Hindcasts Over the Last 40 Years and Projections for the Next Century*. Dalhousie University.

Birnbaum, G., & Lüpkes, C. (2002). A new parameterization of surface drag in the marginal sea ice zone. *Tellus*, *54*, 107–123.

Canadian Hydraulics Centre. (2011). *Blue Kenue Reference Manual*. National Research Council Canada.

Canadian Hydrographic Service. (2019). *Non-Navigational (NONNA-100) Bathymetric Data*. https://open.canada.ca/data/en/dataset/d3881c4c-650d-4070-bf9b-1e00aabf0a1d

Canadian Hydrographic Service. (2020). *Nautical Charts*. https://www.charts.gc.ca/charts-cartes/nautical-marines-eng.html

Canadian Ice Service. (2019). *Ice Archive*. https://iceweb1.cis.ec.gc.ca/Archive/page1.xhtml?lang=en

Chin, D. A. (2013). *Water Resources Engineering (3rd Edition)*. Pearson Education Inc.

Church, J. A., Clark, P. U., Cazenave, A., Gregory, J. M., Jevrejeva, S., Levermann, A., Merrifield, M. A., Milne, G. A., Nerem, R. S., Nunn, P. D., Payne, A. J., Pfeffer, W. T., Stammer, D., & Unnikrishan, A. S. (2013). Sea Level Change. In T. F. Stocker, D. Qin, G.-K. Plattner, M. Tignor, S. K. Allen, J. Boschung, A. Nauels, Y. Xia, V. Bex, & P. M. Midgley (Eds.), *Climate Change 2013: The Physical Science Basis. Contribution of Working Group I to the Fifth Assessment Report of the Intergovernmental Panel on Climate Change*. Cambridge University Press.

Cox, R. J., Shand, T. D., & Blacka, M. J. (2010). *Australian Rainfall and Runoff Revision Project 10: Appropriate Safety Criteria for People* (P10/S1/006). Engineers Australia.

Creach, A., Chevillot-miot, E., Mercier, D., & Pourinet, L. (2016). Vulnerability to coastal flood hazard of residential buildings on Noirmoutier Isalnd (France). *Journal of Maps*, *12*, 371–381. https://doi.org/10.1080/17445647.2015.1027041

Daigle, R. (2011). *Sea-Level Rise Estimates for New Brunswick Municipalities*. R.J. Daigle Enviro.

Daigle, R. (2014). *Updated Sea-Level Rise and Flooding Estimates for New Brunswick Coastal Sections Based on IPCC 5th Assessment Report*. R.J. Daigle Enviro.

Daigle, R. (2017). *Sea-Level Rise and Flooding Estimates for New Brunswick Coastal Sections Based on IPCC 5th Assessment Report*. R.J. Daigle Enviro.

Didier, D., Baudry, J., Bernatchez, P., Dumont, D., Sadegh, M., Bismuth, E., Bandet, M., Dugas, S., & Sévigny, C. (2019). Multihazard simulation for coastal flood mapping: Bathtub versus numerical modelling in an open estuary, Eastern Canada. *Journal of Flood Risk Management*, *12*. https://doi.org/10.1111/jfr3.12505

Didier, D., Bernatchez, P., Boucher-Brossard, G., Lambert, A., Fraser, C., Barnett, R., & Van-Wierts, S. (2015). Coastal Flood Assessment Based on Field Debris Measurements and Wave Runup Empirical Model. *Journal of Marine Science and Engineering*, *3*, 560–590. https://doi.org/10.3390/jmse3030560

Doucet, M. (2010). *Inondation du 21 décembre 2010 (Le Goulet) (Haut-Shippagan). YouTube.* https://www.youtube.com/watch?v=GaL_tjc6sbM

Egbert, G. D., & Erofeeva, S. Y. (2002). Efficient Inverse Modeling of Barotropic Ocean Tides. *Journal of Atmospheric and Ocean Technology*, *19*, 183–204. https://doi.org/10.1175/1520-0426(2002)019<0183:EIMOBO>2.0.CO;2

Environment Canada. (2006). *Impacts of Sea-Level Rise and Climate Change on the Coastal Zone of Southeastern New Brunswick*. Environment Canada.

FEMA. (2016). *Guidance for Flood Risk Analysis and Mapping: Coastal Flood Frequency and Extreme Value Analysis* (Guidance Document 76). Federal Emergency Management Agency.

FEMA. (2021). *Hazus Tsunami Model Technical Manual: Hazus 4.2 Service Pack 3*.

Ferguson, S., Provan, M., Murphy, E., Bérubé, D., Desrosiers, M., Robichaud, A., & Kim, J. (2022). Assessing numerical model skill at simulating coastal flooding using field observations of deposited debris and photographic evidence. *Water*, *14*(4), 589. https://doi.org/10.3390/w14040589

Fine, I., & Thomson, R. (2021). *Storm surge simulations for the southern Strait of Georgia and Boundary Bay for selected future sea level rise predictions*. Fisheries and Oceans Canada.

Fisheries and Oceans Canada. (2019a). *Canadian Tides and Water Levels Data Archive*. https://www.meds-sdmm.dfo-mpo.gc.ca/isdm-gdsi/twl-mne/index-eng.htm#

Fisheries and Oceans Canada. (2019b). *Wave data available on-line*. https://www.isdm.gc.ca/isdm-gdsi/waves-vagues/data-donnees/index-eng.asp

Flather, R. A. (1976). *Results from a storm surge prediction model of the north-west European continental shelf for April, November and December 1973* (Report No. 24). Institute of Oceanographic Sciences.

Foreman, M. G. G. (1977). *Manual for tidal heights analysis and prediction*. Department of Fisheries and Oceans, Institute of Ocean Sciences.

Forrester, W. D. (1983). *Canadian Tidal Manual*. Department of Fisheries and Oceans, Canadian Hydrographic Service.

Garbrecht, T., Lupkes, C., Hartmann, J., & Wolff, M. (2002). Atmospheric drag coefficients over sea ice—Validation of a parameterisation concept. *Tellus*, *54*, 205–219.

GEBCO Compilation Group. (2019). *GEBCO 2019 Grid*. https://doi.org/10.5285/836f016a-33be-6ddc-e053-6c86abc0788e

Goda, Y. (2000). *Random Seas and Design of Maritime Structures (2nd ed.)*. World Scientific Publishing Co.

Government of Canada. (2021). *GPS·H*. https://webapp.geod.nrcan.gc.ca/geod/tools-outils/gpsh.php

Government of New Brunswick. (2019a). *2018 digital elevation model*. NB DEM LiDAR Derived Digital Elevation Models. https://geonb.snb.ca/nbdem/

Government of New Brunswick. (2019b). *Forest*. http://www.snb.ca/geonb1/e/DC/forest.asp

Government of New Brunswick. (2019c). *Non-forest*. http://www.snb.ca/geonb1/e/DC/non-forest.asp

Government of New Brunswick. (2019d). *SNB 2018 LiDAR AOI 2*. LiDAR Download. https://geonb.snb.ca/li/

Government of New Brunswick. (2019e). *Wetlands*. http://www.snb.ca/geonb1/e/DC/RW.asp

Government of New Brunswick. (2021). *Data Catalogue*. GeoNB. http://www.snb.ca/geonb1/e/DC/catalogue-E.asp

Greenan, B. J. W., James, T. S., Loder, J. W., Pepin, P., Azetsu-Scott, K., Ianson, D., Hamme, R. C., Gilbert, D., Tremblay, J.-E., Wang, X. L., & Perrie, W. (2018). *Changes in oceans surrounding Canada; Chapter 7 in (eds.) Bush and Lemmen, Canada's Changing Climate Report* (pp. 343–423). Government of Canada.

Harper, J. R., Henry, R. F., & Stewart, G. G. (1988). *Maximum storm surge elevations in the Tuktoyaktuk region of the Canadian Beaufort Sea*. *41*(1), 48–52. https://www.jstor.org/stable/40510662

Hébert, C., & Aubé, M. (2015). *Évaluation d'options d'adaptation aux changements climatiques: Restauration des dunes à Le Goulet*. Institut de recherche sur les zones côtières inc.

Hersbach, H., Bell, B., Berrisford, P., Biavati, G., Horányi, A., Muñoz Sabater, J., Nicolas, J., Peubey, C., Radu, R., Rozum, I., Schepers, D., Simmons, A., Soci, C., Dee, D., & Thépaut, J.-N. (2018). *ERA5 hourly data on single levels from 1979 to present. Copernicus Climate Change Service (C3S) Climate Data Store (CDS).* https://doi.org/10.24381/cds.adbb2d47

Houghtalen, R. J., Akan, A. O., & Hwang, N. H. C. (2010). *Fundamentals of Hydraulic Engineering Systems (4th Edition)*. Prentice Hall.

IPCC. (2007). *Climate Change 2007: Synthesis Report. Contribution of Working Groups I, II and III to the Fourth Assessment Report of the Intergovernmental Panel on Climate Change* (R. K. Pachauri & A. Reisinger, Eds.). IPCC.

James, T. S., Robin, C., Henton, J. A., & Craymer, M. (2021). *Relative sea-level projections for Canada based on the IPCC Fifth Assessment Report and the NAD83v70VG national crustal velocity model* (Open File 8764). Geological Survey of Canada.

Jardine, D. E., Wang, X., & Fenech, A. L. (2021). Highwater Mark Collection after Post Tropical Storm Dorian and Implications for Prince Edward Island, Canada. *Water*, *13*(22). https://doi.org/10.3390/w13223201

Ji, C., Zhang, Q., & Wu, Y. (2018). An empirical formula for maximum wave setup based on a coupled wave-current model. *Ocean Engineering*, *147*, 215–226. https://doi.org/10.1016/j.oceaneng.2017.10.021

Joyce, B. R., Pringle, W. J., Wirasaet, D., Westerink, J. J., Van der Westhuysen, A. J., Grumbine, R., & Feyen, J. (2019). High resolution modeling of western Alaskan tides and storm surge under varying sea ice conditions. *Ocean Modelling*, *141*. https://doi.org/10.1016/j.ocemod.2019.101421

Kim, J., Murphy, E., Nistor, I., Ferguson, S., & Provan, M. (2021). Numerical Analysis of Storm Surges on Canada's Western Arctic Coastline. *Journal of Marine Science and Engineering*, *9*(3), 326. https://doi.org/10.3390/jmse9030326

Lüpkes, C., Gryanik, V. M., Hartmann, J., & Andreas, E. L. (2012). A parametrization, based on sea ice morphology, of the neutral atmospheric drag coefficients for weather prediction and climate models. *Journal of Geophysical Research: Atmospheres*, *117*. https://doi.org/10.1029/2012JD017630

MacLeod, R. F., & Dallimore, S. R. (2021). Assessment of Storm Surge History as Recorded by Driftwood in the Mackenzie Delta and Tuktoyaktuk Coastlands, Arctic Canada. *Frontiers in Earth Science*, *9*, 698660. https://doi.org/10.3389/feart.2021.698660

Mazas, F., & Hamm, L. (2011). A multi-distribution approach to POT methods for determining extreme wave heights. *Coastal Engineering*, *58*, 385–394. https://doi.org/10.1016/j.coastaleng.2010.12.003

Melton, G., Gall, M., Mitchell, J. T., & Cutter, S. L. (2010). Hurricane Katrina storm surge delineation: Implications for future storm surge forecasts and warnings. *Natural Hazards*, *54*, 519–536. https://doi.org/10.1007/s11069-009-9483-z

Murphy, E., Lyle, T., Wiebe, J., Hund, S. V., Davies, M., & Williamson, D. (2020). *Coastal Flood Risk Assessment Guidelines for Building and Infrastructure Design*. National Research Council Canada.

NOAA. (2021). *Historical Hurricane Tracks*. https://coast.noaa.gov/hurricanes/#map=4/32/-80

NRCan. (2020). *Workshop Summary Report—Introductory Workshop of Coastal Flood Mitigation Canada*.

Provan, M., Ferguson, S., & Murphy, E. (2022). (Accepted) Storm surge contributions to flood hazards on Canada's Atlantic coast. *Journal of Flood Risk Management*.

Pugh, D. T., & Vassie, J. M. (1980). Applications of the joint probability method for extreme sea level computations. *Proceedings of the Institution of Civil Engineers*, *69*, 959–975.

Robichaud, A., Simard, I., Doiron, A., & Chelbi, M. (2011). *Infrastructures à risque dans trois municipalités de la Péninsule Acadienne*. Atlantic Climate Adaptation Solutions Association.

Robin, C., Nudds, S., MacAulay, P., Godin, A., De Lange Boom, B., & Bartlett, J. (2016). Hydrographic vertical separation surfaces (HyVSEPs) for the tidal waters of Canada. *Marine Geodesy*, *39*, 195–222. https://doi.org/10.1080/01490419.2016.1160011

Schubert, J. E., & Sanders, B. F. (2012). Building treatments for urban flood inundation models and implications for predictive skill and modeling efficiency. *Advances in Water Resources*, *41*, 49–64. https://doi.org/10.1016/j.adwatres.2012.02.012

Stockdon, H. F., Holman, R. A., Howd, P. A., & Sallenger, A. H. (2006). Empirical parameterization of setup, swash, and runup. *Coastal Engineering*, *53*, 573–588. https://doi.org/10.1016/j.coastaleng.2005.12.005

United Nations. (2004). *Living with Risk: A global review of disaster reduction initiatives*.

United Nations. (2015). *Sendai Framework for Disaster Risk Reduction 2015-2030*.

WAFO group. (2011). *WAFO - a Matlab Toolbox for Analysis of Random Waves and Loads: Tutorial for WAFO version 2.5*. Lund University.

White, F. M. (2003). *Fluid Mechanics (5th Edition)*. McGraw-Hill.

Wu, J. (1980). Wind-stress coefficients over sea surface near neutralconditions—A revisit. *Journal of Physical Oceanography*, *10*, 727–740.

Wu, J. (1982). Wind-stress coefficients over sea surface from breeze to hurricane. *Journal of Geophysical Research Oceans*, *87*, 9704–9706.

Appendix A – Modelled Flood Extents versus Surveyed High Water Level Indicators

Notes:

- Survey points are shown in pink
- Boxes are drawn around survey locations listed in Table 5 and Table 6

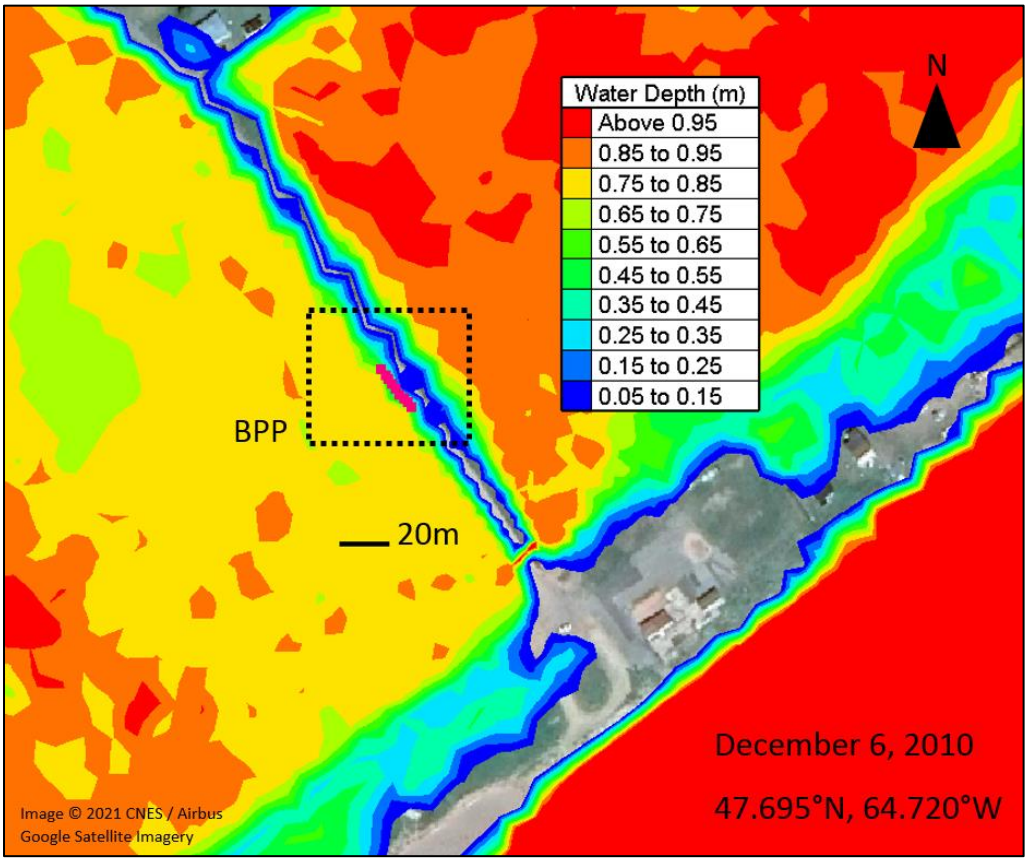
Water Depth (m)
Above 0.95
0.85 to 0.95
0.75 to 0.85
0.65 to 0.75
0.55 to 0.65
0.45 to 0.55
0.35 to 0.45
0.25 to 0.35
0.15 to 0.25
0.05 to 0.15
N
BPP
20m
December 6, 2010
47.695°N, 64.720°W
Image © 2021 CNES / Airbus
Google Satellite Imagery

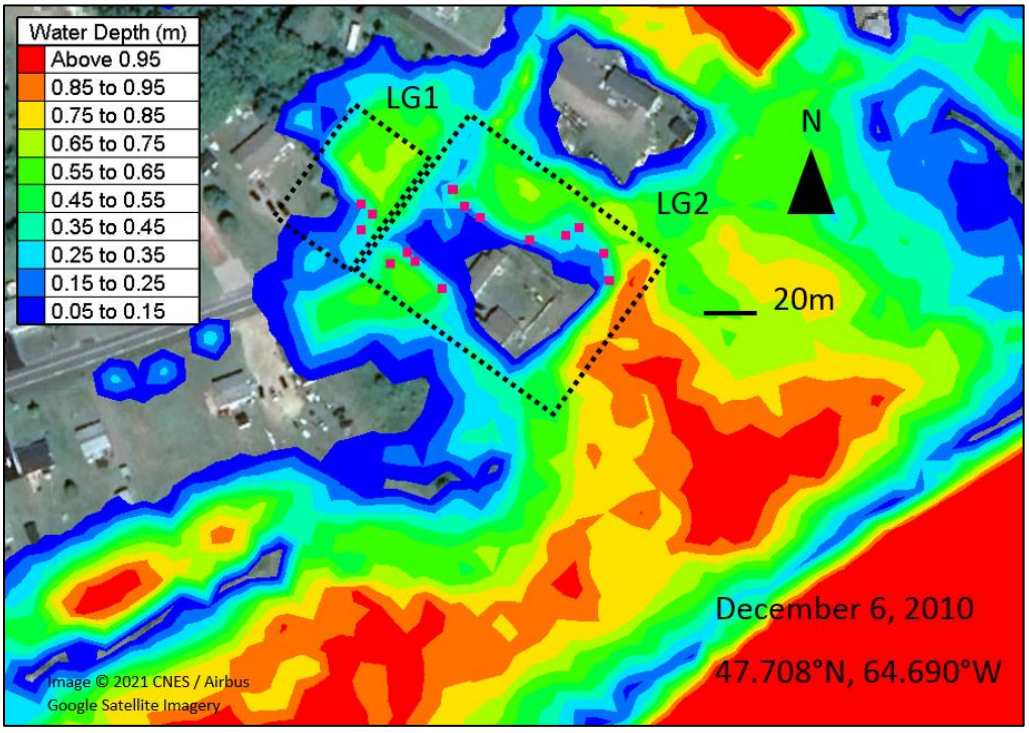
Water Depth (m)
Above 0.95
0.85 to 0.95
0.75 to 0.85
0.65 to 0.75
0.55 to 0.65
0.45 to 0.55
0.35 to 0.45
0.25 to 0.35
0.15 to 0.25
0.05 to 0.15
LG1
LG2
N
20m
December 6, 2010
47.708°N, 64.690°W
Image © 2021 CNES / Airbus
Google Satellite Imagery

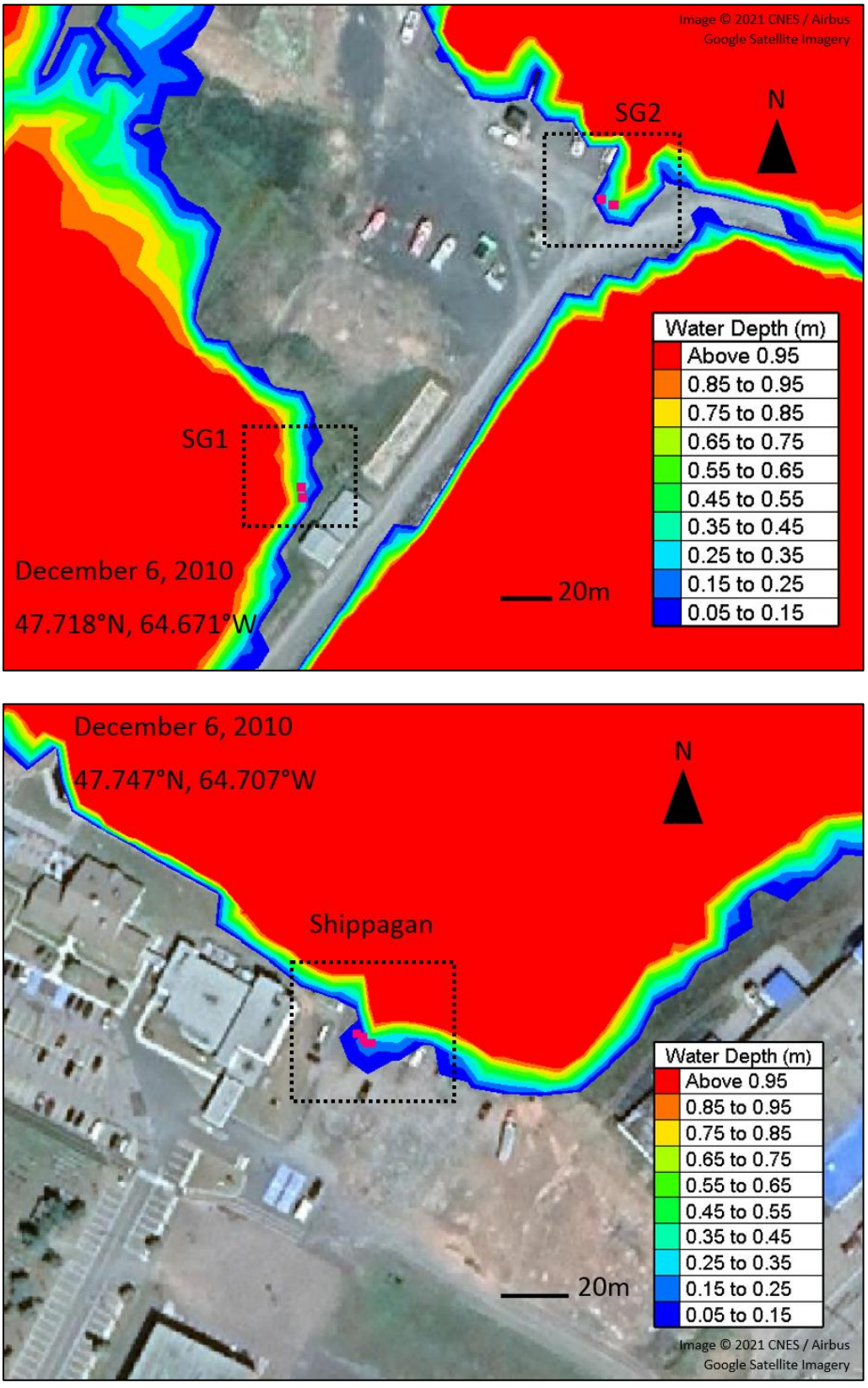
Image © 2021 CNES / Airbus
Google Satellite Imagery
N
SG2
SG1
Water Depth (m)
Above 0.95
0.85 to 0.95
0.75 to 0.85
0.65 to 0.75
0.55 to 0.65
0.45 to 0.55
0.35 to 0.45
0.25 to 0.35
0.15 to 0.25
0.05 to 0.15
December 6, 2010
47.718°N, 64.671°W
20m
December 6, 2010
47.747°N, 64.707°W
N
Shippagan
Water Depth (m)
Above 0.95
0.85 to 0.95
0.75 to 0.85
0.65 to 0.75
0.55 to 0.65
0.45 to 0.55
0.35 to 0.45
0.25 to 0.35
0.15 to 0.25
0.05 to 0.15
20m
Image © 2021 CNES / Airbus
Google Satellite Imagery

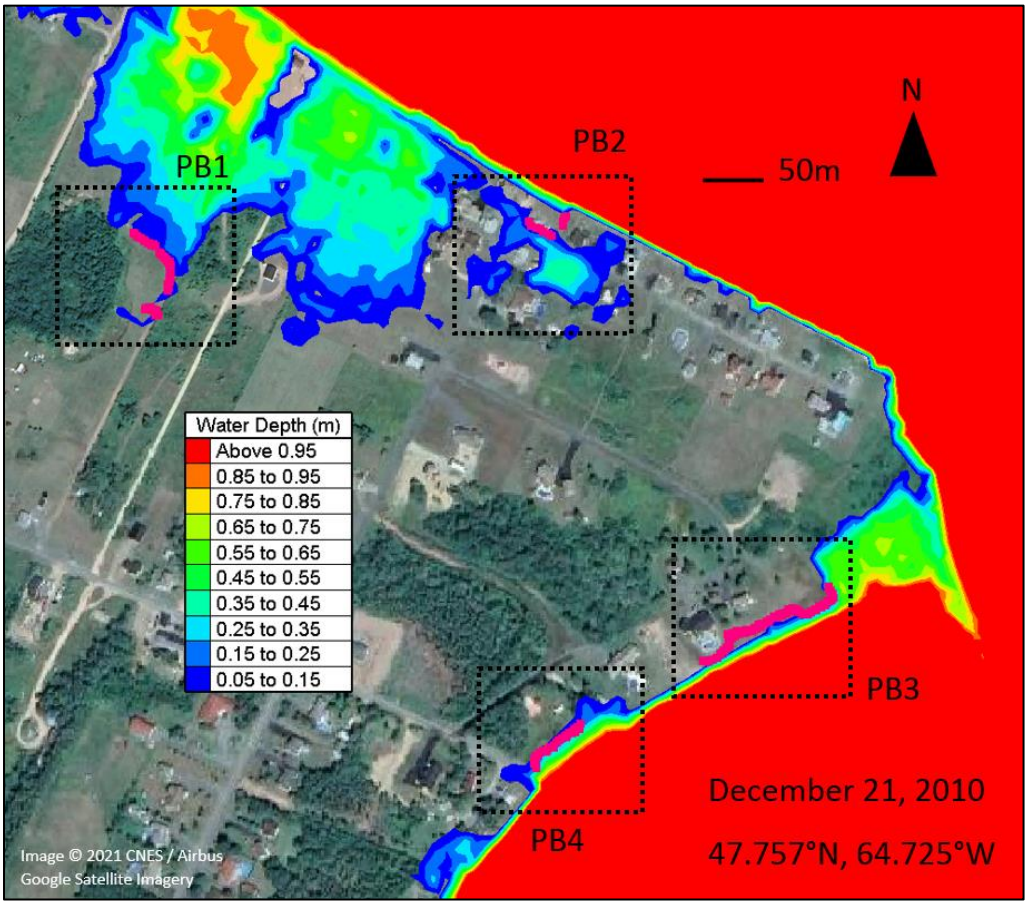
PB1
PB2
PB3
PB4
N
50m
Water Depth (m)
Above 0.95
0.85 to 0.95
0.75 to 0.85
0.65 to 0.75
0.55 to 0.65
0.45 to 0.55
0.35 to 0.45
0.25 to 0.35
0.15 to 0.25
0.05 to 0.15
December 21, 2010
47.757°N, 64.725°W
Image © 2021 CNES / Airbus
Google Satellite Imagery

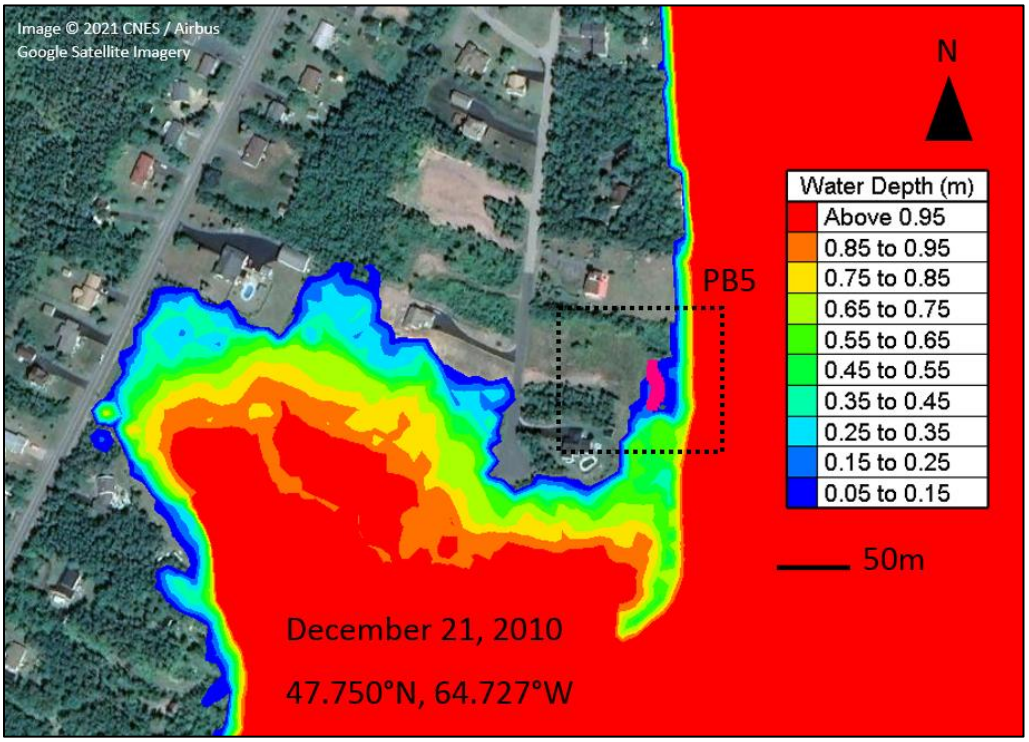
Image © 2021 CNES / Airbus
Google Satellite Imagery
N
PB5
Water Depth (m)
Above 0.95
0.85 to 0.95
0.75 to 0.85
0.65 to 0.75
0.55 to 0.65
0.45 to 0.55
0.35 to 0.45
0.25 to 0.35
0.15 to 0.25
0.05 to 0.15
50m
December 21, 2010
47.750°N, 64.727°W

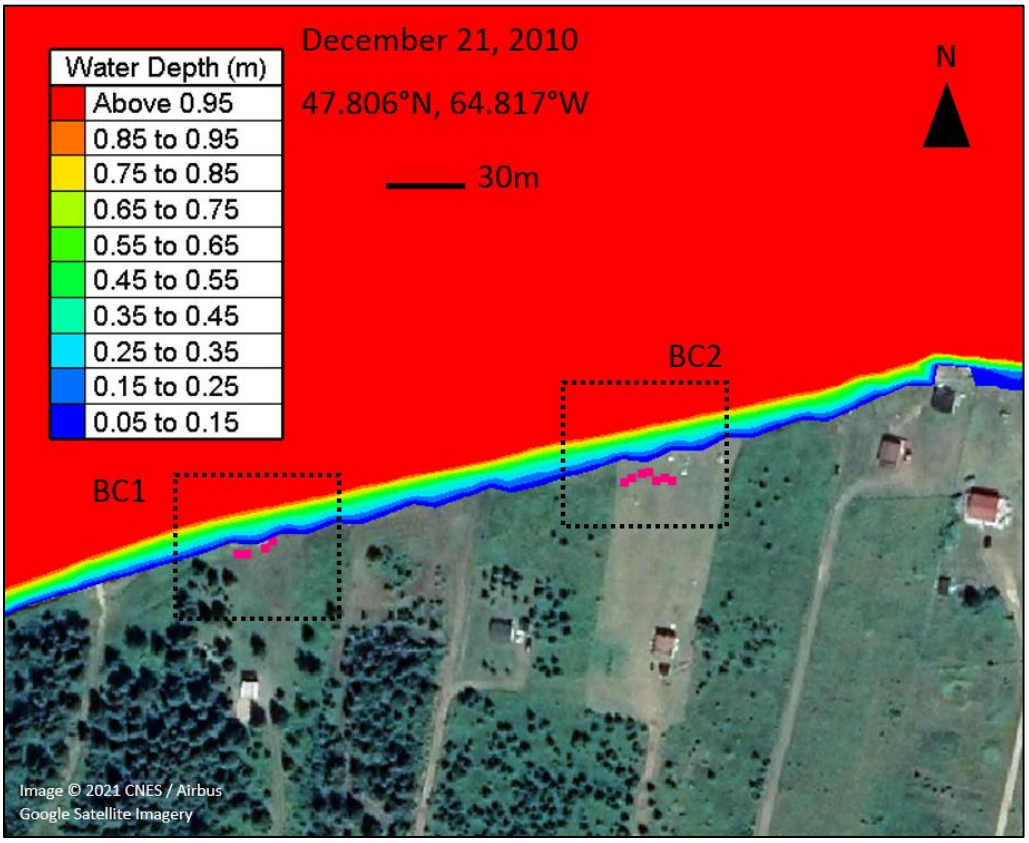
Water Depth (m)
Above 0.95
0.85 to 0.95
0.75 to 0.85
0.65 to 0.75
0.55 to 0.65
0.45 to 0.55
0.35 to 0.45
0.25 to 0.35
0.15 to 0.25
0.05 to 0.15
December 21, 2010
47.806°N, 64.817°W
30m
N
BC1
BC2
Image © 2021 CNES / Airbus
Google Satellite Imagery

Appendix B – Comparison of Modelled Flood Extent with Photographic Evidence of the December 6, 2010 Event

Notes:

- White circles illustrate the location of the observer and black cones illustrate the viewing direction
- Where present, survey points are shown in pink
- Letters indicate corresponding photographs or video clips

QAAD6-A (47.695°N, 64.720°W)

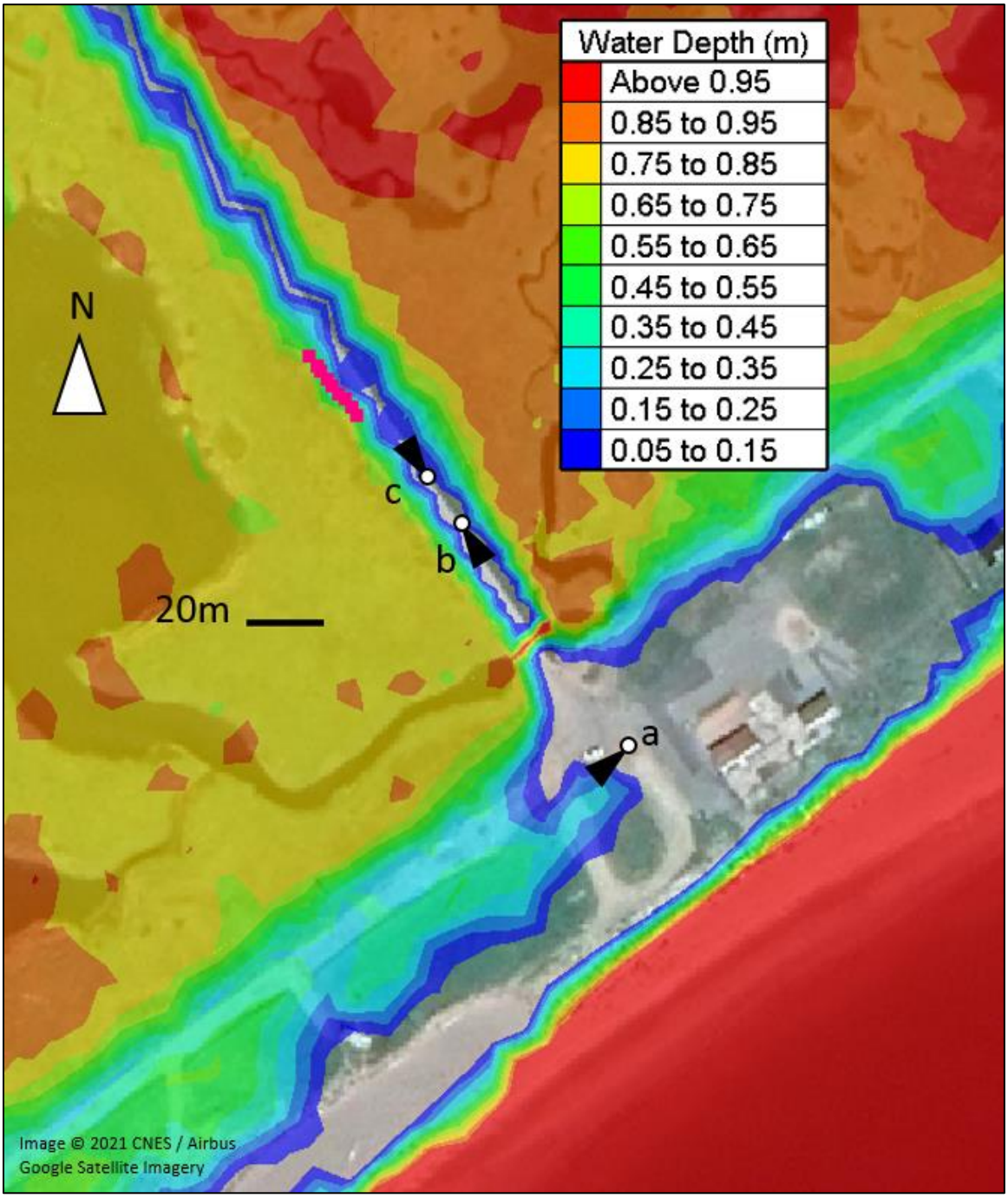

Date: December 6, 2010
Dominique Bérubé & Marc Desrosiers

QAAD6-B (47.698°N, 64.723°W)

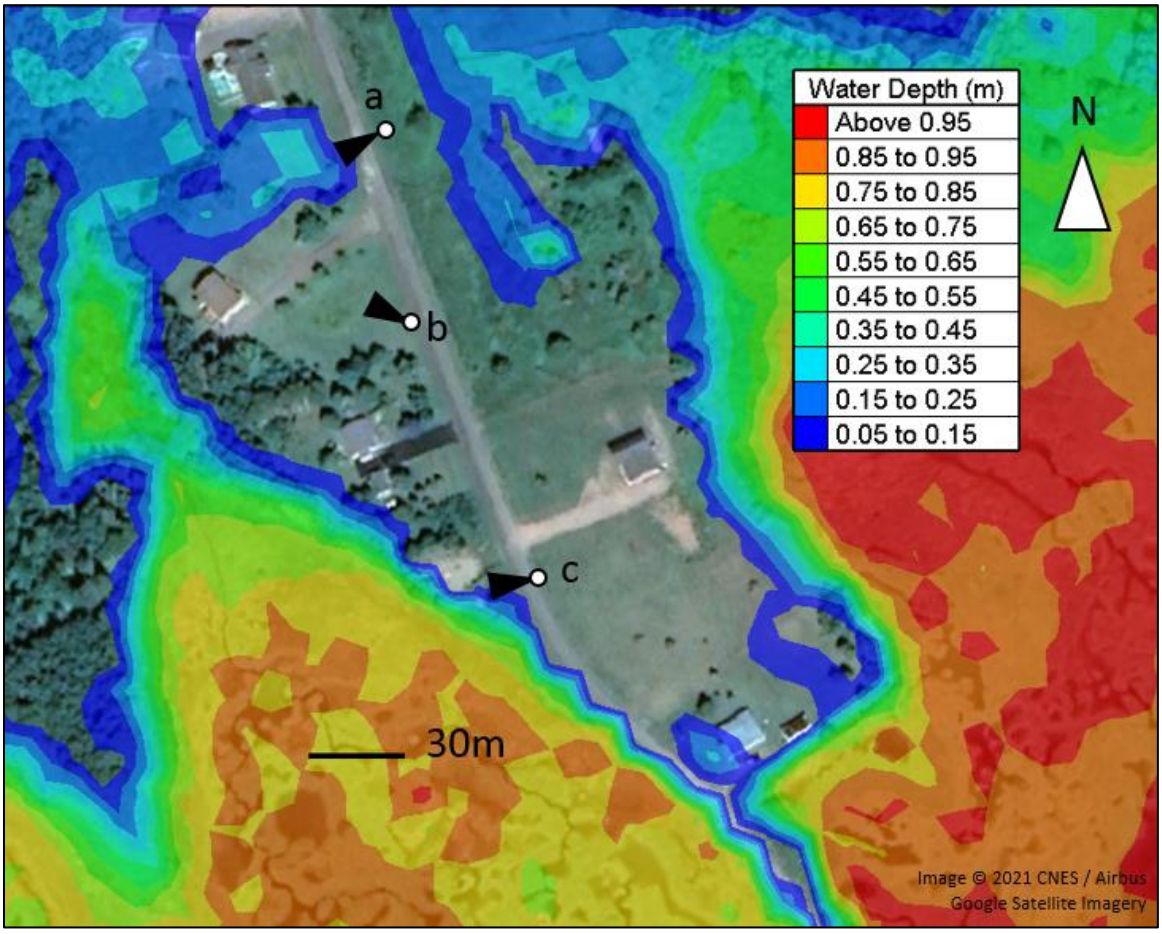

Date: December 6, 2010
Dominique Bérubé & Marc Desrosiers

QAAD6-C (47.708°N, 64.690°W)

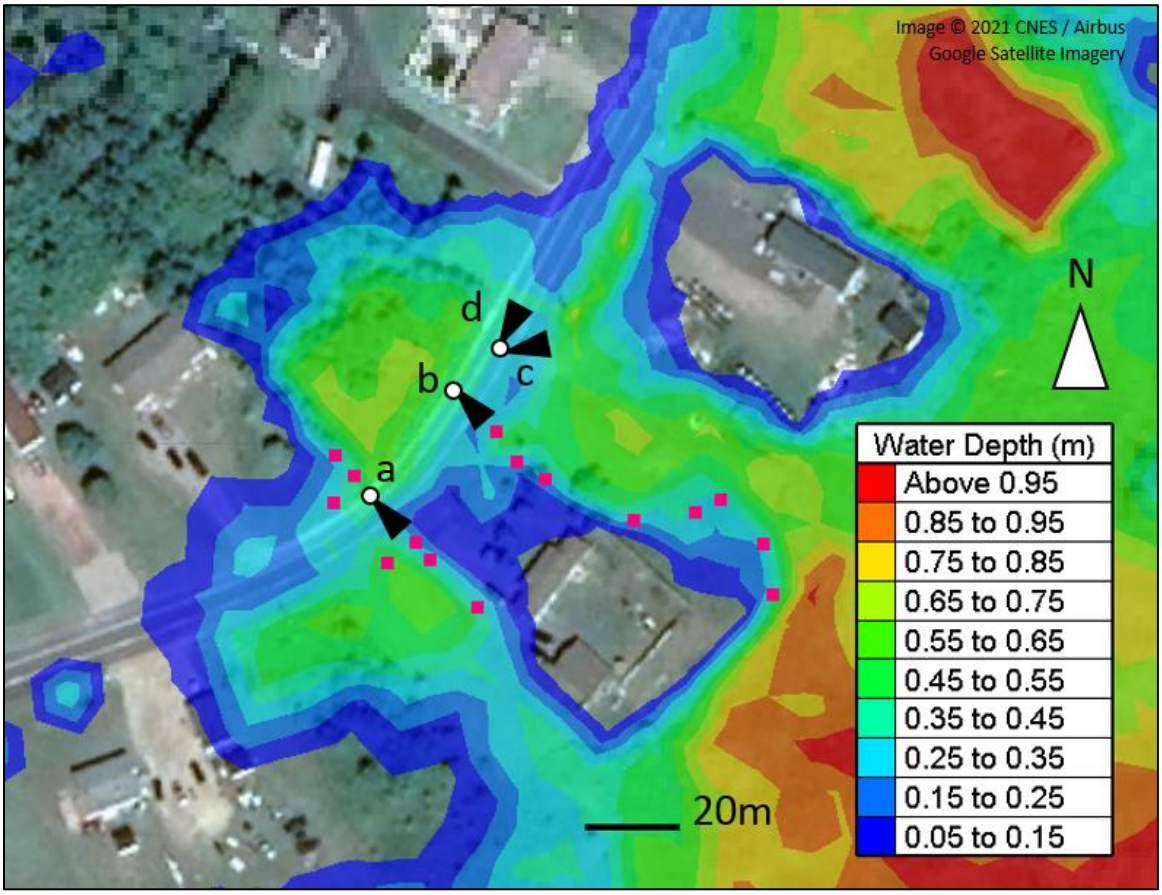

Date: December 6, 2010
Dominique Bérubé & Marc Desrosiers

QAAD6-D (47.711°N, 64.680°W)

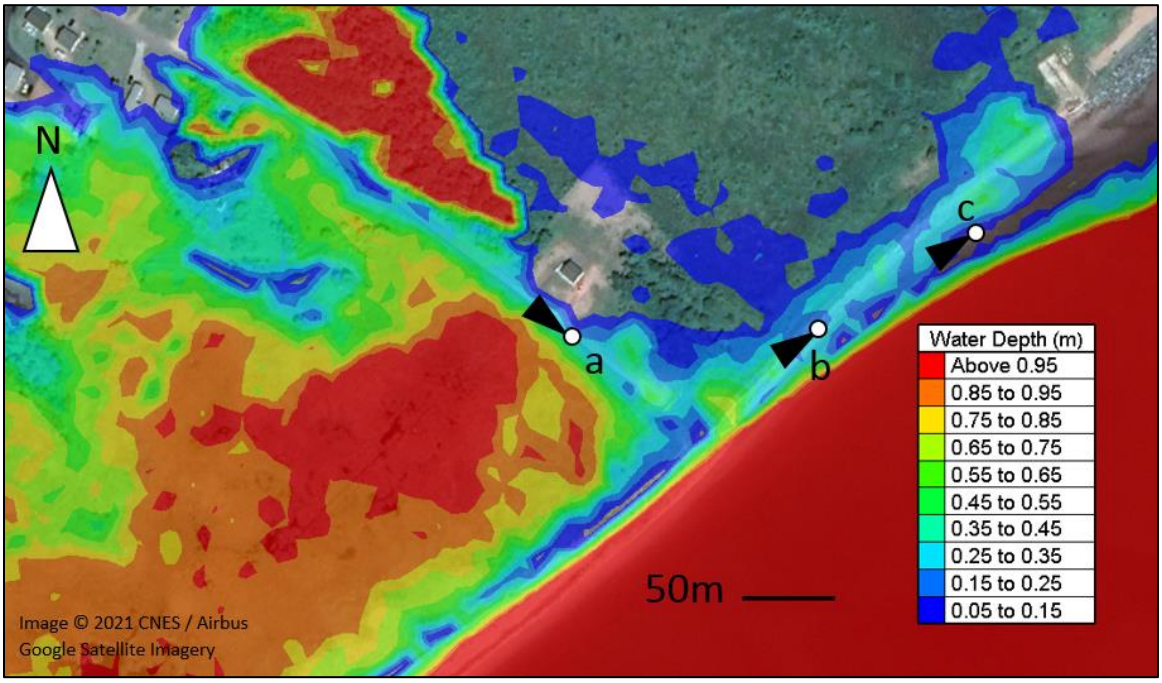


a
Date: December 6, 2010
Dominique Bérubé & Marc Desrosiers


b
Date: May 2, 2011
André Robichaud
Evidence of overtopping


c
Date: May 2, 2011
André Robichaud
Deposited debris and evidence
of slight overtopping

QAAD6-E (47.714°N, 64.677°W)

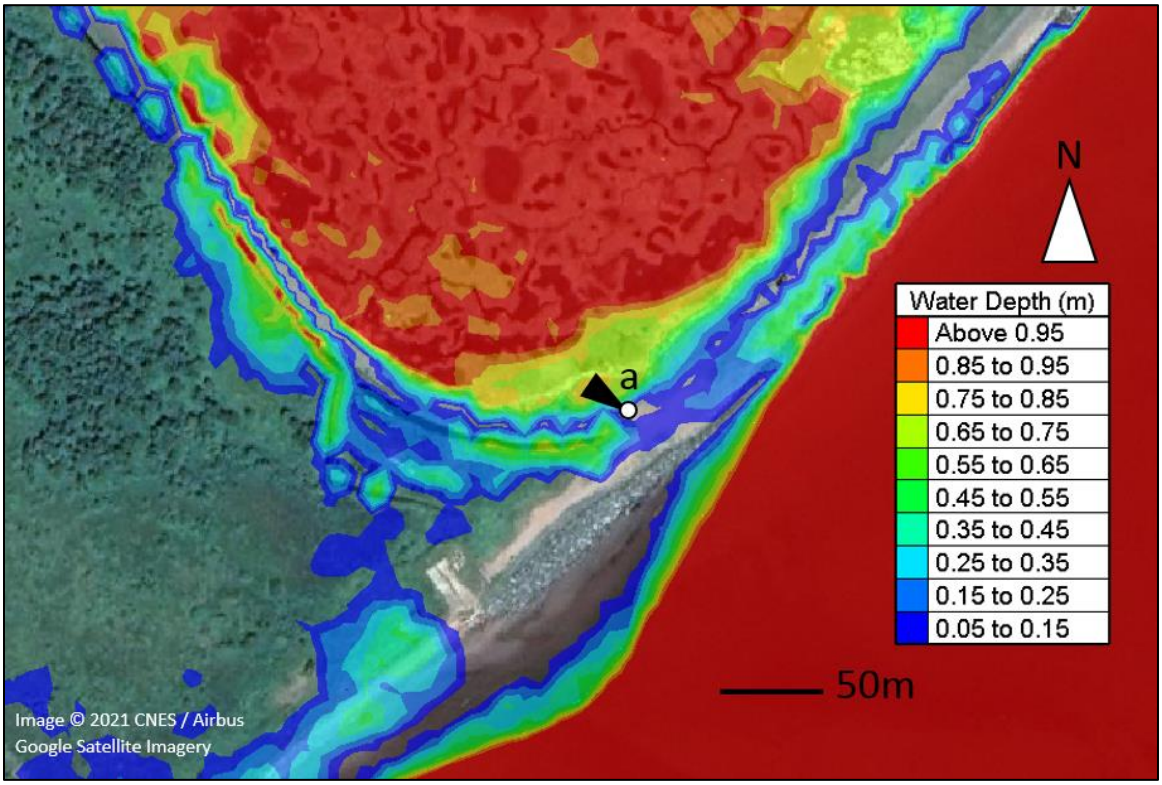


a
Date: December 6, 2010
Dominique Bérubé & Marc Desrosiers

Appendix C – Comparison of Modelled Flood Extent with Photographic and Video Evidence of the December 21, 2010 Event

Notes:

- White circles illustrate the location of the observer and black cones illustrate the viewing direction
- Where present, survey points are shown in pink
- Letters indicate corresponding photographs or video clips

QAAD21-A (47.705°N, 64.696°W)

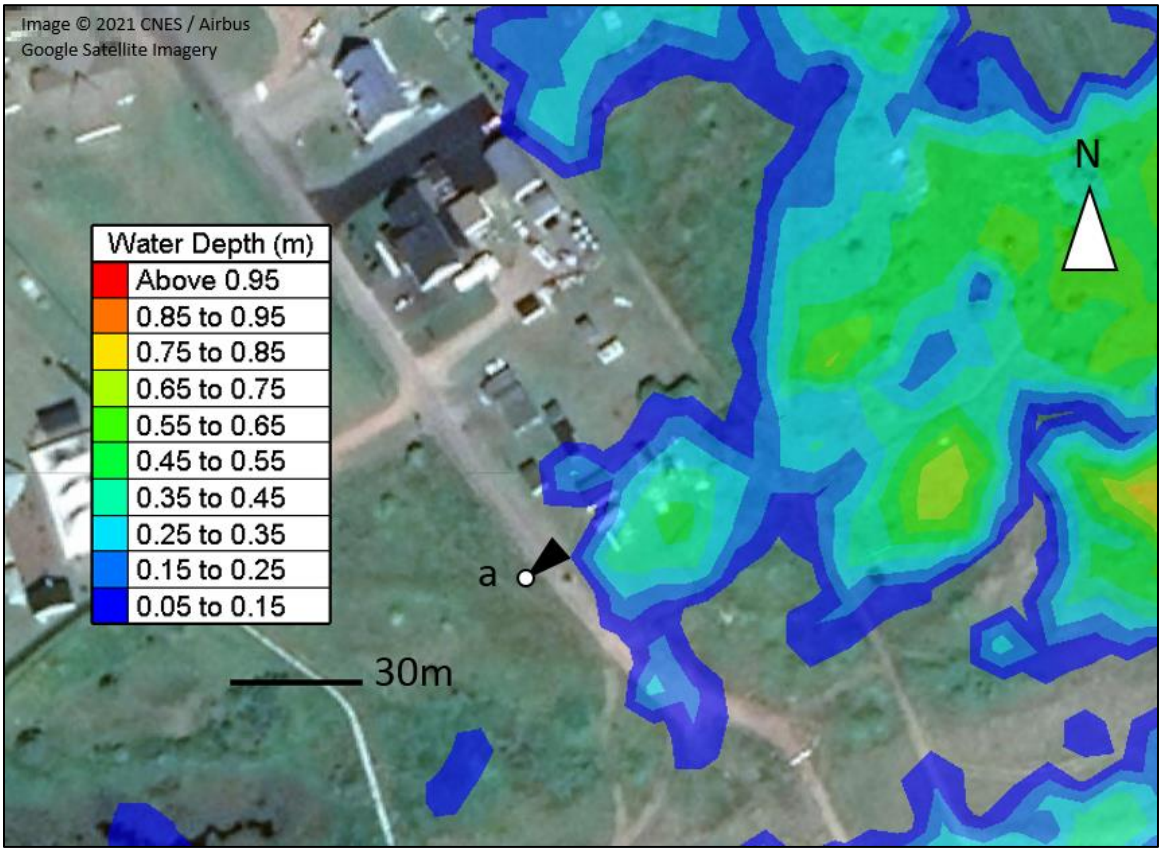


a
Date: December 21, 2010
Maxime Doucet

QAAD21-B (47.708°N, 64.690°W)

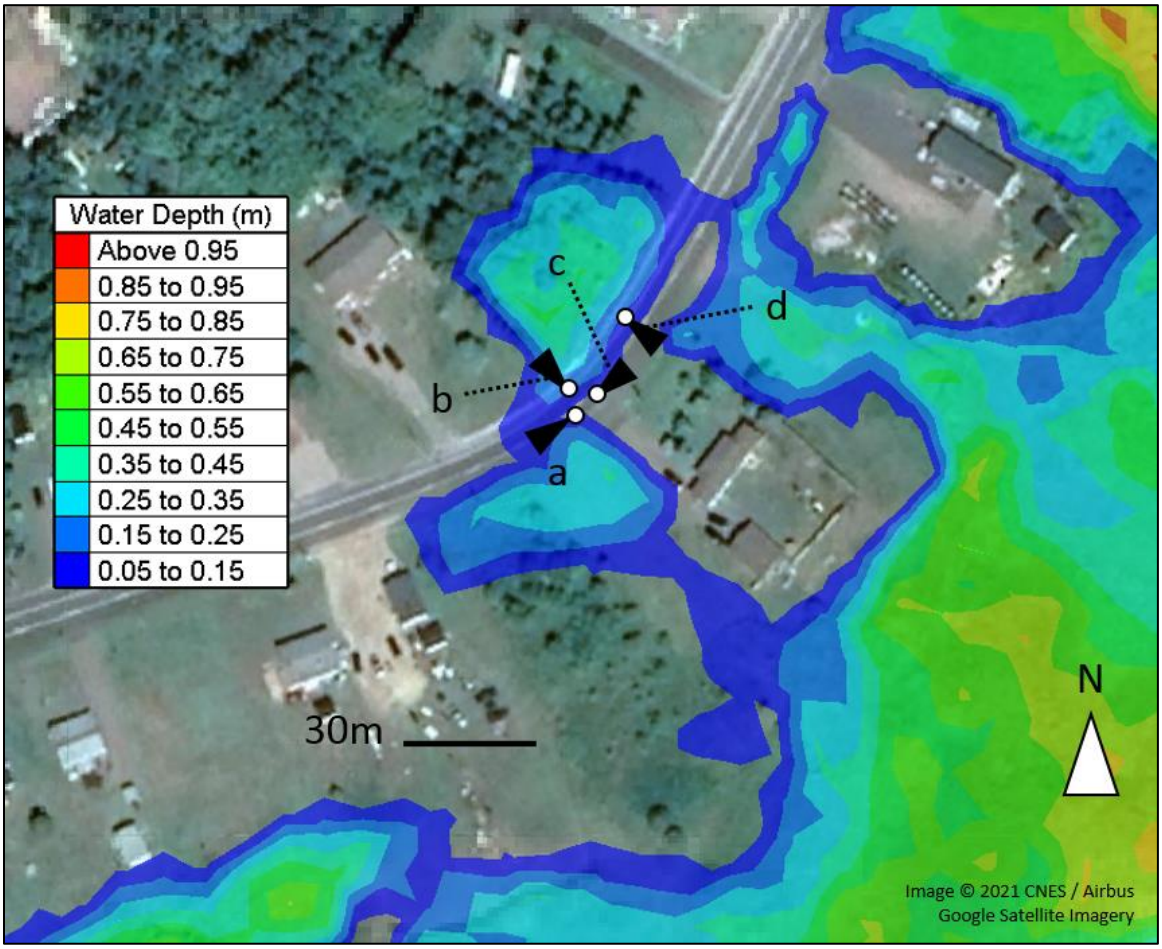

Date: December 21, 2010
Dominique Bérubé & Marc Desrosiers

QAAD21-C (47.712°N, 64.687°W)

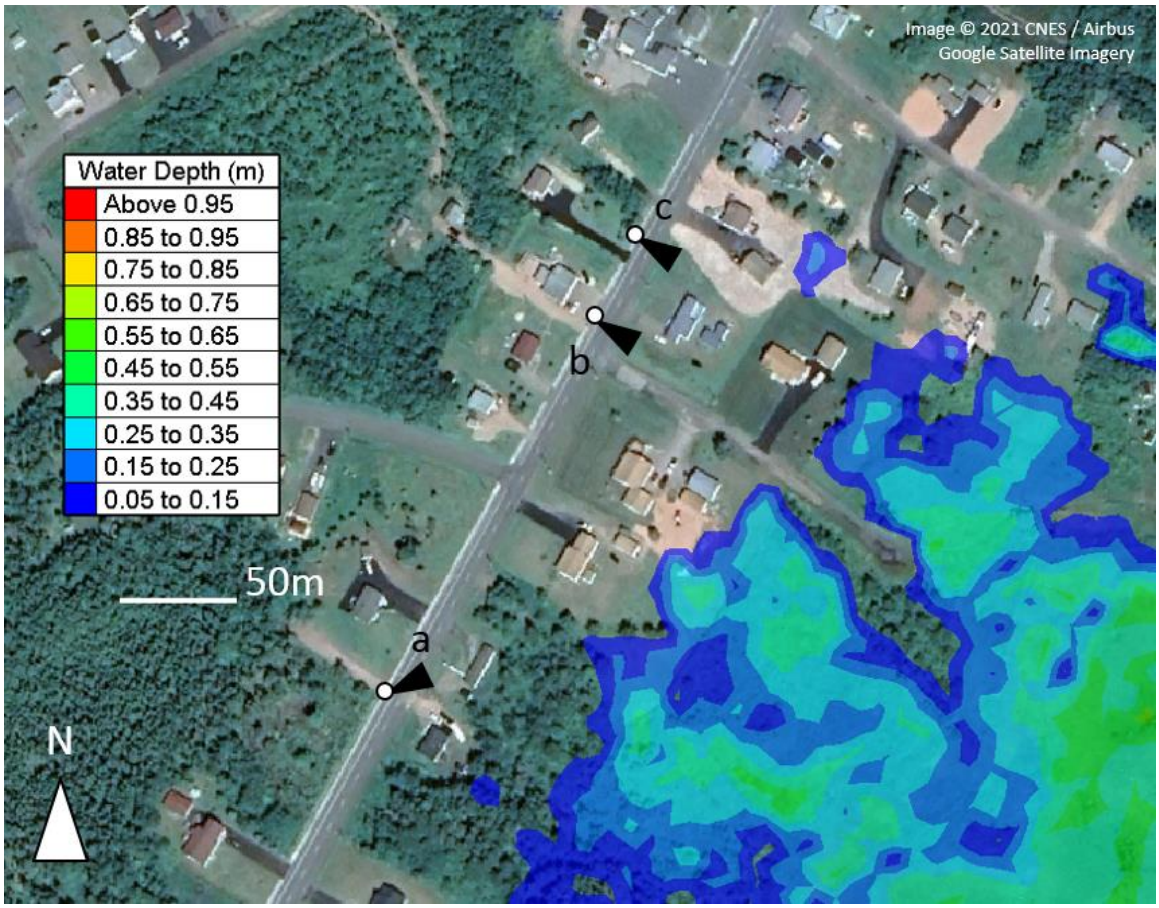


a
Date: December 21, 2010
Dominique Bérubé & Marc Desrosiers


b
Date: December 21, 2010
Maxime Doucet


c
Date: December 21, 2010
Maxime Doucet

QAAD21-D (47.711°N, 64.680°W)

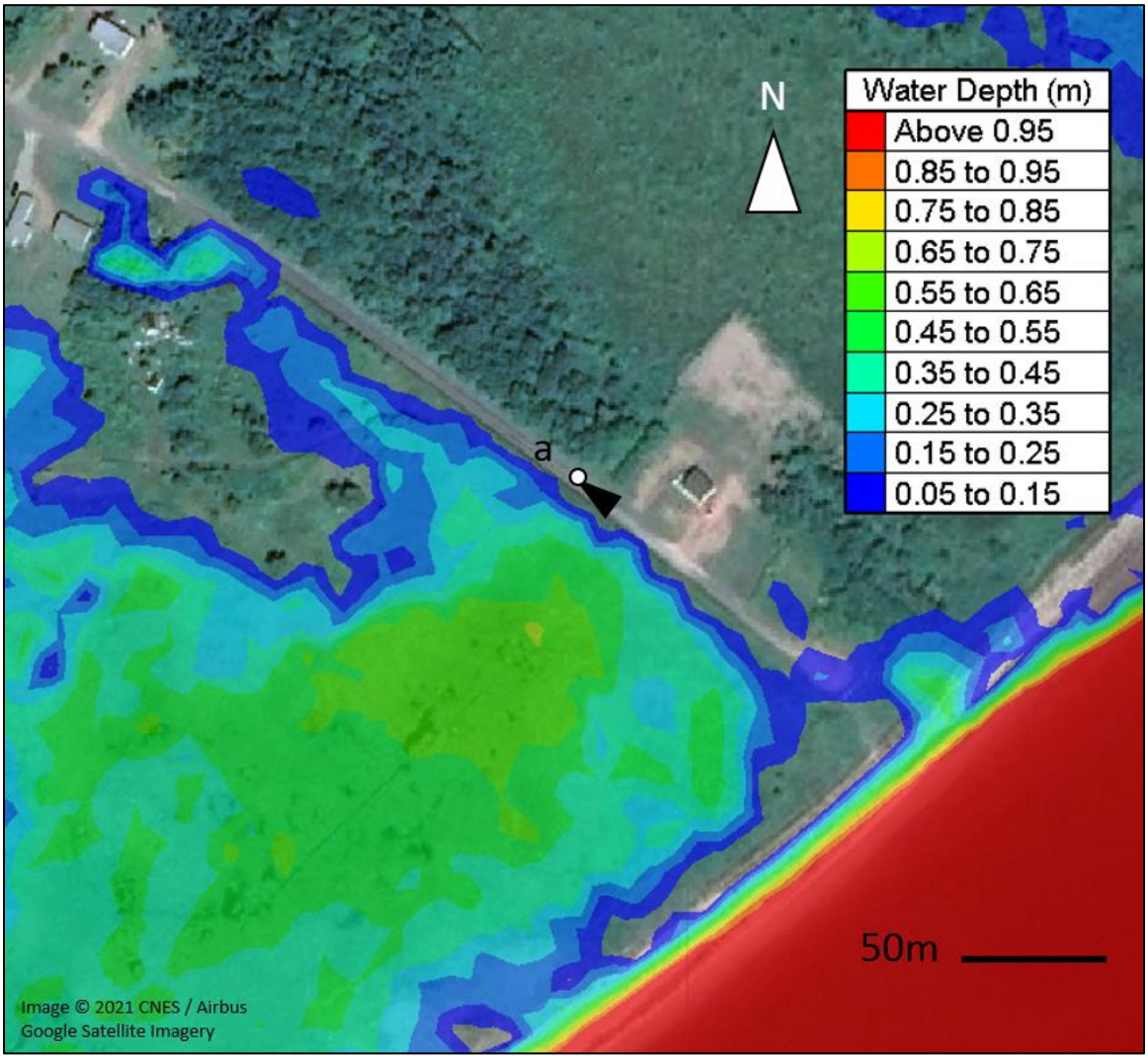


a
Date: December 21, 2010
Dominique Bérubé & Marc Desrosiers

QAAD21-E (47.714°N, 64.677°W)

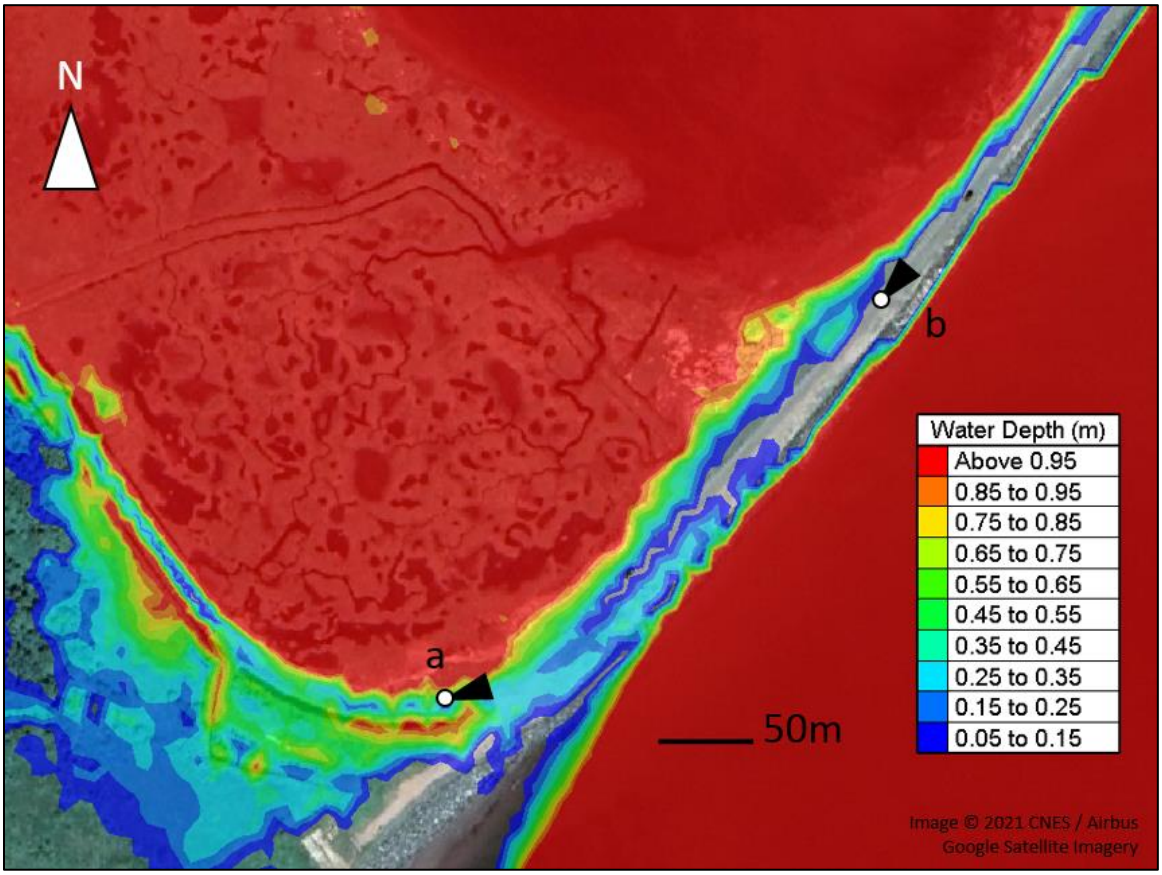

Date: December 21, 2010
Dominique Bérubé & Marc Desrosiers

QAAD21-F (47.743°N, 64.702°W)

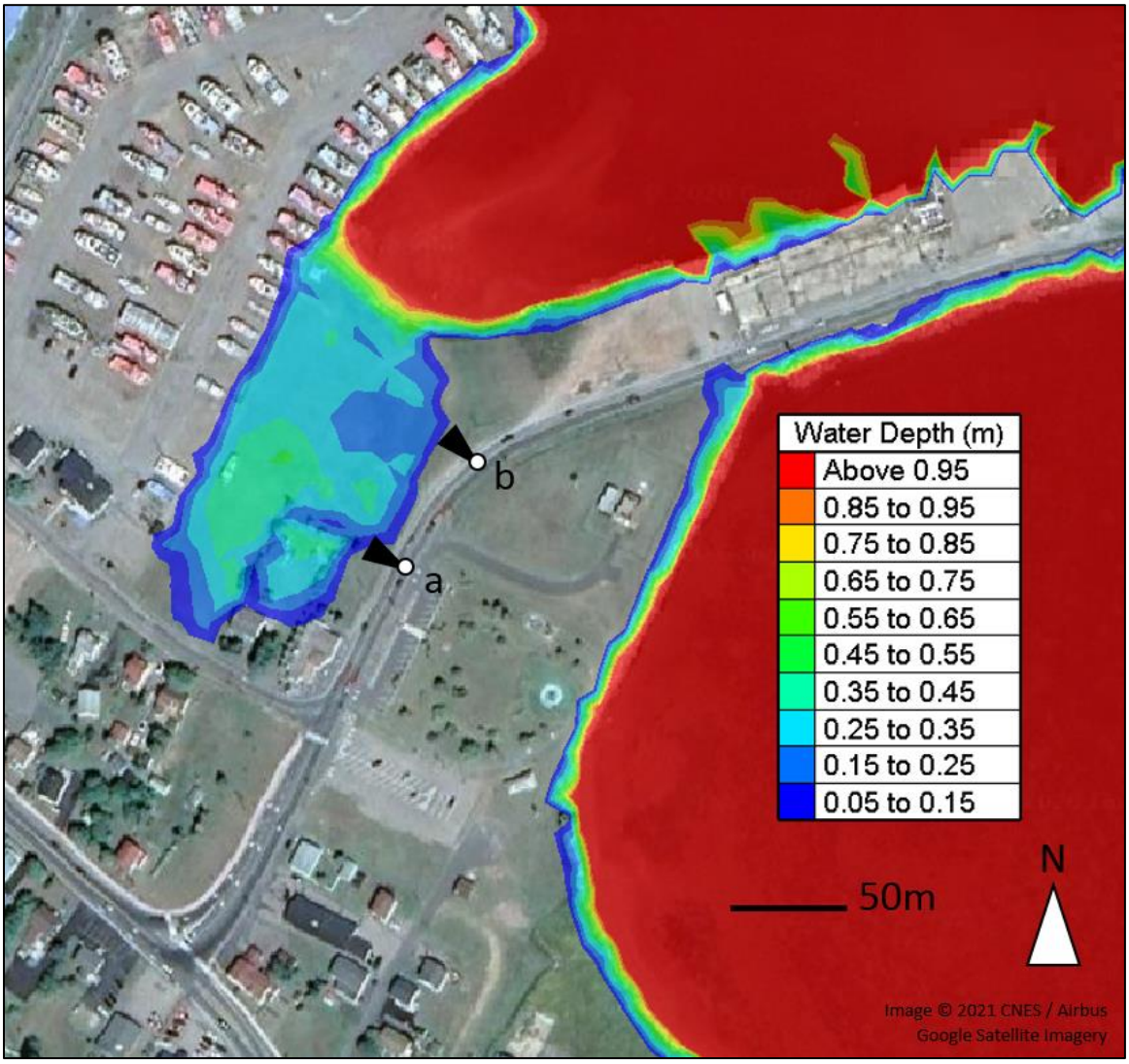

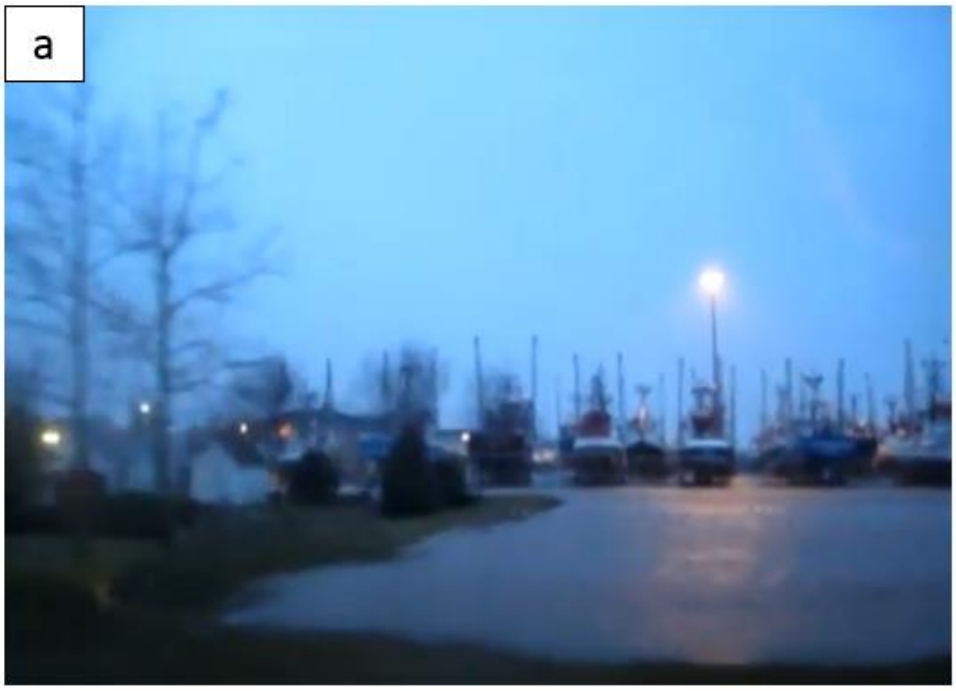

Date: December 21, 2010
Maxime Doucet

QAAD21-G (47.759°N, 64.725°W)

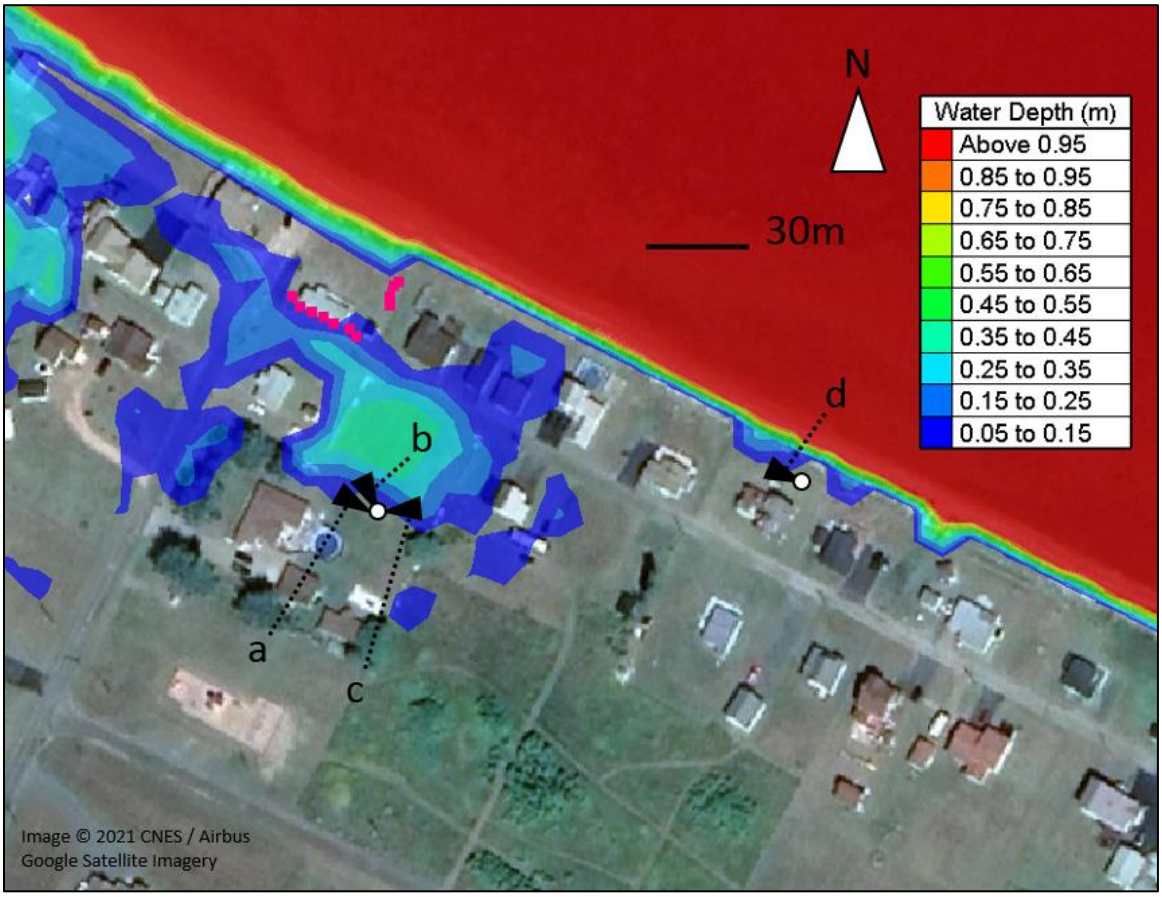


a
Date: December 21, 2010
Maxime Doucet
b
Date: December 21, 2010
Maxime Doucet
c
Date: December 21, 2010
Maxime Doucet
d
Deposited debris
Date: June 14, 2011
André Robichaud

QAAD21-H (47.803°N, 64.872°W)

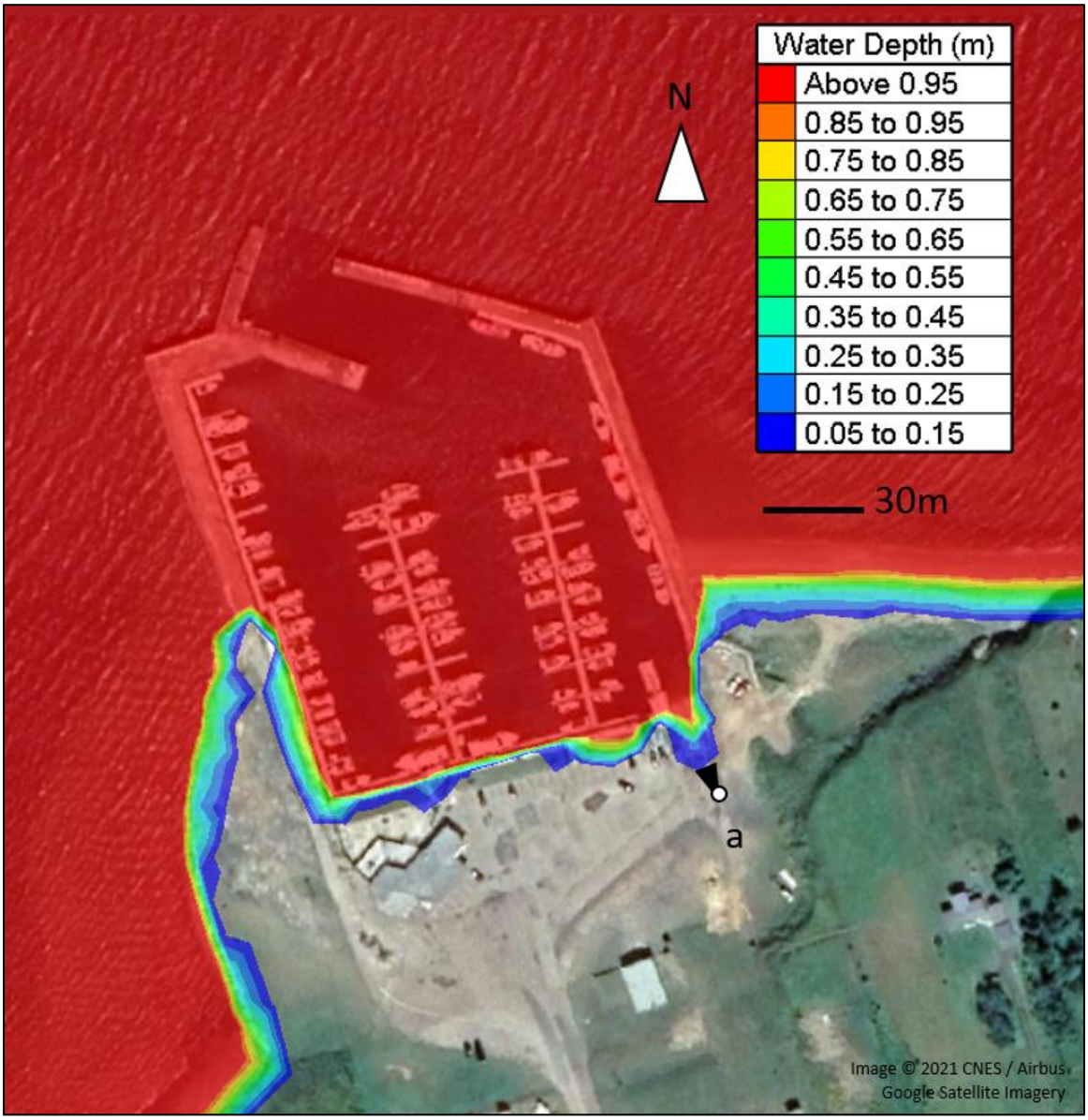


a
Date: December 21, 2010
Dominique Bérubé & Marc Desrosiers

Appendix D – Flood Hazard under Present-Day Conditions

Maximum Flood Extent for all Present-Day Hazard Events

Maisonnette

Caraquet

Bas-Caraquet

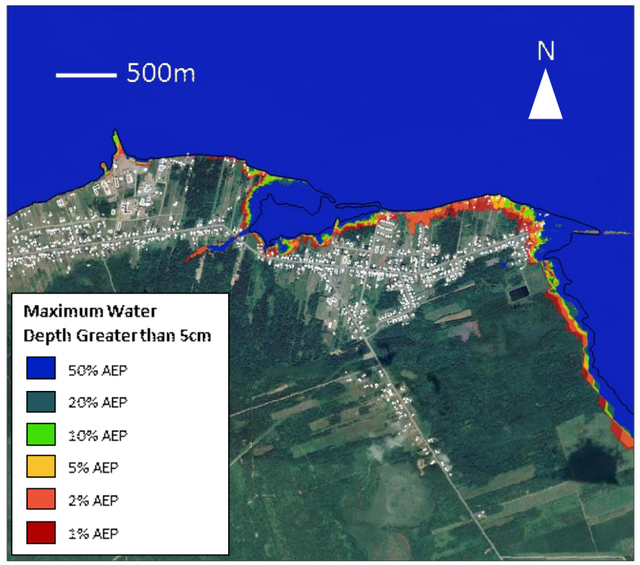

Shippagan and Pointe-Brûlée

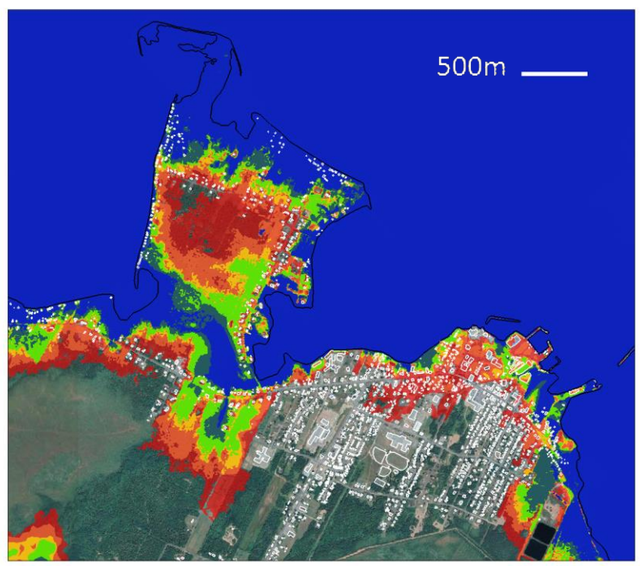

Le Goulet

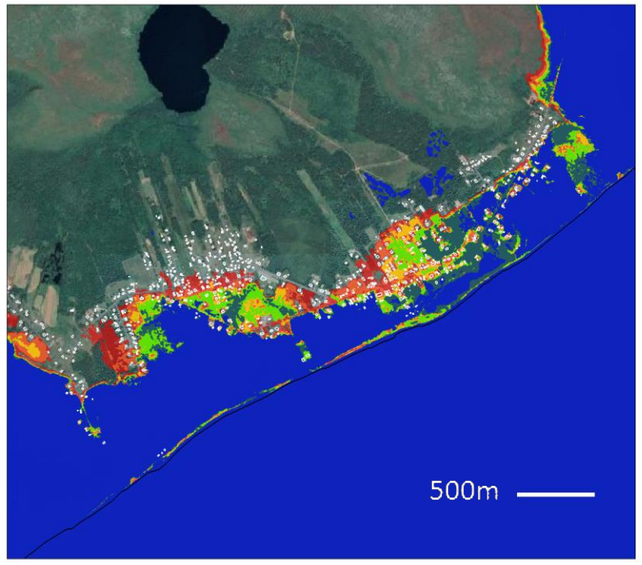

Lamèque

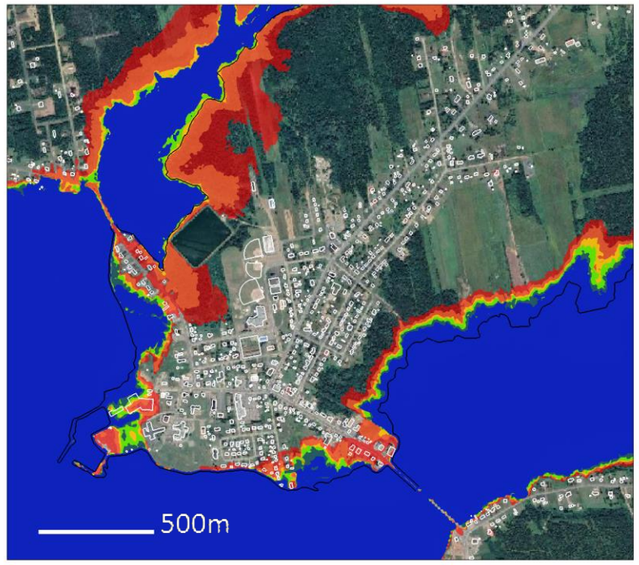

Basemap: Image © 2021 CNES / Airbus; Google Satellite Imagery

Maximum Water Depth for the 50% AEP Present-Day Hazard Event

Maisonnette

Caraquet

Bas-Caraquet

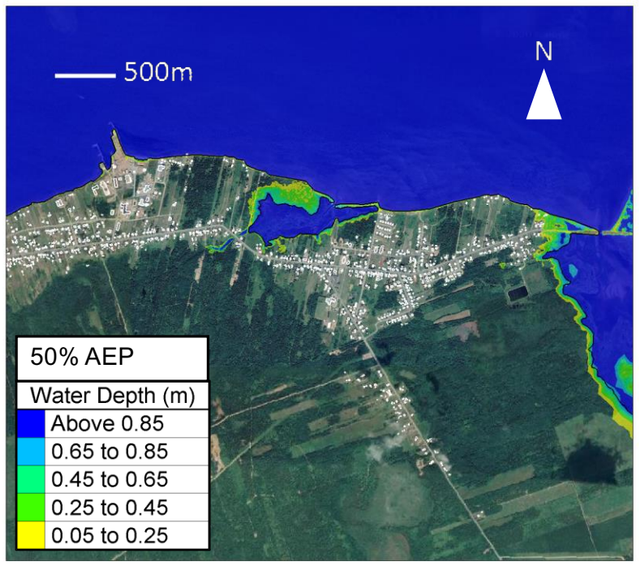

Shippagan and Pointe-Brûlée

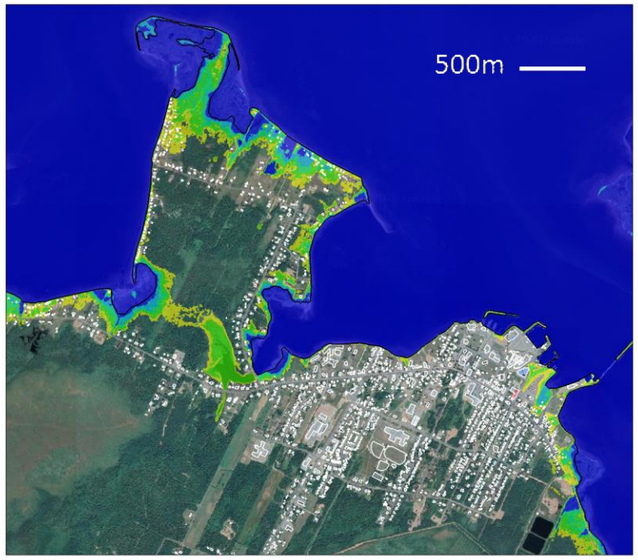

Le Goulet

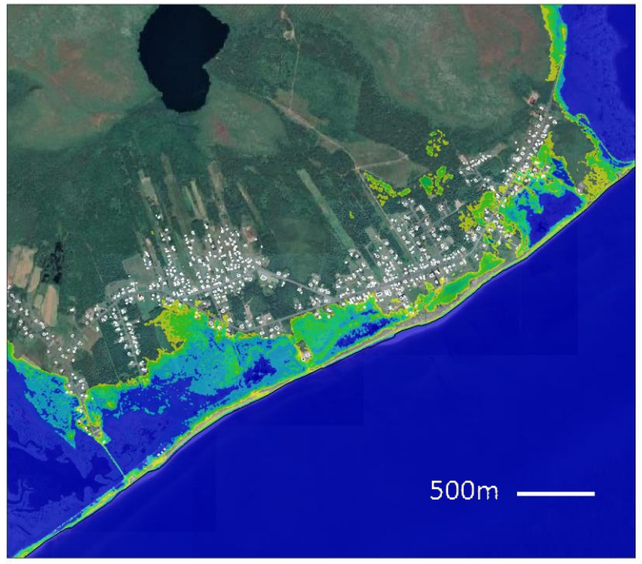

Lamèque

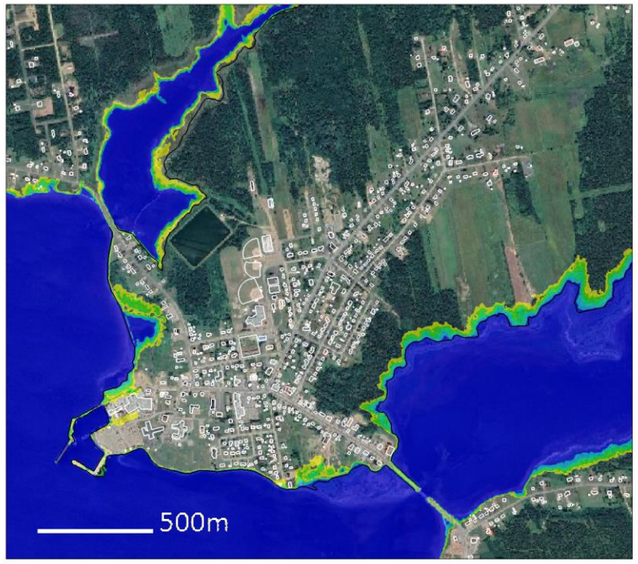

Basemap: Image © 2021 CNES / Airbus; Google Satellite Imagery

Maximum Water Depth for the 1% AEP Present-Day Hazard Event

Maisonnette

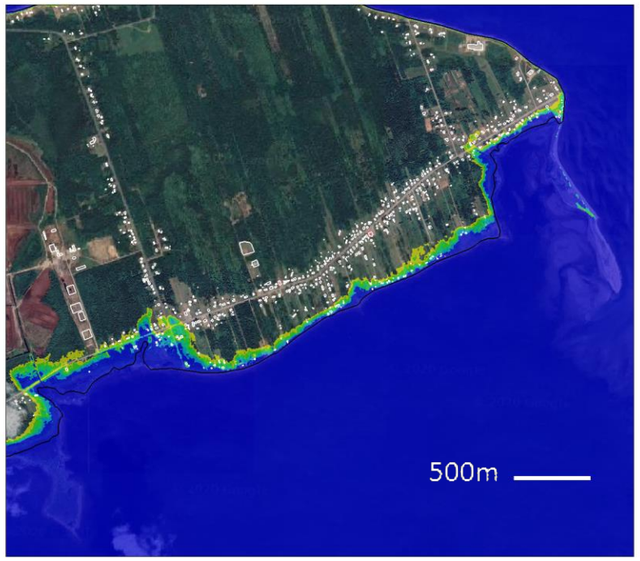

Caraquet

Bas-Caraquet

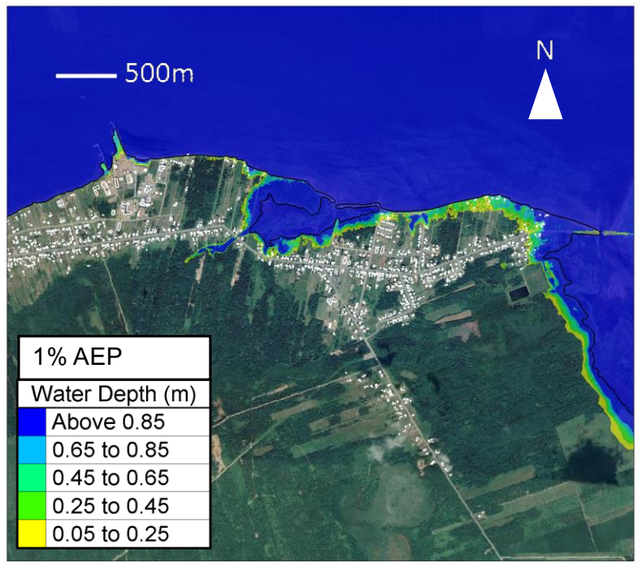

Shippagan and Pointe-Brûlée

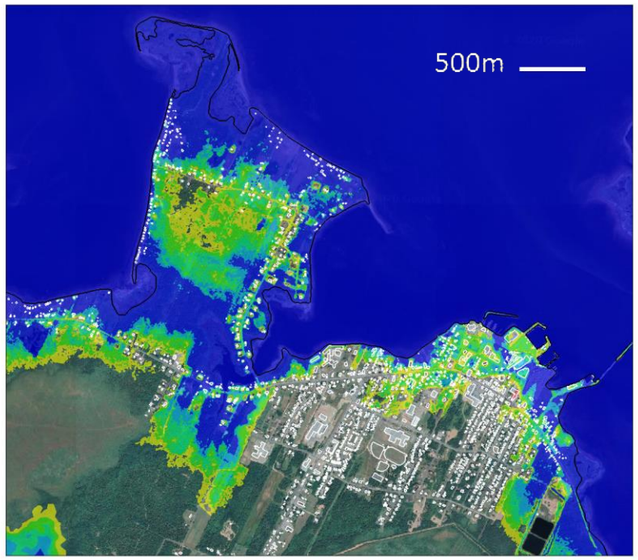

Le Goulet

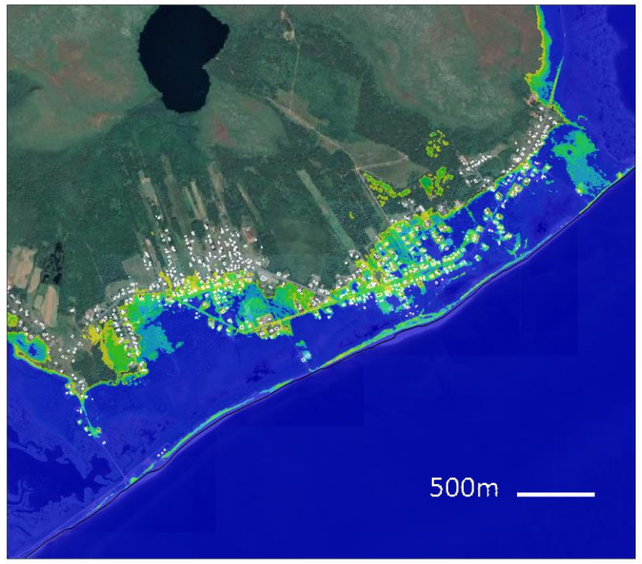

Lamèque

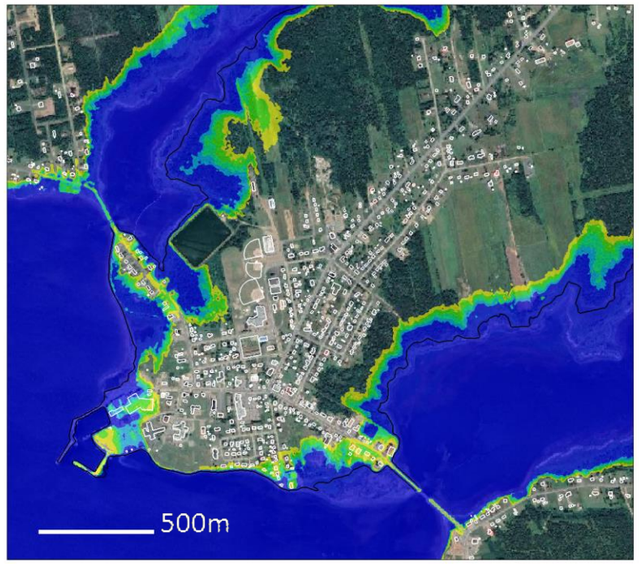

Basemap: Image © 2021 CNES / Airbus; Google Satellite Imagery

Appendix E – Flood Hazard under Future Conditions Accounting for Potential Sea-Level Rise

Maximum Flood Extent for the 50% AEP Hazard Event under Present-Day Sea Levels and Future Sea Levels Accounting for GSLR

Maisonnette

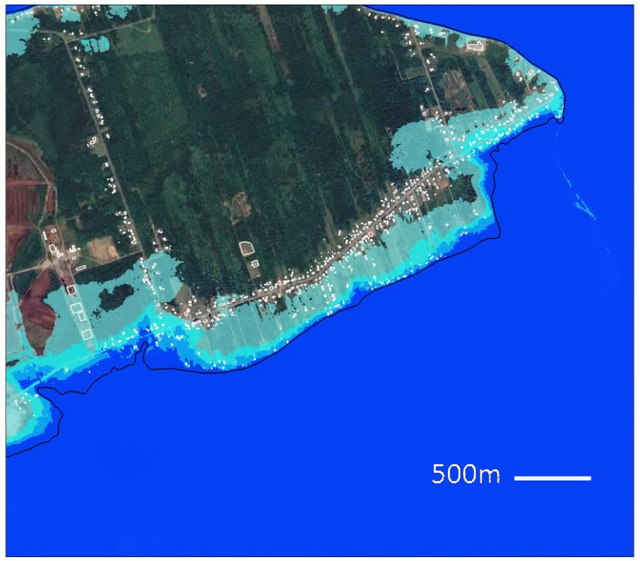

Caraquet

Bas-Caraquet

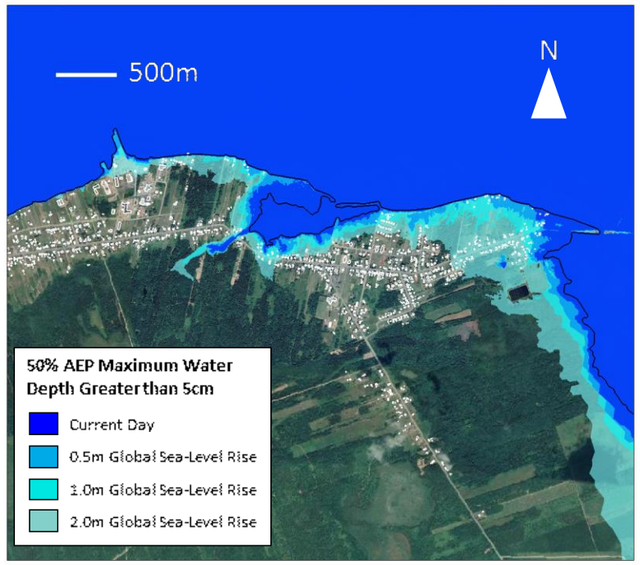

Shippagan and Pointe-Brûlée

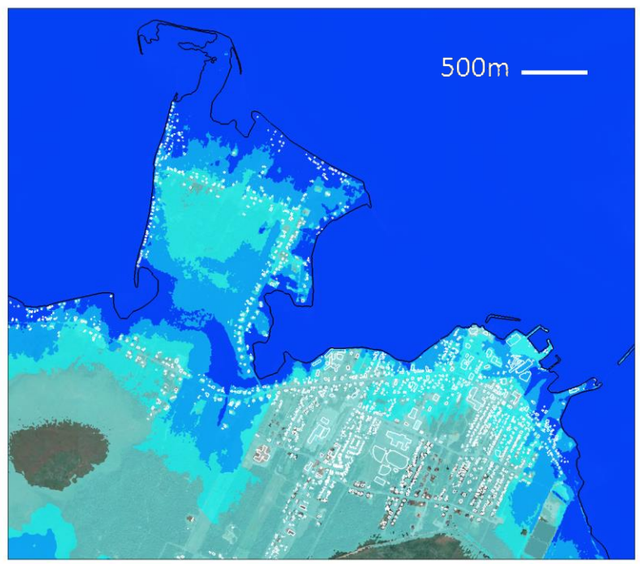

Le Goulet

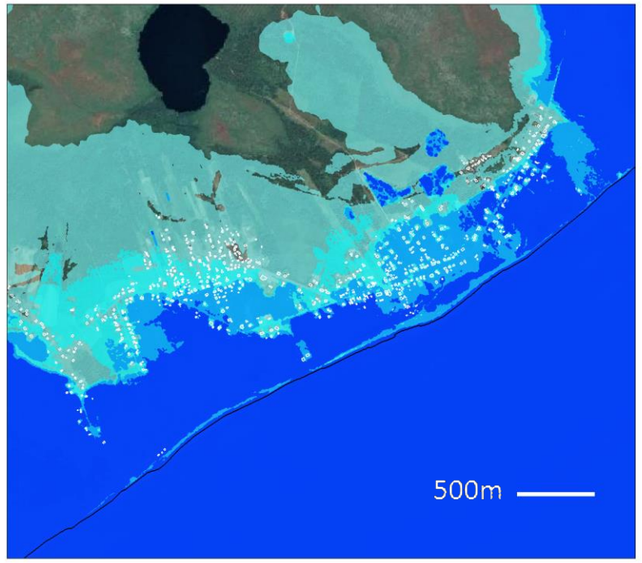

Lamèque

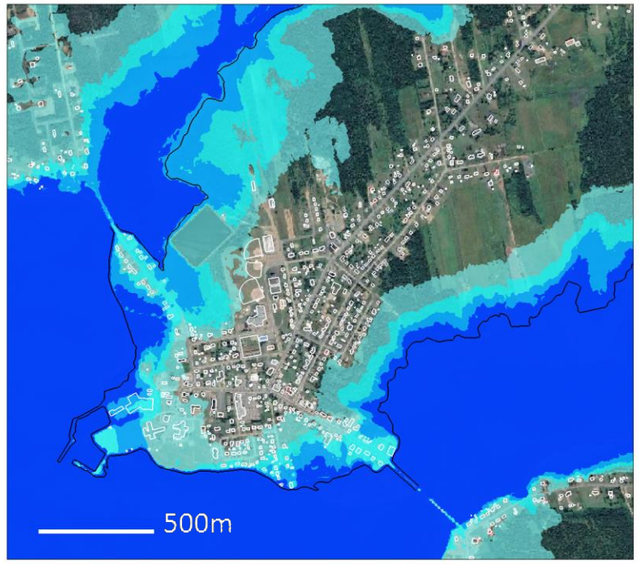

Basemap: Image © 2021 CNES / Airbus; Google Satellite Imagery

Maximum Flood Extent for the 1% AEP Hazard Event under Present-Day Sea Levels and Future Sea Levels Accounting for GSLR

Maisonnette

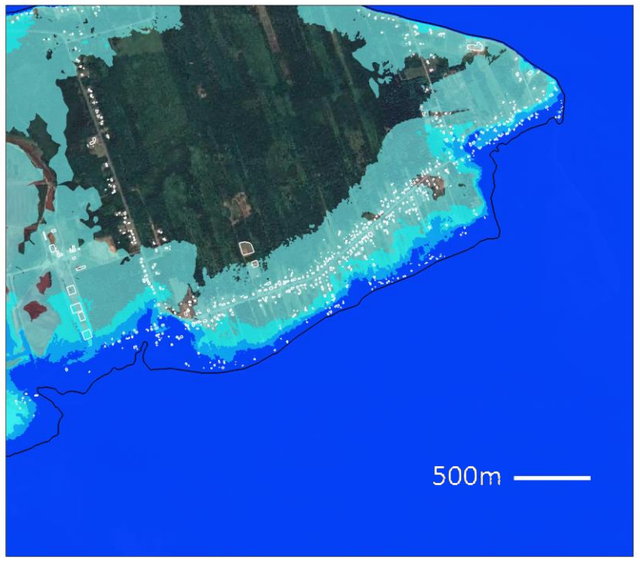

Caraquet

Bas-Caraquet

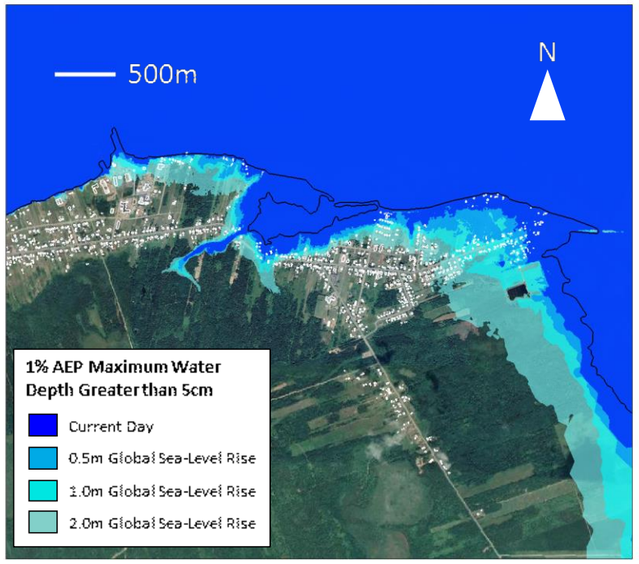

Shippagan and Pointe-Brûlée

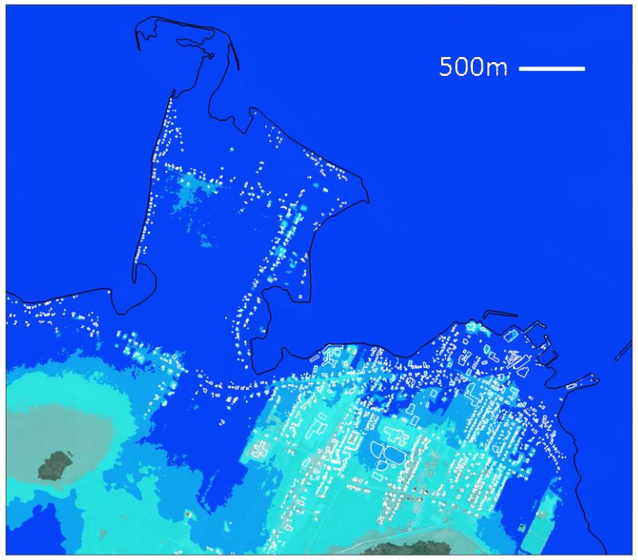

Le Goulet

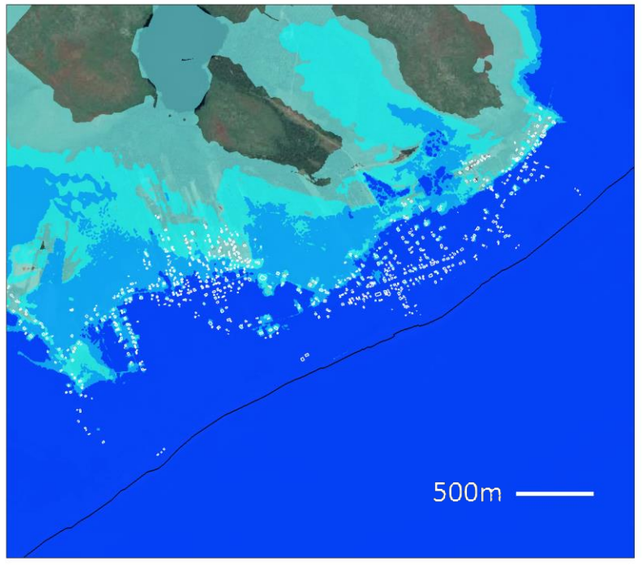

Lamèque

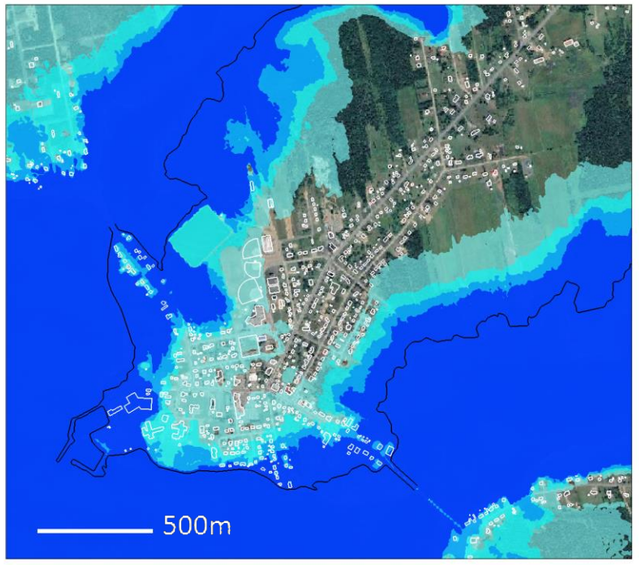

Basemap: Image © 2021 CNES / Airbus; Google Satellite Imagery

Maximum Water Depth for the 1% AEP Hazard Event Accounting for 2.0m GSLR

Maisonnette

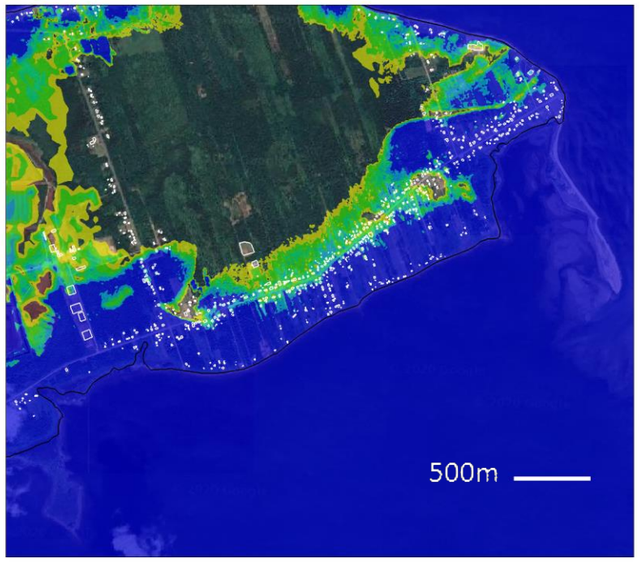

Caraquet

Bas-Caraquet

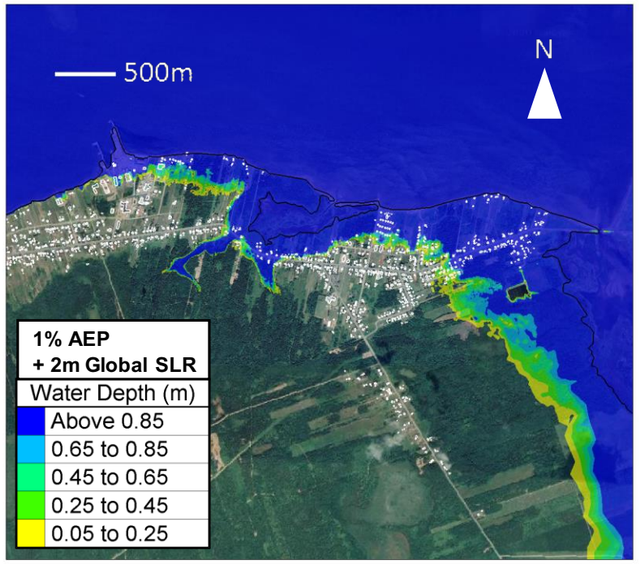

Shippagan and Pointe-Brûlée

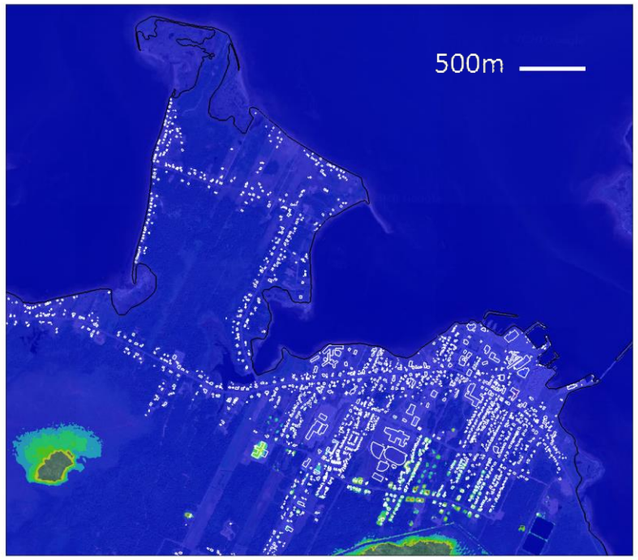

Le Goulet

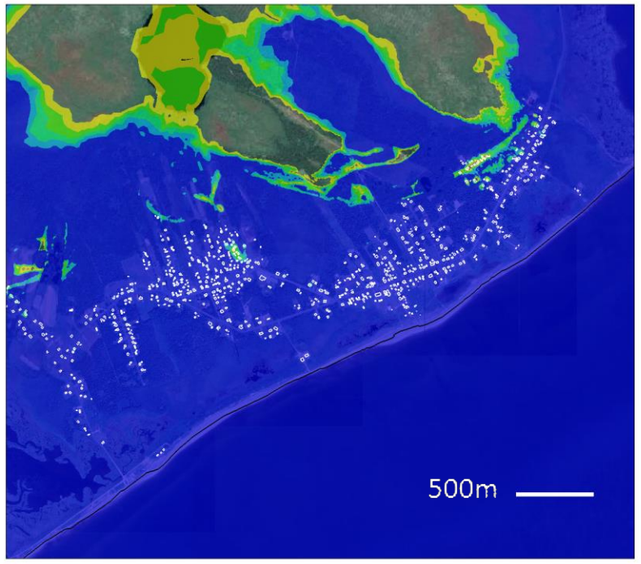

Lamèque

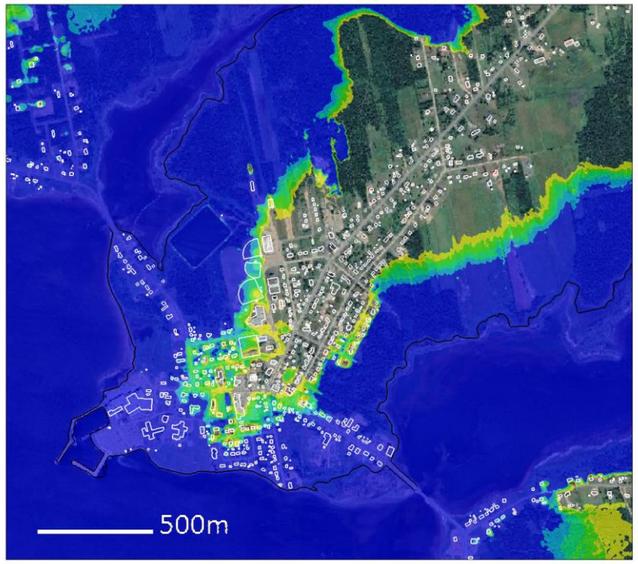

Basemap: Image © 2021 CNES / Airbus; Google Satellite Imagery

Appendix F – Flow-induced Hazard under Present-Day Conditions and Future Conditions Accounting for Potential Sea-Level Rise

Depth-Velocity Product for the 1% AEP Present-Day Hazard Event

Maisonnette

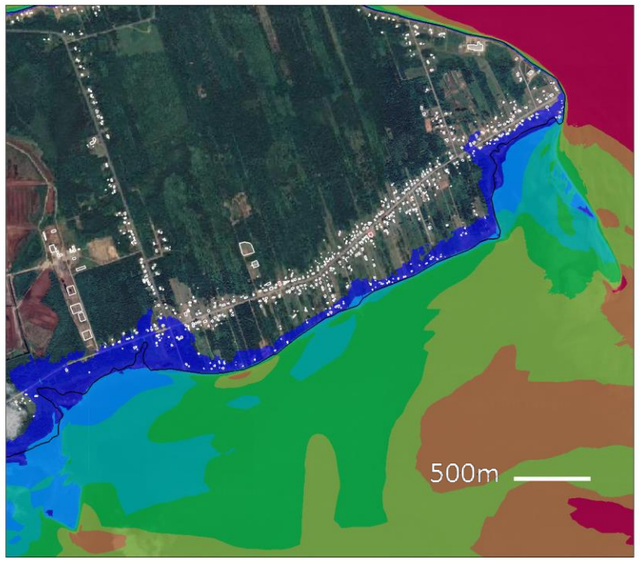

Caraquet

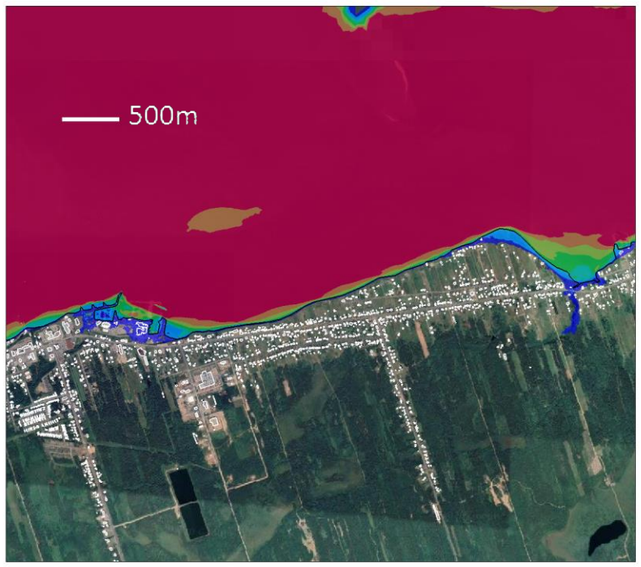

Bas-Caraquet

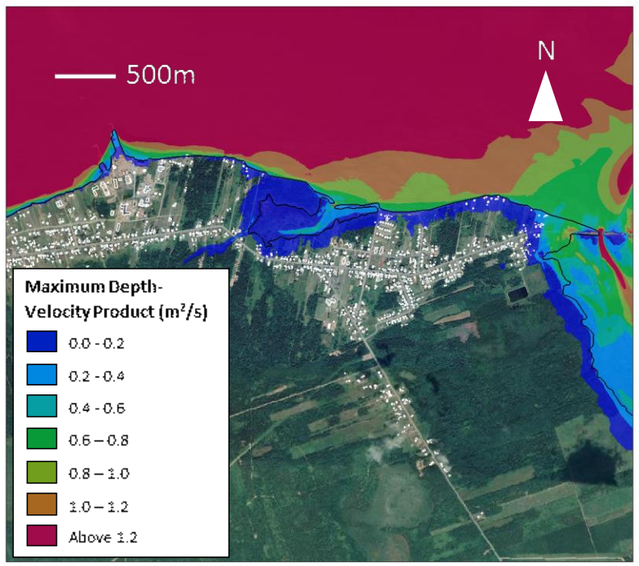

Shippagan and Pointe-Brûlée

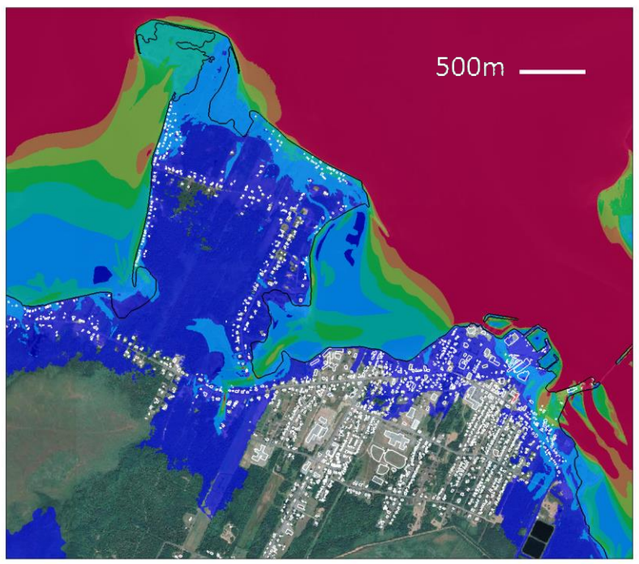

Le Goulet

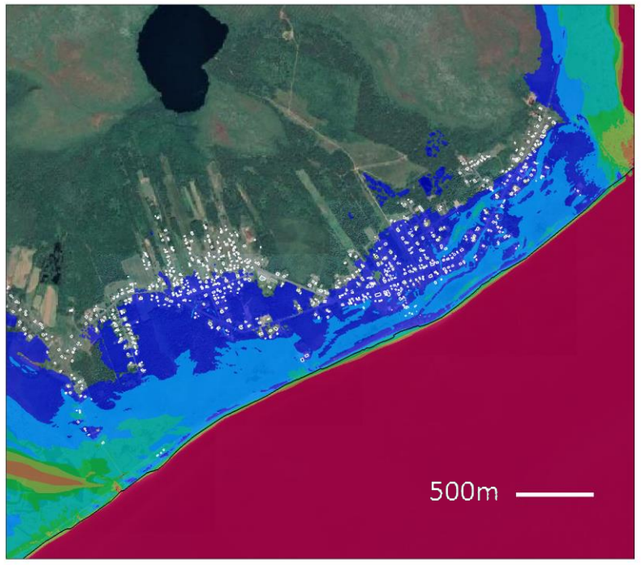

Lamèque

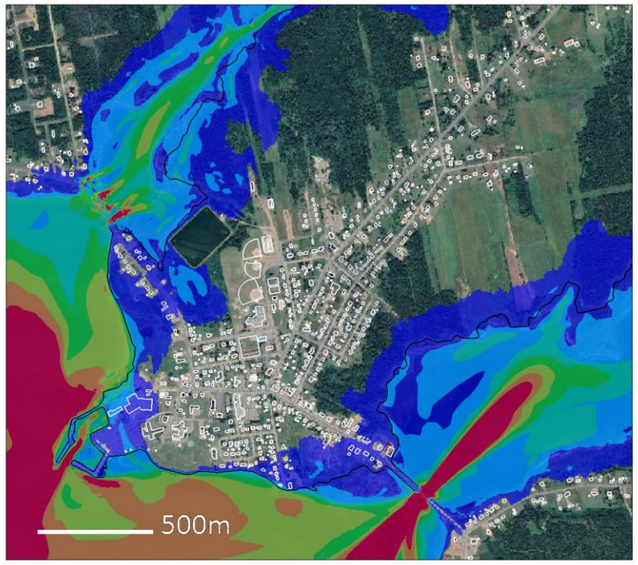

Basemap: Image © 2021 CNES / Airbus; Google Satellite Imagery

Depth-Velocity Product for Present-Day Hazard Events in Bas-Caraquet

50% AEP

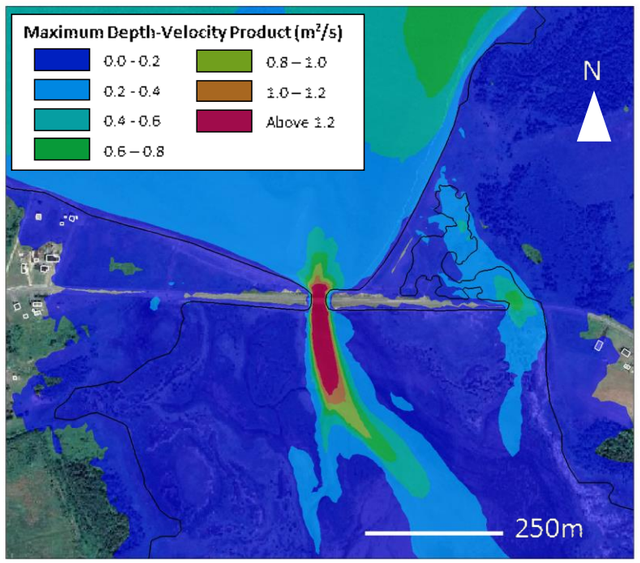

20% AEP

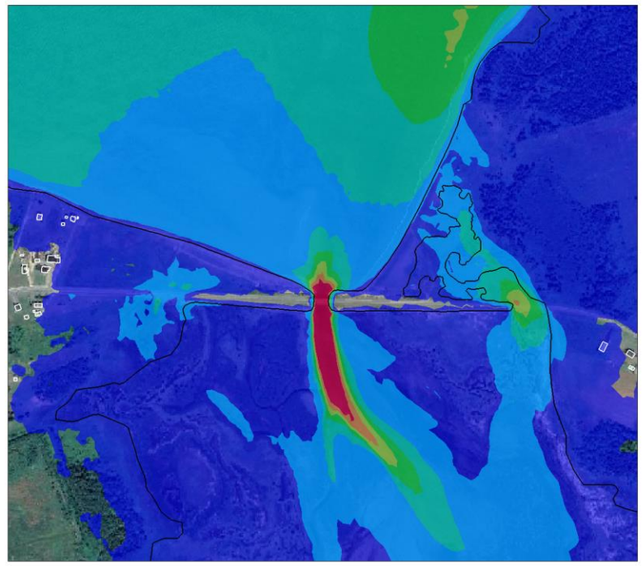

10% AEP

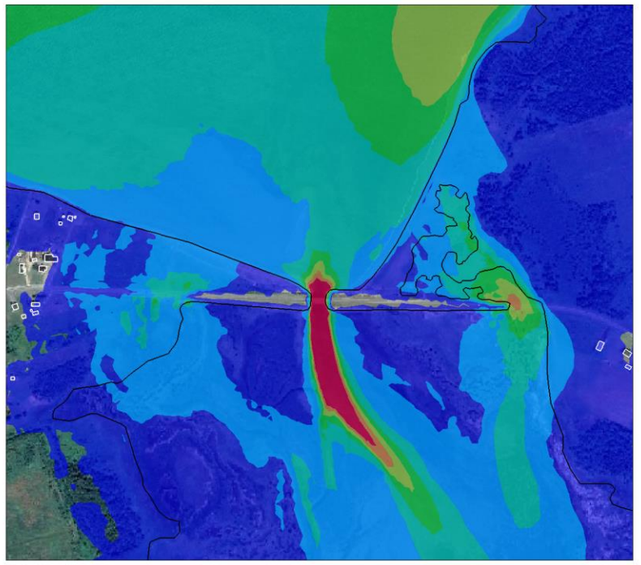

5% AEP

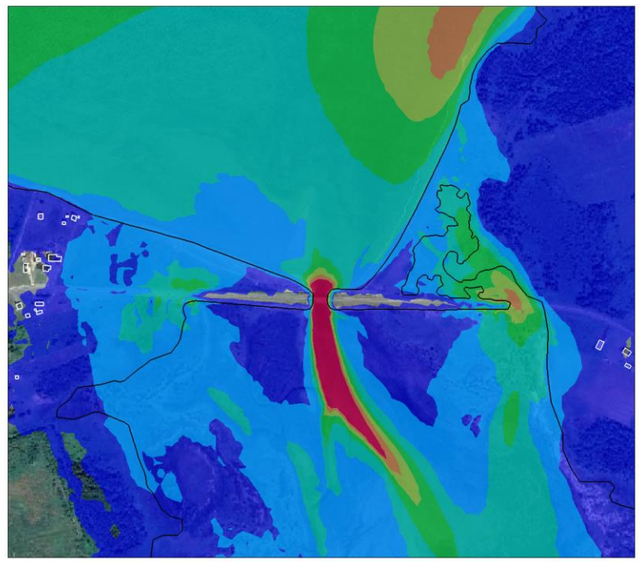

2% AEP

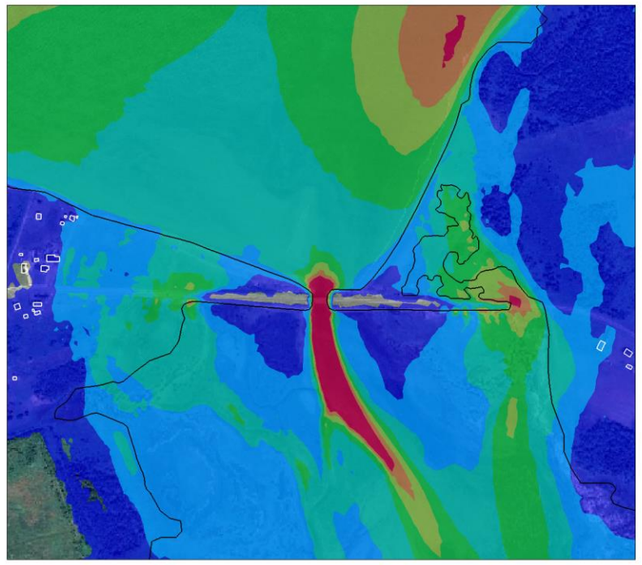

1% AEP

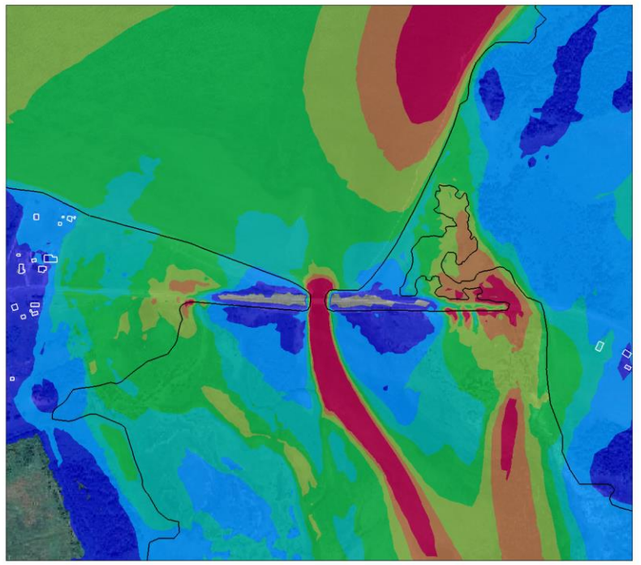

Basemap: Image © 2021 CNES / Airbus; Google Satellite Imagery

Depth-Velocity Product for Present-Day Hazard Events in Shippagan

50% AEP

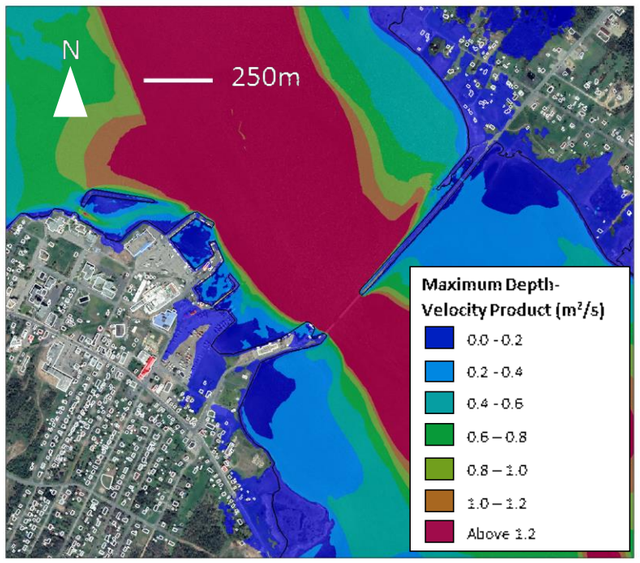

20% AEP

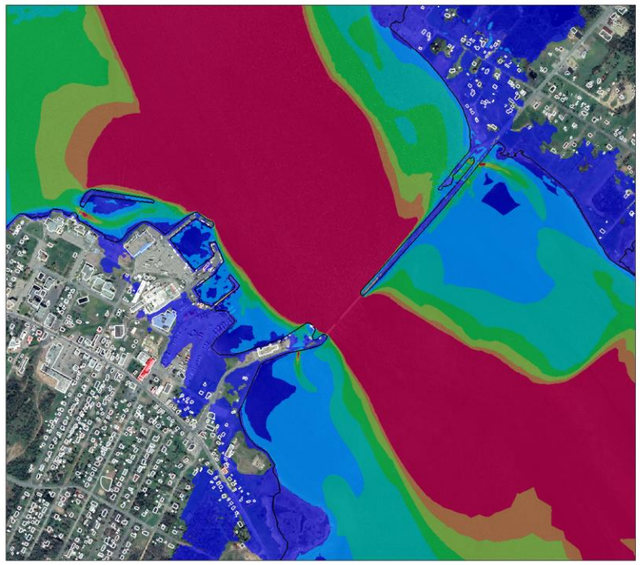

10% AEP

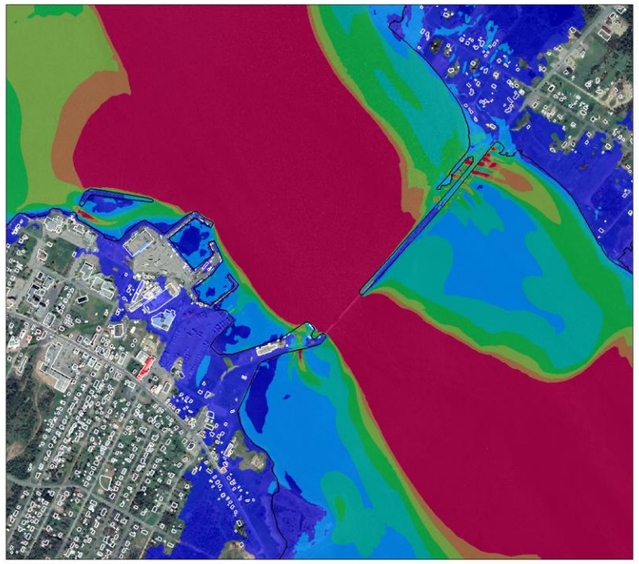

5% AEP

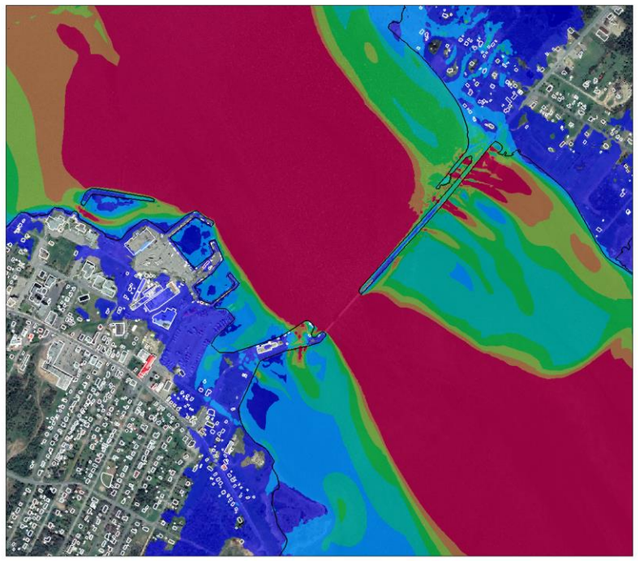

2% AEP

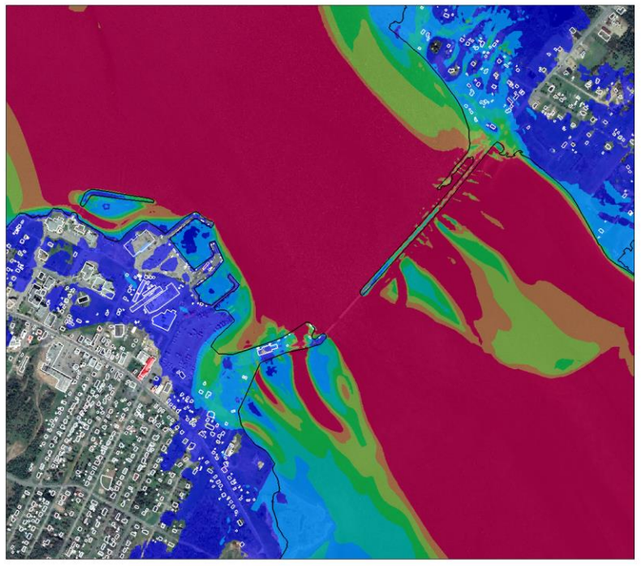

1% AEP

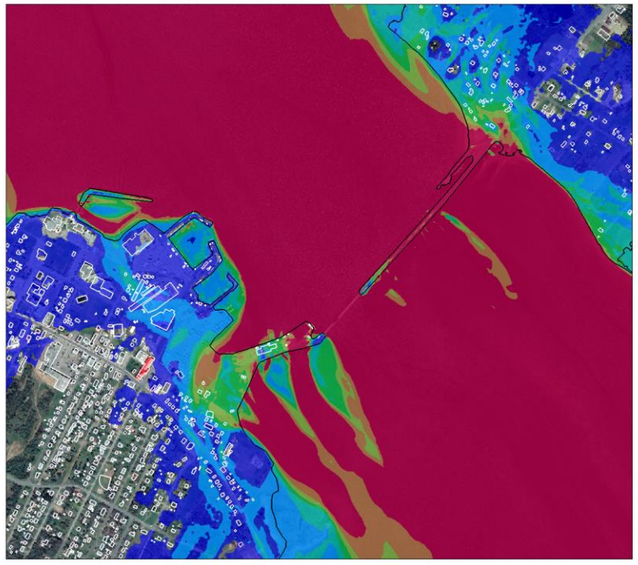

Basemap: Image © 2021 CNES / Airbus; Google Satellite Imagery

Depth-Velocity Product for Present-Day Hazard Events in Lamèque

50% AEP

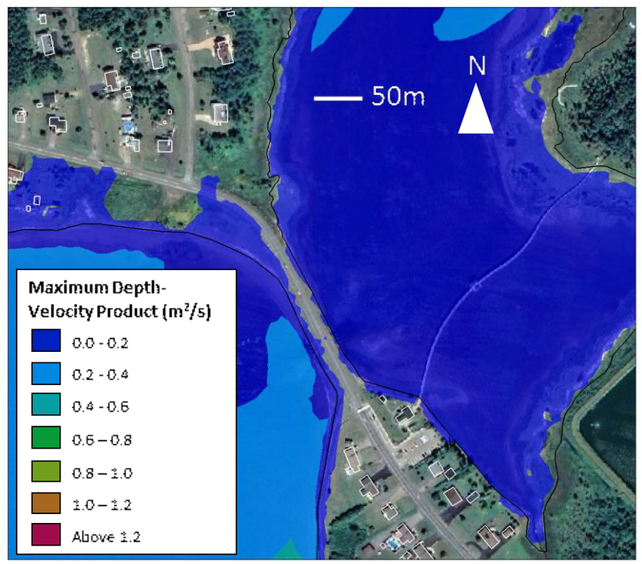

20% AEP

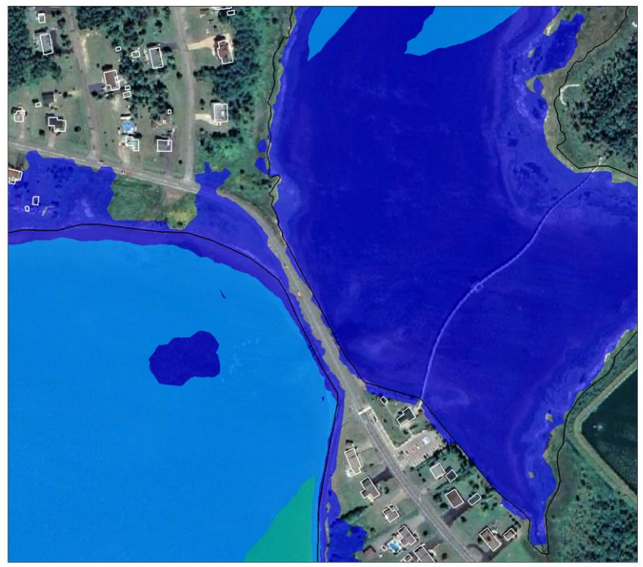

10% AEP

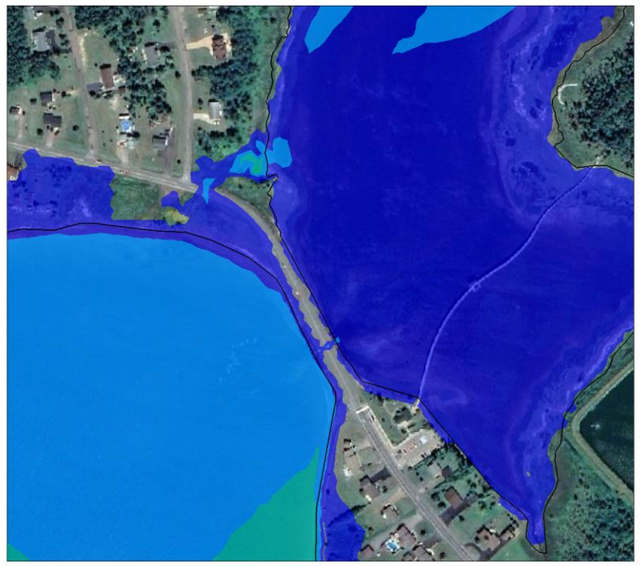

5% AEP

2% AEP

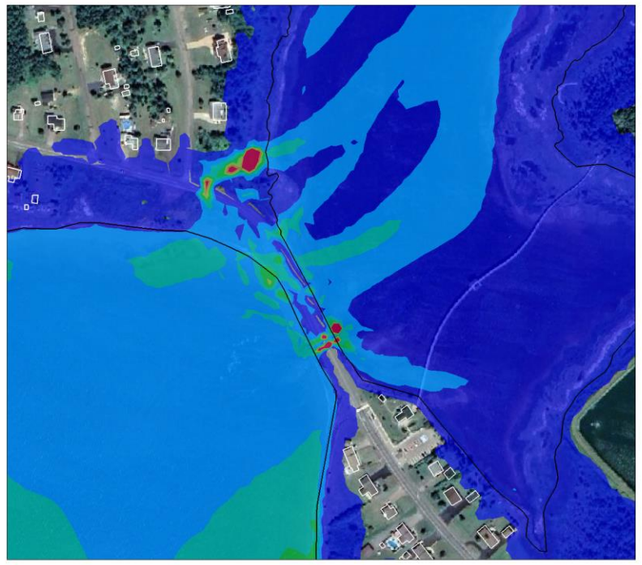

1% AEP

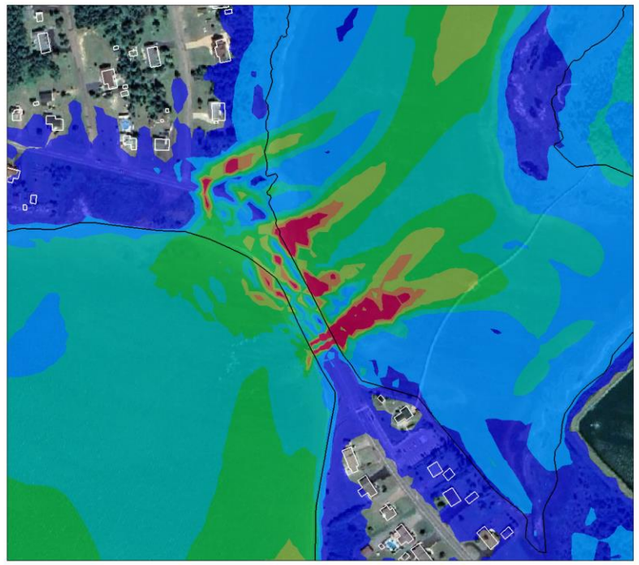

Basemap: Image © 2021 CNES / Airbus; Google Satellite Imagery

Momentum Flux for the 1% AEP Hazard Event under Present-Day Sea Levels and Accounting for 2.0m GSLR

Maisonnette

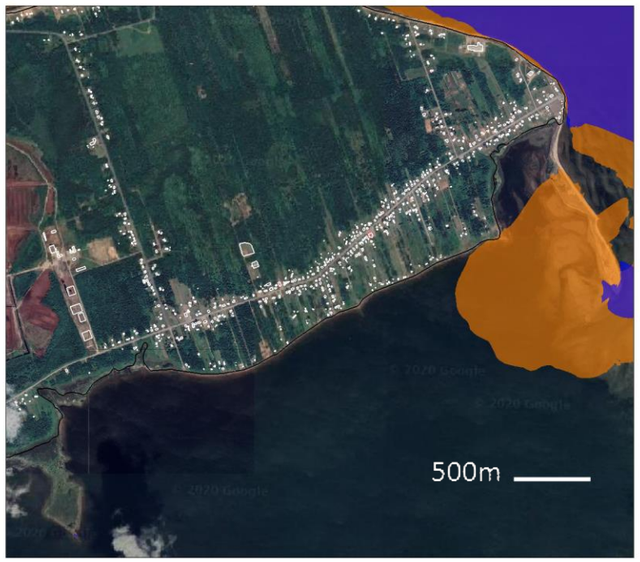

Caraquet

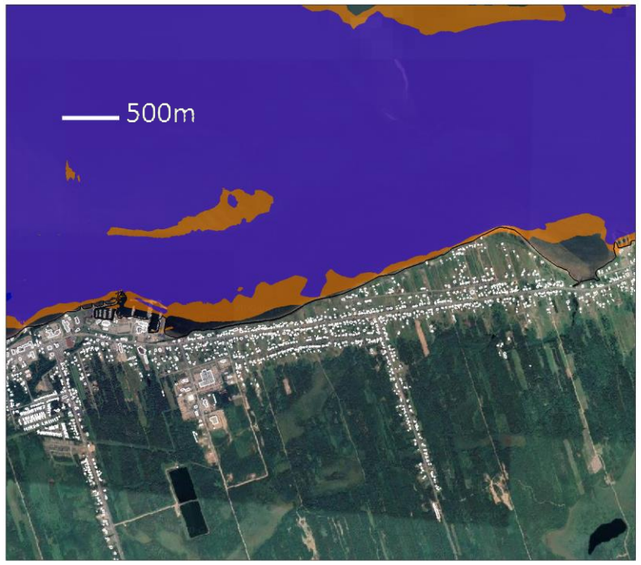

Bas-Caraquet

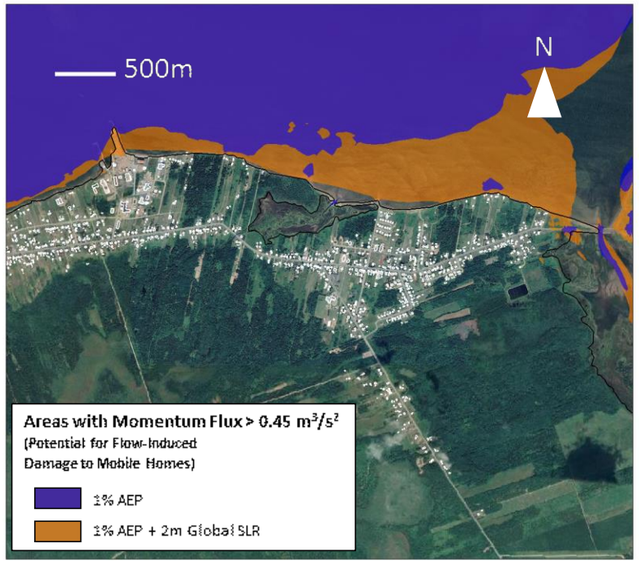

Shippagan and Pointe-Brûlée

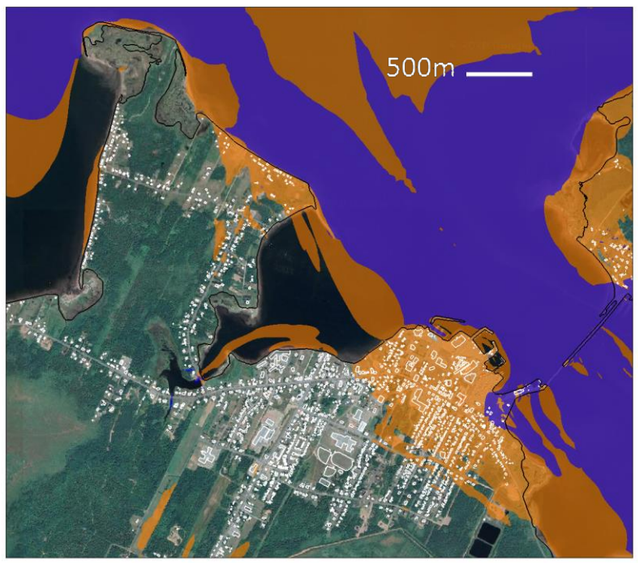

Le Goulet

Lamèque

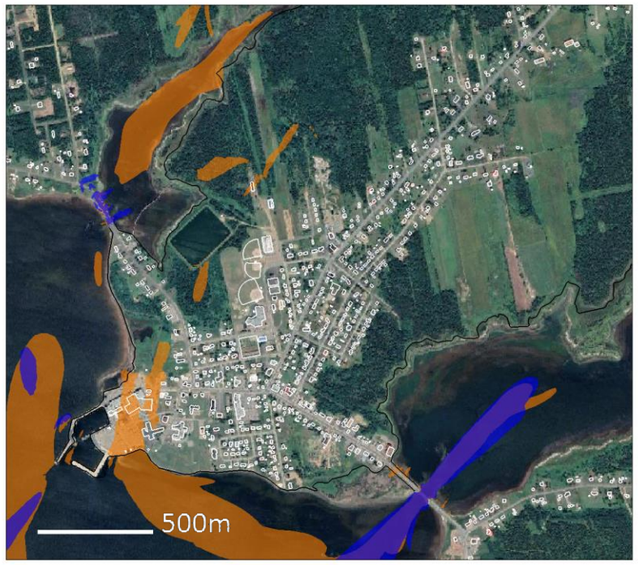

Basemap: Image © 2021 CNES / Airbus; Google Satellite Imagery